

8056

NACA TN 3217

# NATIONAL ADVISORY COMMITTEE FOR AERONAUTICS

TECHNICAL NOTE 3217

THE INFLUENCE OF WHEEL SPIN-UP

ON LANDING-GEAR IMPACT

By W. Flügge and C. W. Coale

Stanford University



Washington

October 1954

0066056



TECH LIBRARY KAFB, NM

AFM20

TECHNICAL REPORT  
AFL 2811



## TABLE OF CONTENTS

	Page
SUMMARY . . . . .	1
INTRODUCTION . . . . .	1
SYMBOLS . . . . .	2
PRELIMINARY STUDY OF SPIN-UP . . . . .	6
DIFFERENTIAL EQUATIONS OF LANDING IMPACT . . . . .	12
Equation of Oleo Strut . . . . .	12
Equations of Motion . . . . .	14
Phase one . . . . .	15
Phase two . . . . .	17
Phase three . . . . .	18
SOLUTION OF IMPACT PROBLEM . . . . .	18
Phase One . . . . .	18
Numerical Integration for Phases Two and Three . . . . .	22
Exact solution . . . . .	22
Numerical example . . . . .	27
Approximate solution . . . . .	30
Further simplification: Large steps . . . . .	33
Analytical Method of Solution . . . . .	34
Regular interval . . . . .	34
Singular interval . . . . .	44
Procedure . . . . .	51
Application of method to numerical example . . . . .	55
Analytic Start of Numerical Integration . . . . .	56
GENERALIZATIONS OF THEORY . . . . .	57
Eccentric Wheel . . . . .	57
Inclined Shock Strut . . . . .	60
Phase one . . . . .	61
Phase two . . . . .	63
Phase three . . . . .	64
BINDING OF SHOCK STRUT . . . . .	66
APPENDIX A - ADDITIONAL ANALYSIS OF SPRING-BACK MOTION . . . . .	73
APPENDIX B - DERIVATION OF EQUATION FOR AXLE MOTION RELATIVE TO UPPER SHOCK-STRUT CYLINDER . . . . .	75

	Page
REFERENCES . . . . .	78
TABLES . . . . .	79
FIGURES . . . . .	88

TECHNICAL NOTE 3217

THE INFLUENCE OF WHEEL SPIN-UP  
ON LANDING-GEAR IMPACT

By W. Flügge and C. W. Coale

SUMMARY

This report is a continuation of Technical Note 2743. It deals with the influence of the wheel drag on the performance of the landing gear. The differential equations are developed and are solved by numerical integration and by an analytical method. Special emphasis has been laid on dropping all influences of minor importance in order to make computations as simple as possible.

The possibilities of an eccentric wheel and of an inclined shock strut have been considered. In both cases the computation is rather involved. The binding of the piston due to ovalization of the shock-strut cylinder does not seem to present a serious problem.

INTRODUCTION

The study of impact forces in landing gears presented in Technical Note 2743 was subject to the restriction that no drag force on the wheel was admitted. The present report deals with the influence of the wheel drag on the performance of the landing gear.

When an airplane approaches the ground, the wheels of the landing gear must be brought from rest to the angular velocity which corresponds to the forward speed of the airplane rolling on the runway. The accelerating moment is supplied by a horizontal force acting between the ground and the wheel, the drag  $D$ . The magnitude of this drag depends, of course, on the vertical force  $F$  and will increase as  $F$  increases, until the wheel has been completely spun up. Then the drag disappears except for a small remainder, the rolling resistance of the wheel, which is of no importance for the problem treated here.

During the spin-up time the horizontal force acts on the cantilever shock strut and presses the bearing parts of the piston and barrel against each other. Through this action the friction of the shock strut is increased and hence its axial force  $F$ , which in turn influences  $D$ . The phenomenon becomes still more involved because of the horizontal deflection of the landing gear. Modern cantilever shock struts are

rather flexible; and, since the drag builds up in a very short time, the wheel mass undergoes a considerable horizontal acceleration. Therefore, the force which is transmitted to the axle of the wheel is different from the drag which acts on its rim.

When the spin-up of the wheel is completed and the drag drops almost to zero, the landing gear is in a state of lateral deflection; and, since the deflecting force has vanished, it will spring back. The ensuing fore-and-aft vibration is damped, but for several cycles it produces appreciable bending moments in the shock strut and its influence on the piston friction is similar to that of the spin-up drag.

This work was conducted at Stanford University under the sponsorship and with the financial assistance of the National Advisory Committee for Aeronautics.

#### SYMBOLS

$A_0$	inner cross section of barrel at oil level
$A_1$	total cross section of piston
$A_2$	inner cross section of piston
$A_3$	cross section of oil jet, equal to area of gap around metering pin times orifice factor
$a$	axial distance between upper and lower bearings for fully extended shock strut (see fig. 6)
$a$	mean radius of cylindrical shell (used only in section "Binding of Shock Strut")
$a_k, \bar{a}_k$	$k$ th coefficient for power-series expansion of $x_1$
$b$	effective width of cylindrical shell (used only in section "Binding of Shock Strut")
$b_k, \bar{b}_k$	$k$ th coefficient for power-series expansion of $x_2$
$c_k, \bar{c}_k$	$k$ th coefficient for power-series expansion of $x$
$D$	wheel drag (see figs. 1 and 8)
$d_k, \bar{d}_k$	$k$ th coefficient for power-series expansion of $y$

E	modulus of elasticity of shock-strut barrel
e	eccentricity of wheel
F	vertical force applied to wheel axle
$F_a$	part of $F_1$ due to air pressure in oleo strut
$F_p$	resultant force of oil pressure acting on surface of piston
$F_1$	compressive force in shock strut
$F_2$	compressive force between wheel and ground, normal to runway
H	force transmitted at wheel axle, directed normal to shock strut
I	mass moment of inertia of wheel
k	spring constant, used in preliminary study
$k_2$	spring constant of tire
$k_3$	spring constant for spring-back vibration
l	axial distance between axle and upper bearing attached to inner cylinder (see fig. 6)
M	bending moment in circular ring
m	wheel mass
$m_1$	part of airplane mass attributed to landing gear
$m_2$	unsprung mass (wheel and lower part of shock strut)
$m_3$	mass for spring-back motion
N	total normal force
$N_1, N_2$	normal forces between piston and barrel
$p_0$	initial air pressure in oleo strut
$p_1, p_2$	air pressure in upper and lower chamber of shock strut, respectively

q	resultant force per unit area of strip of middle surface of cylinder (see section "Binding of Shock Strut")
r	radius of wheel (distance of its center from runway)
T	total friction force
$T_1, T_2$	friction forces connected with normal forces $N_1$ and $N_2$
t	time
t	wall thickness of shock-strut barrel (used only in section "Binding of Shock Strut")
V	vertical velocity of airplane at contact
$V_h$	horizontal velocity of airplane
$W_1$	load on airplane (weight minus lift)
$W_1^* = W_1/m_1$	
$w_0$	ovalization of shock-strut barrel
x	stroke of shock strut
$x_1$	vertical displacement of mass $m_1$
$x_2$	vertical displacement of wheel center
Y	amplitude of $y$ for spring-back vibration
y	deflection of shock strut, measured at wheel axle
$\alpha$	angle between oleo strut and vertical
$\alpha_k, \bar{\alpha}_k$	kth coefficient for power-series expansion of $A_3$ as a function of $\tau$
$\beta$	coefficient (see eq. (17))
$\beta_k, \bar{\beta}_k$	definitions precede equations (31) and (45), respectively
$\gamma$	polytropic exponent of air in oleo strut
$\theta$	polar coordinate (see fig. 23)
$\theta_0, \theta_1$	coefficients (see eq. 25))

$\kappa_1, \kappa_2, \kappa_3$  parameters explained and used in section "Analytical Method of Solution"

$$\lambda = \sqrt{k/m}$$

$\lambda_1$  frequency of vertical vibration of airplane

$\lambda_3$  frequency of spin-up vibration

$\lambda_3'$  frequency of spring-back vibration

$\mu$  wheel friction coefficient

$\mu_r$  coefficient of friction between runway and wheel

$\mu_s$  coefficient of friction of shock strut

$\nu$  Poisson's ratio

$\rho$  mass density of oil in oleo strut

$\sigma$  bending stress in shock-strut barrel

$\sigma_1, \sigma_2$  coefficients (see eq. (26))

$\tau$  time variable, counted from start of an interval

$\phi_0, \phi_1$  coefficients (see eq. (24))

$\omega$  angular velocity of spinning wheel

Subscripts:

max maximum value

n value at start of interval n

o initial conditions

t value at transition from phase two to phase three

l value at start of phase two

## PRELIMINARY STUDY OF SPIN-UP

Since the real landing-gear problem is rather involved, it is useful to study first some simplified problems which may easily be solved and which will indicate the general character of the solutions to be expected for the landing gear.

This preliminary study is concerned with a wheel which is restrained horizontally by a spring as indicated in figure 1. This wheel is originally at rest and at  $t = 0$  is pressed against a horizontal plane which moves with the constant speed  $V_h$  toward the right. The vertical force  $F$  applied to the axle of the wheel is a given function of time. It will here be assumed zero for  $t < 0$  and equal to a constant value for  $t \geq 0$ . Because of the relative motion between the wheel and the ground a drag  $D = \mu F$  is developed which tends to spin the wheel up. But it also pushes the wheel to the right, producing a deflection  $y$ , varying with time.

The equations of motion of the wheel may easily be written. If  $m$  is its mass and  $I$ , its moment of inertia, one has

$$m\ddot{y} = \mu F - ky \quad (1a)$$

$$I\dot{\omega} = \mu Fr \quad (1b)$$

These equations hold while the wheel is spinning up, that is, while the horizontal velocity of its rim at the point of contact is smaller than the ground speed:

$$\dot{y} + r\omega < V_h$$

The initial conditions express the fact that the motion starts from rest:

$$\text{At } t = 0: y = 0, \dot{y} = 0, \omega = 0$$

The solution which satisfies these conditions is

$$\left. \begin{aligned} y &= \frac{\mu F}{k} (1 - \cos \lambda t) \\ \lambda^2 &= k/m \\ \omega &= \mu F r t / I \end{aligned} \right\} \quad (2)$$

It is shown in figure 2.

While the force acting at the rim of the wheel is always equal to  $\mu F$ , the force at the axle is  $ky$  and varies between 0 and  $2\mu F$ . In the case of a landing gear this variable force is responsible for the bending moment in the shock strut and for the piston friction.

The spin-up phase is terminated at a certain time  $t = t_t$  (see fig. 3) when

$$\dot{y} + r\omega = V_h$$

For  $t > t_t$ , the drag can no longer be  $\mu F$ , and equations (1) must be written:

$$m\ddot{y} = D - ky \quad (3a)$$

$$I\dot{\omega} = Dr \quad (3b)$$

where  $D$  is now a third unknown. Two things might occur:  $D$  may be restricted between the limits  $\pm\mu F$ , but otherwise unknown, and then there exists as a third equation the condition of rolling:

$$\dot{y} + r\omega = V_h \quad (3c)$$

On the other hand, the drag might attain the value  $D = -\mu F$ , and there would be slipping in the opposite direction,

$$\dot{y} + r\omega > V_h$$

It will be shown that the second case never occurs.

Equations (3a) to (3c) may easily be solved. Equations (3b) and (3c) are used to eliminate  $D$  and  $\omega$  from equation (3a) without increasing the order of this differential equation:

$$\left(m + \frac{I}{r^2}\right)\ddot{y} + ky = 0 \quad (4)$$

Evidently this equation describes a free vibration about the undeflected position, but with a fictitious mass  $m + I/r^2$ .

The solution of equation (4) is subject to the conditions that, for  $t = t_t$ , one has:

$$y = y_t$$

$$\dot{y} = \dot{y}_t$$

that is, those values which are found for the end of the spin-up phase. The following solution satisfies these conditions:

$$y = y_t \cos \lambda' (t - t_t) + \frac{\dot{y}_t}{\lambda'} \sin \lambda' (t - t_t) \quad (5a)$$

with

$$(\lambda')^2 = \frac{kr^2}{I + mr^2}$$

From it one finds with the help of equations (3c), (4), and (3a):

$$\omega = \frac{1}{r} \left[ v_h + y_t \lambda' \sin \lambda' (t - t_t) - \dot{y}_t \cos \lambda' (t - t_t) \right] \quad (5b)$$

$$D = \frac{Ik}{I + mr^2} y \quad (5c)$$

The maximum of the displacement  $y$  (in either direction) is

$$Y = \sqrt{y_t^2 + \frac{\dot{y}_t^2}{(\lambda')^2}}$$

and, when here  $y = y_t$  from equation (2) is introduced, one obtains:

$$y^2 = \left(\frac{\mu F}{k}\right)^2 \left[ (1 - \cos \lambda t_t)^2 + \frac{I + mr^2}{mr^2} \sin^2 \lambda t_t \right]$$

Necessarily,  $mr^2 > I$ , and one may easily prove that the expression within the brackets cannot get larger than 4; hence,

$$kY \leq 2\mu F$$

and, since the drag, equation (5c), is still less than one-half of that, sliding will never occur again, once the spring-back motion has started.

Some of the possible motions are shown in figure 4 for the following data (ref. 1):

$$\mu F = 4,840 \text{ lb}$$

$$I = 54.4 \text{ lb in. sec}^2$$

$$m = 0.286 \text{ lb in.}^{-1} \text{ sec}^2$$

$$k = 4,470 \text{ lb in.}^{-1}$$

$$r = 16.50 \text{ in.}$$

The diagrams lead to the following conclusions of general validity:

During the spin-up period the deflection varies periodically between 0 and  $2\mu F/k$ . The average of the spring force  $k y$  is  $\mu F$ , the spin-up drag.

In the spring-back period the deflection varies periodically with the average zero. Since the amplitude of this vibration depends on the landing speed and on the coefficient of friction, it will be different in successive landings. In the extremes, it may be zero or equal to the peak value of the spin-up period; that is, the force  $k y$  may be as high as  $\pm 2\mu F$ . The time average of the absolute value is then  $1.274\mu F$ . When analyzing drop tests, one may expect any value within these limits, and an unsuspected change of  $\mu$  may present puzzles or may be called upon as an excuse for scattering results. In design work, however, one must consider the worst, that is, the case with the greatest spring-back force.

The case  $F = \text{Constant}$  reveals some essential features of the drag-force problem, but it is not realistic enough for immediate application to a landing gear. This will be possible if it is assumed that  $F$  increases linearly with time, say

$$F = \dot{F}t \quad \text{for } t \geq 0$$

with constant  $\dot{F}$ . This must be introduced into the differential equations of the spin-up motion, equations (1). Their solution is then

$$\left. \begin{aligned} y &= \frac{\mu \dot{F}}{k} \left( t - \frac{1}{\lambda} \sin \lambda t \right) \\ \omega &= \frac{\mu \dot{F} r t^2}{2I} \end{aligned} \right\} \quad (6)$$

In this case, the displacement  $y$  represents a monotonic movement in the direction of the drag, but with a velocity dropping periodically to zero.

The spin-up phase is again terminated at a time  $t_t$  when the rim of the wheel has reached the velocity  $V_h$  of the ground, that is, when

$$\dot{y} + r\omega = \frac{\mu \dot{F}}{k} \left( 1 - \cos \lambda t_t + \frac{k r^2}{2I} t_t^2 \right) = V_h$$

The spring-back motion is again described by equations (3) with the only difference that now the values  $y_t$ ,  $\dot{y}_t$ , and  $\omega_t$  must be used which result for  $t = t_t$  from equations (6). It is shown in appendix A that the spring-back motion cannot be interrupted by phases of tire skidding which would require a separate analytical treatment.

The motion is represented in figure 5 for some typical choices of the transition time  $t_t$ . During the spin-up time the deflection is never far away from the static value  $y_{\text{stat}} = \mu \dot{F} t / k$ , and the amplitude of the spring-back vibration would not be much different if the static deflection were used for computing  $y_t$  and  $\dot{y}_t$ .

One may, therefore, do so and compute the greatest deflections in this way:

Given  $\dot{F}$ ,  $\mu$ , and  $V_h$ , the time needed to spin the wheel up is

$$t_t = \frac{1}{r} \sqrt{\frac{2IV_h}{\mu \dot{F}} - \frac{2I}{k}}$$

the deflection at this time,

$$y_t = \frac{\mu \dot{F}}{k} t_t = \frac{1}{kr} \sqrt{2I\mu \dot{F} V_h}$$

and the rate of deflection,

$$\dot{y}_t = \frac{y_t}{t_t} = \frac{\mu \dot{F}}{k}$$

The spring-back vibration is found from equation (5a), and its amplitude is

$$Y = \sqrt{y_t^2 + \frac{\dot{y}_t^2}{(\lambda')^2}} = \frac{\mu \dot{F}}{k} \sqrt{t_t^2 + \frac{I + mr^2}{kr^2}}$$

The maximum of the force at the axle is  $kY$ . The average is zero, but the average of the absolute value is  $2kY/\pi = 0.637kY$ .

### DIFFERENTIAL EQUATIONS OF LANDING IMPACT

In this section the landing impact is investigated under the following assumptions: At the beginning of the impact period the wheel does not rotate (or at least not with that angular velocity which is required for rolling). There are friction forces between the wheel and the ground and inside the shock strut which influence the impact force. The axis of the shock strut is vertical and lies either in the plane of the wheel or in the plane of symmetry between two equal wheels.

#### Equation of Oleo Strut

Figure 6 represents an idealized section through an oleo shock strut. The piston is shown separately with the forces applied to it. The force  $F_p$  is the resultant of the oil pressure acting on the surface of the piston. It has been shown earlier (ref. 2) that this force is composed of two parts, that due to the air pressure in the upper chamber  $p_1$  and that due to the pressure difference  $p_2 - p_1$  between the two chambers:

$$F_p = \frac{A_1 p_0}{\left[1 - (A_1 x / A_0 z_0)\right]^\gamma} + \frac{\rho A_2^3}{2A_3^2} \dot{x}^2$$

The forces  $N_1$  and  $N_2$  have to balance the horizontal force  $H$  at the axle of the wheel. Since the vertical forces make only small contributions to the moment equilibrium, one may write with good approximation:

$$N_1 = H \frac{l - a - x}{a + x}$$

$$N_2 = H \frac{l}{a + x}$$

These forces are transmitted through normal pressures in the contact area between two cylindrical surfaces. This area will extend over a certain part of the circumference. The length of the arc (fig. 7) in which the two parts are in contact depends on the elasticity of these

parts, and its central angle may be anything between  $0^\circ$  and  $180^\circ$ . If the angle is large, part of the contact pressure contributes only with a component to the resultant  $N_1$  or  $N_2$ , while the total pressure contributes to the frictional force. Therefore, if one simply puts  $T = \mu_s N$ , it must be expected that the coefficient  $\mu_s$  is greater than that for plane surfaces under similar conditions and that it depends on the wall thickness of the cylinders and on other parameters which may influence the size of the contact area. One of these parameters is the force  $N$  itself, so that the relation between  $T$  and  $N$  is necessarily nonlinear.

These considerations should be kept in mind when results of different tests are compared. However, the present information on the value of the coefficient of friction is so scarce that it seems more than good enough to write

$$T_1 = \mu_s N_1$$

$$T_2 = \mu_s N_2$$

with a coefficient of shock-strut friction  $\mu_s$  somewhere between 0.02 and 0.15 or still more (ref. 3), but assumed to be constant throughout the stroke of the shock strut. It follows that

$$T_1 + T_2 = \mu_s H \frac{2l - a - x}{a + x}$$

If the force  $H$  changes sign, the points of application of the forces  $T_1$  and  $T_2$  will change, but their direction will still be vertically downward. The formula just derived will remain correct if  $|H|$  is written instead of  $H$ .

The force  $F_1$  must be in equilibrium with  $F_p$ ,  $T_1$ , and  $T_2$ , whence:

$$F_1 = \frac{A_1 p_0}{\left[1 - (A_1 x / A_0 z_0)\right]^\gamma} + \frac{\rho A_2^3}{2A_3^2} \dot{x}^2 + \mu_s |H| \frac{2l - a - x}{a + x} \quad (7)$$

This equation holds true as long as  $\dot{x} > 0$ . When the rate of stroke changes sign, the second and third terms to the right must have a minus sign. However, for the reverse stroke other changes must be made which have been mentioned before (ref. 2) and of which little is known so far.

Equation (7) relates  $F_1$  to the stroke  $x$  and its first derivative and may be called the differential equation of the shock strut. The orifice area  $A_3$  depends on  $x$ , while  $H$  may be a given function of time or may be related to  $F_1$  by another differential equation.

The force  $F_1$  is not exactly the force transmitted from the wheel; otherwise equation (7) ought to have a term which represents the inertia of the piston. This term has been omitted here because it is simpler to take care of it in the equations of motion, lumping together the masses of the piston and of the wheel.

When the shock strut is fully extended, the air pressure  $p_0$  presses the piston with the force  $p_0 A_1$  against its seat. As long as  $F_1 < p_0 A_1$ , the shock strut certainly cannot be compressed. But, if there is a horizontal force  $H$ , then the friction forces  $T_1$  and  $T_2$  also must be overcome, and the minimum force  $(F_1)_1$  needed to make the piston move is the force obtained from equation (7) for  $x = \dot{x} = 0$ ; that is,

$$(F_1)_1 = A_1 p_0 + \mu_s H \frac{2l - a}{a} \quad (8)$$

In the early part of the landing impact, before  $F_1$  has built up to this limit, equation (7) must be replaced by the equation  $\dot{x} = 0$ .

#### Equations of Motion

When the horizontal deflection of the landing gear is taken into account, a three-degree-of-freedom system must be considered (fig. 8). The mass  $m_1$  represents the airframe. It moves only in a vertical direction. The total unsprung mass of the landing gear is  $m_2$ . It represents the inertia of all parts which move vertically with the velocity  $\dot{x}_2$ . Because of the bending elasticity of the landing gear, the wheel moves also in the horizontal direction, but only a portion of the unsprung mass participates in this movement. This portion will be called  $m_3$ .

The mass  $m_3$  is held horizontally by the spring  $k_3$  which represents the elastic stiffness of the landing gear. As the shock strut

collapses, the spring constant  $k_3$  will increase. This effect will be neglected in the present investigation, since it is not expected that the influence of this variability on the vertical impact is important enough to make additional computational labor worth while.

The member connecting the mass  $m_2$  with  $m_1$  is the oleo strut, the spring  $k_2$  represents the tire,  $F_2$  and  $H$  are the forces in the springs  $k_2$  and  $k_3$ , respectively, and  $F_1$  as given by equation (7) is the force in the oleo strut.

In the study made here it is convenient to assume that the model (except for the mass  $m_3$ ) moves only in the vertical direction and that the ground moves with the speed  $V_h$  under it.

The motion during the landing impact, as far as it is studied here, may be divided into three phases, which are governed by different sets of differential equations:

Phase one: The motion before the prestressing of the shock strut has been overcome.

Phase two: The remainder of the spinning-up of the wheel.

Phase three: The motion which takes place after the wheel has been spun up. This phase terminates when the stroke  $x$  has reached its maximum.

The fourth phase, the recoil motion, is not yet accessible to a rational analysis for the reasons already mentioned.

Phase one.- When the landing gear strikes the ground, the wheels are for some time the only elastic element and the oleo strut is inoperative; that is:

$$x \equiv x_1 - x_2 \equiv 0$$

The whole mass  $m_1 + m_2$  moves then as a rigid body and is acted upon by the load  $W_1$  (weight minus lift) from above and the ground reaction  $F_2$  from below. The latter is

$$F_2 = k_2 x_2 \quad (9a)$$

and the equation of motion is

$$(m_1 + m_2)\ddot{x}_2 + k_2x_2 = W_1 \quad (9b)$$

This is a differential equation in  $x_2$  only. When it has been solved, the force in the shock strut is found from the equation of motion of the mass  $m_2$ :

$$F_1 = m_2\ddot{x}_2 + k_2x_2 \quad (9c)$$

The drag force is

$$D = \mu_r F_2 = \mu_r k_2 x_2$$

It produces a lateral displacement  $y$  of the mass  $m_3$  according to the differential equation

$$m_3\ddot{y} + k_3y = \mu_r k_2 x_2 \quad (9d)$$

and an angular velocity  $\omega$  of the wheel

$$\omega = \int_0^t \frac{Dr}{I} dt$$

In this equation,  $r$  represents the distance between the wheel axis and the runway. Because of the elastic deformation of the tire, it decreases during the landing impact and might be written as

$$r = r_0 - x_2$$

However, the deformation of the tire has a fore-and-aft asymmetry such that the vertical force is moved rearward and restores part of the moment which the drag loses through the decrease of  $r$ . Since exact information on this subject is hard to obtain, it may be good enough

to assume  $r$  as a constant. This has been done in all examples prepared for this report, but one may, of course, easily introduce any other assumption which is judged to be better.

With  $r = \text{Constant}$  one has

$$\omega = \frac{\mu_r k_2 r}{I} \int_0^t x_2 dt \quad (9e)$$

Equations (9a) to (9e) determine the motion during phase one of the landing impact. This phase is terminated when  $F_1$  as computed from equation (9c) reaches the value  $(F_1)_1$  given by equation (8).

Phase two.- In phases two and three  $x_1$  and  $x_2$  are no longer equal, and the vertical motion of the masses  $m_1$  and  $m_2$  must be considered independently. This yields the two equations:

$$m_1 \ddot{x}_1 + F_1 = W_1 \quad (10a)$$

$$m_2 \ddot{x}_2 - F_1 + k_2 x_2 = 0 \quad (10b)$$

Besides the displacements, these two equations contain as a third unknown the shock-strut force  $F_1$ . Therefore another equation is needed, the differential equation of the shock strut, equation (7). It contains a new variable, the horizontal force  $H$ , equal here to  $k_3 y$ , whence

$$F_1 = \frac{A_1 p_0}{\left[1 - (A_1 x / A_0 z_0)\right]^\gamma} + \frac{\rho A_2^3}{2A_3^2} \dot{x}^2 + \mu_s k_3 \frac{2l - a - x}{a + x} |y| \quad (10c)$$

This equation seems to introduce two new unknowns,  $x$  and  $y$ . One of them stands merely as an abbreviation;

$$x = x_1 - x_2$$

but for  $y$  another equation is needed, equation (9d) for the motion of the mass  $m_3$ . These four equations for the four unknowns  $x_1$ ,  $x_2$ ,  $F_1$ , and  $y$  must be treated together.

When they have been solved, equation (9e) may be used again to find the angular velocity  $\omega$ . The backward velocity of the lowest point of the wheel is then  $\dot{y} + r\omega$ ; and, when that becomes equal to  $V_h$ , phase two is terminated.

Phase three.- In phase three equations (10a) to (10c) of phase two are still valid, but the drag force on the right-hand side of equation (9d) is no longer  $\mu_r k_2 x_2$ , but just enough to keep the wheel rolling without skidding. Equation (9d) must therefore be replaced by equations (1a) and (1b) in which the notations  $m$ ,  $k$ ,  $\mu$ , and  $F$  must be replaced by  $m_3$ ,  $k_3$ ,  $\mu_r$ , and  $F_1$ , respectively. Since the wheel does not skid, there is also the kinematic relation

$$r\dot{\omega} = -\dot{y}$$

which serves to eliminate  $\dot{\omega}$  from equation (1b). Then the drag  $\mu_r F_1$  may be eliminated from both equations, and thus the equation is obtained which takes the place of equation (9d):

$$\left(m_3 + \frac{I}{r^2}\right)\ddot{y} + k_3 y = 0 \quad (10d)$$

In each of the three phases the differential equations represent an initial-value problem. All displacements and velocities at the beginning of the phase must be equal to those obtained for the end of the preceding one or, in phase one, equal to those which the landing gear is supposed to have at the moment of first contact with the ground.

## SOLUTION OF IMPACT PROBLEM

### Phase One

Since the shock strut remains at rest during phase one of the impact, all complications which arise from its nonlinear behavior are absent. The load  $W_1$  may certainly be assumed constant during the rather short time interval, and equation (9b) may be solved at once.

The initial conditions are:

$$t = 0: \quad x_1 = x_2 = 0, \quad \dot{x}_1 = \dot{x}_2 = V$$

and the solution satisfying these conditions is

$$x_1 = x_2 = \frac{W_1}{k_2} (1 - \cos \lambda_1 t) + \frac{V}{\lambda_1} \sin \lambda_1 t$$

with

$$\lambda_1^2 = \frac{k_2}{m_1 + m_2}$$

This must be introduced into the right-hand term of equation (9d). The solution  $y$  has to fulfill the initial conditions

$$t = 0: \quad y = 0, \quad \dot{y} = 0$$

and it will consist of a static deflection, a free vibration with the frequency

$$\lambda_3 = \sqrt{k_3/m_3}$$

and a forced vibration with the frequency  $\lambda_1$ :

$$y = \frac{\mu_r W_1}{k_3} \left( 1 + \frac{\lambda_1^2 \cos \lambda_3 t - \lambda_3^2 \cos \lambda_1 t}{\lambda_3^2 - \lambda_1^2} \right) +$$

$$\frac{\mu_r V k_2 \lambda_3}{k_3 \lambda} \frac{\lambda_3 \sin \lambda_1 t - \lambda_1 \sin \lambda_3 t}{\lambda_3^2 - \lambda_1^2}$$

The force  $F_1$  follows from equation (9c):

$$F_1 = W_1 - W_1 \frac{m_1}{m_1 + m_2} \cos \lambda_1 t + \frac{V k_2}{\lambda_1} \frac{m_1}{m_1 + m_2} \sin \lambda_1 t$$

Since the unsprung mass  $m_2$  is small as compared with  $m_1$ , this formula may be replaced by

$$F_1 = W_1(1 - \cos \lambda_1 t) + \frac{V k_2}{\lambda_1} \sin \lambda_1 t \quad (11)$$

Phase one ends when the force  $F_1$  has built up to the value  $(F_1)_1$  as given by equation (8). With  $H = k_3 y$  this yields the following equation for the duration  $t_1$  of this period:

$$F_1 = A_1 p_0 + \mu_s k_3 \frac{2l - a}{a} y \quad \text{for } t = t_1 \quad (12)$$

When the expressions just found for  $F_1$  and  $y$  are inserted here, a rather unwieldy transcendental equation will result.

Fortunately, however, phase one is of rather short duration. In the numerical example used in reference 2,  $\lambda_1 = 10.98 \text{ second}^{-1}$  and  $t_1 = 0.0088 \text{ second}$ ; hence,  $\lambda_1 t_1 = 0.097 = 5.5^\circ$ . The situation is not quite so favorable regarding  $\lambda_3 t$ , but usually it is small enough also that all trigonometric functions may be expressed by a few terms of this power series.

Instead of introducing these series in the preceding equations, one may more conveniently make a fresh start, assuming power series for the unknowns,

$$x_1 = x_2 = \sum_{k=0}^{\infty} \frac{a_k}{k!} t^k$$

$$y = \sum_{k=0}^{\infty} \frac{d_k}{k!} t^k$$

and introducing them into differential equations (9b) and (9d). Proceeding in the usual way, one obtains the following solutions:

$$x_1 = x_2 = Vt + \frac{1}{2} \frac{W_1}{k_2} \lambda_1^2 t^2 - \frac{1}{6} V \lambda_1^2 t^3 - \frac{1}{24} \frac{W_1}{k_2} \lambda_1^4 t^4 + \frac{1}{120} V \lambda_1^4 t^5 + \dots \quad (13a)$$

$$y = \frac{\mu_r k_2}{m_3} \left( \frac{1}{6} V t^3 + \frac{1}{24} \frac{W_1}{k_2} \lambda_1^2 t^4 + \dots \right) \quad (13b)$$

As before,  $m_2$  may be neglected. If this is done, equation (9c) yields

$$F_1 = k_2 V t + \frac{1}{2} W_1 \lambda_1^2 t^2 - \frac{1}{6} k_2 V \lambda_1^2 t^3 - \dots \quad (13c)$$

One may now put  $t = t_1$  in all these series and then introduce them into equation (12), which then becomes an equation for  $t_1$ . If terms beyond  $t^3$  are discarded, it reads as follows:

$$k_2 V t_1 + \frac{1}{2} W_1 \lambda_1^2 t_1^2 - \frac{1}{6} k_2 V \lambda_1^2 t_1^3 = A_1 p_0 + \mu_s k_3 \frac{2l - a}{a} \frac{1}{6} \frac{\mu_r k_2}{m_3} V t_1^3$$

In this equation the terms with  $t_1^2$  and  $t_1^3$  are not large, and it is best solved by iteration. One obtains a first approximation by neglecting the small terms altogether:

$$t_1 = A_1 p_0 / k_2 V \quad (14a)$$

and proceeds then with the help of the formula

$$t_1 = \frac{A_1 p_0}{k_2 V \left[ 1 - \frac{1}{6} \left( \lambda_1^2 + \mu_r \mu_s \lambda_3^2 \frac{2l - a}{a} \right) t_1^2 \right] + \frac{1}{2} W_1 \lambda_1^2 t_1} \quad (14b)$$

which yields a sequence of improved approximations when one introduces for  $t_1$  on the right-hand side the best value so far available.

After  $t_1$  has been computed, the corresponding values of  $x_1 = x_2$ ,  $y$ ,  $\dot{y}$ ; and  $F_1$  may be obtained from the series forms (13) for these variables.

In order to check the progress of the spinning-up, it is necessary to find the angular velocity  $\omega = \omega_1$  of the wheel at  $t = t_1$ . It is found from equation (9e):

$$\omega_1 = \frac{\mu_r k_2 r}{I} \left( \frac{1}{2} v t_1^2 + \frac{1}{6} \frac{W_1}{k_2} \lambda_1^2 t_1^3 - \frac{1}{24} v \lambda_1^2 t_1^4 \right) \quad (15)$$

#### Numerical Integration for Phases Two and Three

Exact solution.- As soon as equation (7) comes into action, the problem becomes nonlinear and a closed-form solution can no longer be expected. Among the different methods available for a numerical solution, the most flexible is the step-by-step integration. Since it is possible to control the error and to keep it below any desired limit, this method can be considered as exact. In its practical application, however, the requirements of accuracy are usually not high, and its merits must then be judged by the time needed for the computation. The method will now be applied to phases two and three of the landing-gear impact.

Phase two: In phase two the spinning-up of the wheel is completed, and the motion is described by equations (10a) to (10c) and (9d). Since these equations are rather involved, it is advisable to introduce at once every reasonable simplification. Now it has been shown in reference 2 that the influence of the unsprung mass  $m_2$  is not very large and that in most cases it will be possible to assume  $m_2 = 0$ . This does not necessarily mean that  $m_3$  must be neglected also. Although  $m_3$  is smaller than  $m_2$ , it controls the horizontal vibration and hence the friction in the shock strut and it may well be worth while to have these details.

For this degree of simplification  $F_1 = F_2$ , and equations (10a) to (10c) and (9d) may be brought into the following form:

$$m_1 \ddot{x}_1 + F_1 = W_1 \quad (16a)$$

$$F_1 = k_2 x_2 \quad (16b)$$

$$m_3 \ddot{y} + k_3 y = \mu_s F_1 \quad (16c)$$

$$F_1 = \frac{A_1 p_0}{\left[1 - (A_1 x / A_0 z_0)\right]^\gamma} + \frac{\rho A_2^3}{2 A_3} \dot{x}^2 + \mu_s k_3 \frac{2l - a - x}{a + x} y \quad (16d)$$

Since  $y$  is always positive during spin-up, the absolute signs have been dropped in the last term.

When these equations are solved by step-by-step integration as explained in reference 2, the values may be arranged as shown in table 1.

In the first group of columns (marked by the double lines) the values for  $t = t_1$  may be filled in from the initial conditions (asterisks) and with the relation  $x = x_1 - x_2$ . The next three groups are used to obtain from the differential equations the values of the highest derivative of each unknown. The computation of  $\dot{x}$  for column (9) must be done in a separate table, using equation (16d) in the form

$$\dot{x} = \frac{A_3}{A_2} \sqrt{\frac{2}{\rho A_2}} \sqrt{F_1 - F_a - \beta y} \quad (17)$$

with

$$F_a = \frac{A_1 p_0}{\left[1 - (A_1 x / A_0 z_0)\right]^\gamma}$$

$$\beta = \mu_s k_3 \frac{2l - a - x}{a + x}$$

Since the air force  $F_a$  and the factor  $\beta$  depend only on the stroke  $x$ , it is useful to prepare large-scale diagrams for both functions from which individual values may easily be picked during the integration.

If the numerical integration is done by one of the more elaborate methods, the values of  $\dot{x}_2$ ,  $\ddot{x}_1$ , and  $\ddot{y}$  are copied into special integration tables and handled as described in reference 2.

If the simpler formulas described below are used, it is necessary to group those columns together which refer to the same variable as in table 2. Again a special table is needed to evaluate  $\dot{x}$  from equation (16d), but now there are no additional integration tables. An example for this kind of computation is given in table 3.

The most convenient method among all tested is Milne's method (ref. 4). It works as follows:

When for a variable  $z$  and its derivative  $\dot{z}$  the values in four lines are known (in particular,  $z_{n-3}$  and  $\dot{z}_{n-2}$ ,  $\dot{z}_{n-1}$ , and  $\dot{z}_n$ ), one may find an approximate value of  $z_{n+1}$  by passing a quadratic parabola through the three points of the  $\dot{z}$  diagram and integrating the segment under the parabola over the four intervals from  $n-3$  to  $n+1$ . This yields Milne's "predictor" formula:

$$z_{n+1} = z_{n-3} + \frac{4}{3} \Delta t (2\dot{z}_{n-2} - \dot{z}_{n-1} + 2\dot{z}_n) + \frac{14}{45} \Delta t \Delta^4 \dot{z}_{n-1} + \dots \quad (18)$$

The last term of this formula cannot be used, since the fourth difference

$$\Delta^4 \dot{z}_{n-1} = \dot{z}_{n-3} - 4\dot{z}_{n-2} + 6\dot{z}_{n-1} - 4\dot{z}_n + \dot{z}_{n+1}$$

cannot be computed,  $\dot{z}_{n+1}$  still being unknown. This term represents the next improvement which might be applied if more information were available, and it is a measure for the possible error of the calculation using the other terms only.

When this formula is applied to the present problem, identifying  $\dot{z}$  first with  $\dot{x}_2$  and then with  $\ddot{y}$ , values of  $x_2$  and of  $\ddot{y}$  for the

line  $n + 1$  are obtained. It is then possible to calculate  $\ddot{x}_1$  for this line from equation (16a), and now all the remaining integrations may be made under much more favorable circumstances. For each of them the value  $\dot{z}_{n+1}$  of the derivative in the new line is already known, and one may use Simpson's formula in the double interval from  $n - 1$  to  $n + 1$ :

$$z_{n+1} = z_{n-1} + \frac{\Delta t}{3} (\dot{z}_{n-1} + 4\dot{z}_n + \dot{z}_{n+1}) - \frac{1}{90} \Delta t \Delta^4 \dot{z}_n + \dots \quad (19)$$

As one may recognize by comparing the terms with  $\Delta^4 \dot{z}$ , this formula is much better than the predictor formula; and, when at last  $\ddot{x}_2$  and  $\ddot{y}$  have been computed from  $\dot{x}_1 - \dot{x}$  and from equation (16c), respectively, one may use equation (19) as a "corrector formula" to obtain improved values of  $x_2$  and  $\dot{y}$ . Looking at the terms with  $\Delta^4 \dot{z}$  in both formulas, one may conclude that the integration error still remaining is about one twenty-ninth of the correction just applied, and the step  $\Delta t$  should be so chosen that this remaining error is negligible.

Nevertheless, this correction of  $x_2$  and  $\dot{y}$  is not final, since it entails corrections of  $\dot{x}_1$  and  $y$  and hence most or all of the values already computed in the line  $n + 1$ . However, the time step should be so chosen that the iterative process thus started stabilizes rapidly to final values everywhere.

The two operations described by equations (18) and (19) may conveniently be carried out with the help of two templates. They are shown here as applied to the integration of the  $\dot{x}_2$  column:

Predictor equation (18)

$t - t_0$	$\dot{x}_2$	$x_2$	$\ddot{x}_1$
0.025	83.61	3.756	-453
0.		4.161	2
0.	+2	74.25	8
0.	-1	69.63	1
0.	+2	64.91	2
0.			
0.055			

$\left. \begin{matrix} 74.25 \\ 69.63 \\ 64.91 \end{matrix} \right\} \times \frac{4\Delta t}{3}$

Corrector equation (19)

$t - t_0$	$\dot{x}_2$	$x_2$	$\ddot{x}_1$
0.025	83.61	3.756	-453
0.030	79.01	4.161	-502
0.			8
0.	1	69.63	1
0.	4	64.91	2
0.	1	60.21	0
0.055			

$\left. \begin{matrix} 69.63 \\ 64.91 \\ 60.21 \end{matrix} \right\} \times \frac{\Delta t}{3}$

The application of predictor formula (18) is not possible until four lines of table 2 have been filled by other means. Therefore, between the filling of the first line as described before and the continuous application of the two templates some intermediate computation is needed. This is best done in the following way:

The first integrations which yield the values of  $x_2$  and  $\dot{y}$  in line 2 can be done only with the simple Euler formula, equation (29) of reference 2. For the other integrations the improved Euler formula, equation (30) of reference 2, may be used; and, when the line has been completed, one may check and correct the first two integrations with the help of the improved formula. Of course, the whole line must then be corrected until agreement has been reached everywhere.

Line 3 may be started in the same way, using equation (29) of reference 2, but instead of using the improved Euler formula one may now resort to equation (19) and the corresponding template. This will yield appreciably better results for the same width of the time step. If the computer has a sufficiently clear idea of the values of  $\dot{x}_2$  and  $\dot{y}$  to be expected in this line, he may guess them and start at once with equation (19). Of course, a second run through the line is needed to justify or to improve the initial guess.

Line 4 must be handled in exactly the same way, except that here an advance guess is easier, since more information is already available.

If each line is iterated until the values therein are perfectly stabilized, the integrations leading to lines 3 and 4 have the same degree of exactness as those of the ensuing regular computation. Only the first time step is less accurate, and it is therefore advisable to start the whole computation with a sufficiently small time step. As soon as two steps have been made, one may double the increment  $\Delta t$ , since then the higher accuracy of Simpson's formula is available. If, after some time, one finds that the predictor formula predicts so well that the corrector formula finds nothing to be corrected, it is advisable to increase again the time step as described in reference 2.

The methods of numerical integration described here have the disadvantage of all numerical solutions of initial-value problems: Any error once made, whether a mistake or a rounding error, is carried on through the computation without much chance of later discovery. It is therefore advisable to develop difference tables for  $x_2$  and  $y$  in separate tables and to watch the regular change of figures in these columns. Any irregularity in one of the differences is a hint that some mistake has been made, and the integration should be halted until the mistake has been found and corrected. Additionally, the more exact integration formulas (31) of reference 2 may be applied at any time to

the difference scheme as a check of sufficient accuracy of equations (18) and (19).

In tables 1 and 2 columns (14) and (15) have been added, in which the force  $F_1 = k_2 x_2$  is integrated, and the velocity  $\dot{w} + \dot{y}$  is computed with the help of equation (9e). From it the time  $t = t_t$  is found when the wheel is fully spun up and when this integration scheme must be modified.

Phase three: As soon as the wheel is fully spun up, equation (9d) must be replaced by equation (10d). This new equation is independent of the other three and may be solved in advance:

$$y = Y \sin \lambda_3'(t - T)$$

with

$$(\lambda_3')^2 = \frac{k_3 r^2}{m_3 r^2 + I}$$

$$Y^2 = y_t^2 + \left( \frac{\dot{y}_t}{\lambda_3'} \right)^2$$

and

$$\tan \lambda_3'(t_t - T) = \frac{\lambda_3' y_t}{\dot{y}_t}$$

When  $y$  has been calculated from this formula, equations (10a) to (10c) may be subjected to numerical integration. The table used for this work is quite similar to table 2, except that columns (7), (8), (14), and (15) are now dropped. The computation may be continued until  $\dot{x} = 0$ . For the recoil motion ( $\dot{x} < 0$ ) the radical in equation (17) must be taken with a minus sign and additional changes in this formula will be necessary if foam is present in the oil which flows back through the orifice of the oleo strut.

Numerical example.- The example which has already been used in reference 2 has been used again to test the integration procedures recommended in this report and to obtain some information on the influence of shock-strut friction on shock-strut performance.

The following data have been used in this example:

Airplane mass, $m_1$ , lb sec <sup>2</sup> /in. . . . .	103.6
Unsprung mass (neglected), $m_2$ . . . . .	0
Wheel mass for y-vibration, $m_3$ , lb sec <sup>2</sup> /in. . . . .	3.89
Vertical velocity, $V$ , in./sec . . . . .	120
Horizontal velocity, $V_h$ , in./sec . . . . .	1,672
Landing-gear load (weight minus lift), $W_1$ . . . . .	0
Spring constants:	
Tire, $k_2$ , lb/in. . . . .	12,500
Horizontal, $k_3$ , lb/in. . . . .	7,810
Shock-strut data:	
$A_1 = A_2$ , sq in. . . . .	39.8
$A_3$ , sq in. . . . .	See fig. 9
$A_0 z_0 / A_1$ , in. . . . .	23.5
$P_0$ , lb/sq in. . . . .	310
$\rho$ , lb in. <sup>-4</sup> sec <sup>2</sup> . . . . .	$8.42 \times 10^{-5}$
$\gamma$ . . . . .	1.1
$l$ , in. . . . .	40
$a$ , in. . . . .	13
Wheel data:	
$I$ , lb in. sec <sup>2</sup> . . . . .	686
$r$ , in. . . . .	20
Friction coefficients:	
Wheel and runway, $\mu_r$ . . . . .	0.5
Piston and barrel, $\mu_s$ . . . . .	0.1

Since phase one is rather short, the only items of interest are its duration  $t_1$  and the values of all variables at the end of the phase. Equation (14a) yields as the first approximation for the duration of the phase:

$$t_1 = 0.00822 \text{ sec}$$

and then the first application of equation (14b) yields the improved value

$$t_1 = \frac{0.00822}{1 - (106.3)(0.00822)^2} = 0.00828 \text{ sec}$$

The improvement is so little that a second application of equation (14b) does not improve the result further, and  $t_1 = 0.00828$  second is final.

Having calculated  $t_1$ , one obtains from equations (13) all the values for the end of phase one:

$$(x_1)_1 = (x_2)_1 = 0.993 \text{ in.}$$

$$(\dot{x}_1)_1 = (\dot{x}_2)_1 = 119.5 \text{ in./sec}$$

$$y_1 = 0.018 \text{ in.}$$

$$\dot{y}_1 = 6.56 \text{ in./sec}$$

and from equation (15):

$$\omega_1 = 0.751 \text{ sec}^{-1}$$

These are the initial values for phase two, and from them the numerical integration must be started.

Since the numerical integration is rather time consuming, a judicious choice of the time step  $\Delta t$  is of great importance. The accuracy requirements of landing-impact calculations are not very high; average slide-rule work is certainly enough. To get an idea of what is really necessary to obtain this degree of accuracy, the numerical example of reference 2 has been repeated with wider steps and it has been found that there is no need of being very particular about the sharp breaks in the  $A_3(x)$  curve.

Therefore, for the present computations the small time step  $\Delta t = 0.0025$  second has been used only to get a smooth start, but when four lines were computed, the values for  $t - t_1 = 0, 0.0050, \text{ and } 0.0100$  were entered in a new table which then was run with  $\Delta t = 0.005$  second, using Milne's method. For the first step in this table Milne's predictor formula (18) could not be used since it requires that four lines be already established. Instead, an advance guess was made for the result of the first integration, and then Simpson's formula could at once be applied.

In each time step equation (17) must be used which contains three functions of the stroke  $x$ . One may speed up the work by plotting these functions at a large scale. In order to preserve accuracy, these plots should be drawn to a sufficiently large scale. The plots used for the computations described in this report had twice the size of the samples given in figures 9, 10, and 11.

While the computation in phase two proceeds, an occasional check of  $\omega$  is made to find the time when the wheel is fully spun up. This occurs at  $t - t_1 = 0.100$  second. Then phase three begins, which requires only minor changes in the arrangement of the computation table. The work has been continued to  $t - t_1 = 0.18$  second. The results are represented as solid lines in figures 12, 13, and 14, together with those obtained for  $\mu_r = 1.0$  and with the results obtained previously for the frictionless case.

Figure 12 shows that the friction in the shock strut reduces the stroke  $x$ , but that it takes some time before the difference is felt in the downward motion of the airplane. Figure 13 reveals more details of the motion. There appears at once a substantial difference in the rate of stroke  $\dot{x}$ . When the orifice opens, the rise in  $\dot{x}$  is moderated by the friction, while after transition the spring-back motion produces a marked waviness of the curve quite different from the continuous decrease of  $\dot{x}$  in the frictionless case. The zero of  $\dot{x}$ , that is, the maximum stroke, is reached earlier and has, as figure 12 shows, a lower value the higher the friction. The oscillations of the spring-back phase are also visible in the force diagram (fig. 14) although there they are not so pronounced. The peak value of the impact force is considerably higher than in the frictionless case, and it varies widely with  $\mu_r$ . This indicates that the coefficient of runway friction must be fairly well known if computations of the kind presented here are to be of practical value.

Approximate solution.- The numerical integration as described on the preceding pages solves the problem and yields reliable results, but the amount of computation involved is considerable. Therefore, it is desirable to develop methods which are sufficiently accurate to satisfy the needs of the designer, but which omit cumbersome details.

One way to speed up the work is to use larger time steps. In attempting this, one must contend with the rather high frequency of the horizontal vibrations.

In the example, the frequencies are  $\lambda_3 = 44.8 \text{ second}^{-1}$  in phases one and two and  $\lambda_3' = 37.37 \text{ second}^{-1}$  in phase three. With  $\Delta t = 0.005$  second, as used in the computation, one has about seven

intervals for one quarter period (the rise of  $\sin \lambda_3 t$  from 0 to 1) which is sufficient for good representation. However, a serious increase in  $\Delta t$  will not be possible without losing the details of the  $y$ -vibration.

This raises the question of whether these details are really important for the main purpose, the determination of the maximum force  $F_1$ . A negative answer is suggested by figure 5 which shows that during the spin-up the  $y$ -curve wriggles around the straight line representing the static deflection

$$y = D/k_3$$

and that the deviations from this line are never very large. When one plots in the same way  $y = y(t)$  from the example represented by figures 12 to 14, the diagram shown as figure 15 is obtained which confirms this idea to some degree.

It seems, therefore, reasonable to drop the dynamic term  $m_3 \ddot{y}$  in equation (16c), at least in phase two. If this is done,

$$y = \mu_r F_1 / k_3$$

may at once be introduced into equation (16d) or (17). This yields

$$\dot{x} = \frac{A_3}{A_2} \sqrt{\frac{2}{\rho A_2}} \sqrt{\left(1 - \frac{\beta \mu_r}{k_3}\right) F_1 - F_a}$$

and, with equation (16b),

$$\dot{x} = \frac{A_3}{A_2} \sqrt{\frac{2}{\rho A_2}} \sqrt{\left(1 - \frac{\beta \mu_r}{k_3}\right) k_2 x_2 - F_a} \quad (20)$$

When this equation is used, the time step is essentially determined by the variability of the effective orifice area  $A_3$ , that is, by the shape of the metering pin.

There seems to be no advantage in applying the same simplifying assumption also to phase one, since there everything is already simple enough. However, if this is not done, it will not be possible to fit the two phases together at  $t = t_1$ . For this reason it is necessary to assume from the very beginning that  $m_3 = 0$ .

The formula for  $x_1 = x_2$  is then the same as before and so is the expression for  $F_1$ , but

$$y = \frac{\mu_r W_1}{k_3} (1 - \cos \lambda_1 t) + \frac{\mu_r k_2 V}{k_3 \lambda_1} \sin \lambda_1 t$$

Also equation (8) is affected, since now  $H$  is equal to the drag  $D$ , that is,

$$H = \mu_r F_1$$

and the condition  $F_1 = (F_1)_1$  which determines  $t_1$  appears in the form

$$F_1 = \frac{A_1 p_0}{1 - \mu_s \mu_r \frac{2l - a}{a}}$$

This particular value of  $F_1$  may be computed from the data of the problem and then introduced into equation (13c) where one puts  $t = t_1$ . This yields an equation for  $t_1$ :

$$k_2 V t_1 + \frac{1}{2} W_1 \lambda_1^2 t_1^2 - \frac{1}{6} k_2 V \lambda_1^2 t_1^3 = \frac{A_1 p_0}{1 - \mu_r \mu_s \frac{2l - a}{a}}$$

It may be solved by iteration. The first approximation is

$$t_1 = \frac{A_1 p_0}{\left(1 - \mu_r \mu_s \frac{2l - a}{a}\right) k_2 V} \quad (21a)$$

and, starting from it, improved values may be obtained by using the iteration formula

$$t_1 = \frac{A_1 p_0}{\left(1 - \mu_r \mu_s \frac{2l - a}{a}\right) \left(k_2 V + \frac{1}{2} W_1 \lambda_1^2 t_1 - \frac{1}{6} k_2 V \lambda_1^2 t_1^2\right)} \quad (21b)$$

These formulas take the place of equations (14).

It is not possible to extend the same idea of approximation also to phase three. There, the static deflection  $y$  is zero, and with  $y = 0$  one would not obtain any shock-strut friction at all. Since in phase three it is possible to compute  $y$  in advance, the need for simplification is less urgent. One must, of course, match the value of  $y = y_t$  at  $t = t_t$ , the end of the spin-up. As a rule it will be possible to neglect the influence of  $\dot{y}$  and to write simply

$$y = y_t \cos \lambda_3'(t - t_t)$$

for  $t \geq t_t$ .

Further simplification: Large steps.— The simplification introduced in the preceding section removes the essential obstacle to using large time steps. The deviation of the solid line from the dotted line in figure 16 shows the error introduced by the changes in the equations, without additional inaccuracies which might be caused by wider steps  $\Delta t$ .

One may now ask how far one may go in increasing  $\Delta t$  without losing much more in accuracy. This has been tried in the example by repeating the computation with  $\Delta t = 0.02$  second. The computation for phases two and three has been reproduced in full in table 3. The quantities  $F_a$ ,  $\beta$ , and  $A_3$  were read from prepared graphs as functions of  $x$ .

The results of this integration have been marked by the small circles in figure 16. They check so well with the solid curve that one might feel tempted to increase the time step still more. This, however, seems inadvisable, not because of the accuracy of the numerical integration, but because a certain number of points are needed for plotting the curve.

When one inspects the column  $|y|$  in the second part of the integration table, one recognizes that there are sharp ups and downs and that the values representing the influence of  $y$  on the shock-strut friction

are rather arbitrary samples. It seems therefore wiser not to rely on the incidental appearance of large and small values in this column, but to replace the variable  $y$  by its average, which is  $\frac{2}{\pi} y_t$ .

### Analytical Method of Solution

As an alternative to numerical integration of the differential equations of motion an analytical method is developed in this section. This method has several advantages over numerical integration: (1) It provides a start which takes account of the singularity which exists in the solution at time  $t_1$ . (2) It allows much larger steps with the same accuracy. (3) It takes into account sharp breaks in the  $A_3(x)$  curve. The disadvantages are: (1) The computation scheme is not so simple as that of step-by-step integration. (2) More skill and judgment are required of the computer. (3) Curve fitting is needed in every interval.

In the analytical method the time is divided into a series of intervals with the  $n$ th interval extending from  $t_n$  to  $t_{n+1}$ . The length of successive intervals is determined during computation, as will be discussed later. Certainly any discontinuity in the slope of the  $A_3(x)$  curve will require termination of an interval.

In each interval the dependent variables  $x_1$ ,  $x_2$ ,  $x$ ,  $y$ , and  $\omega$  are developed in power series in terms of a local time variable

$$\tau = t - t_n$$

In the section "Phase One" this has already been done for phase one, and that calculation represents the interval  $n = 0$  for the analytic method. For the intervals following, the form of the solution depends on whether or not  $\dot{x}$  becomes zero. An interval where this does not happen will be called a regular interval; one where  $\dot{x}$  starts from or reaches zero will be called a singular interval. Since  $\dot{x} = 0$  at the start of phase two, the interval  $n = 1$  of the analytic solution will be a singular one. However, it is more convenient to explain the regular interval first.

Regular interval.- For the purposes of this analysis it is desirable to revise the form of the differential equations somewhat. Equations (10a) and (10b) and equations (10b) and (10c) (neglecting, as previously,  $m_2$ ) may be combined to eliminate  $F_1$ :

$$m_1 \ddot{x}_1 + k_2 x_2 = W_1 \quad (22a)$$

$$k_2 x_2 = \frac{A_1 p_0}{\left[1 - (A_1 x / A_0 z_0)\right]^\gamma} + \frac{\rho A_2^3}{2A_3^2} \dot{x}^2 + \mu_s k_3 \frac{2l - a - x}{a + x} |y| \quad (22b)$$

Equation (22b) is then solved for  $\dot{x}$  as

$$\dot{x} = A_3 \sqrt{\frac{2k_2}{\rho A_2^3} \left[ x_2 - \frac{A_1 p_0}{k_2 \left[1 - (A_1 x / A_0 z_0)\right]^\gamma} - \mu_s \frac{k_3}{k_2} \frac{2l - a - x}{a + x} |y| \right]} \quad (23)$$

In order to make a series solution of this equation feasible several approximations are introduced.

First approximate in the interval of expansion the term

$$f_1(x) = \frac{A_1 p_0}{k_2 \left[1 - (A_1 x / A_0 z_0)\right]^\gamma}$$

by a linear function

$$f_1(x) = \phi_0 + \phi_1 x \quad (24)$$

Figure 17 illustrates  $f_1(x)$  and the straight-line segments used to represent it for the example treated in the section "Numerical example." Similarly, the function

$$f_2(x) = \frac{\mu_s k_3}{k_2} \frac{2l - a - x}{a + x}$$

is approximated in each interval by a linear function

$$r_2(x) = \theta_0 + \theta_1 x \quad (25)$$

This approximation is illustrated in figure 18. Finally, a parabolic (or linear) curve

$$A_3 = (A_3)_n \left( 1 + \sigma_1 \xi + \frac{1}{2} \sigma_2 \xi^2 \right) \quad (26)$$

with

$$\xi = x - (x)_n$$

is fitted to the graph of  $A_3(x)$  to represent this function in the  $n$ th interval. This form seems best suited to fit the orifice curve since it is an exact representation in every conical section of the metering pin (see fig. 9, which consists only of a straight line and parabolas).

Putting the above simplifications into equation (23), one obtains

$$\dot{x} = A_3 \sqrt{\frac{2k_2}{\rho A_2^3}} \sqrt{x_2 - \phi_0 - \phi_1 x - (\theta_0 + \theta_1 x) |y|} \quad (27)$$

To make the equations more manageable it is convenient to introduce the following parameters:

$$\lambda_1^2 = k_2/m_1$$

$$\lambda_3^2 = k_3/m_3$$

$$W_1^* = W_1/m_1$$

$$\kappa_1 = \sqrt{2k_2/\rho A_2^3}$$

$$\kappa_2 = \mu_r k_2/m_3$$

$$\kappa_3 = \mu_r k_2 r/I$$

The resulting full set of equations (from eqs. (9d), (9e), (22a), (26), and (27)) is thus:

$$\ddot{x}_1 + \lambda_1^2 x_2 = W_1^* \tag{28a}$$

$$\dot{x} = \kappa_1 A_3 \sqrt{x_2 - \phi_1 x - \theta_0 |y| - \theta_1 x |y| - \phi_0} \tag{28b}$$

$$\ddot{y} + \lambda_3^2 y = \kappa_2 \kappa_2 \tag{28c}$$

$$A_3 = (A_3)_n \left( 1 + \sigma_1 \xi + \frac{1}{2} \sigma_2 \xi^2 \right), \quad \xi = x - (x)_n \tag{28d}$$

$$x_2 = x_1 - x \tag{28e}$$

$$\dot{\omega} = \kappa_3 x_2 \tag{28f}$$

The expression for  $A_3(x)$  has been retained as a separate equation to avoid overcomplication of equation (28b).

One may now proceed with the solution of these equations in the interval  $n$ . Power series are assumed for all the dependent variables:

$$\left. \begin{aligned} x_1 &= \sum_0^{\infty} \frac{a_k}{k!} \tau^k \\ x_2 &= \sum_0^{\infty} \frac{b_k}{k!} \tau^k \\ x &= \sum_0^{\infty} \frac{c_k}{k!} \tau^k \\ y &= \sum_0^{\infty} \frac{d_k}{k!} \tau^k \\ A_3 &= (A_3)_n \sum_0^{\infty} \frac{\alpha_k}{k!} \tau^k \\ \alpha_0 &= 1 \end{aligned} \right\} \tag{29}$$

Substitution in equation (28a), equating of coefficients of like powers of  $\tau$ , and application of the initial conditions yield

$$\left. \begin{aligned} a_0 &= (x_1)_n \\ a_1 &= (\dot{x}_1)_n \\ a_2 &= -\lambda_1^2 b_0 + W_1^* \\ a_k &= -\lambda_1^2 b_{k-2} \quad (k > 2) \end{aligned} \right\} \quad (30)$$

Equation (28b) is likewise solved by substitution and equating of coefficients of like terms. The process is more involved for this equation, however. Upon substitution,

$$\sum_0^{\infty} \frac{c_k \tau^k}{k!} \tau^{k-1} = \kappa_1 (A_3)_n \left( \sum_0^{\infty} \frac{\alpha_k \tau^k}{k!} \right) \left( \sum_0^{\infty} \frac{b_k \tau^k}{k!} - \phi_1 \sum_0^{\infty} \frac{c_k \tau^k}{k!} - \theta_0 \sum_0^{\infty} \frac{d_k \tau^k}{k!} - \theta_1 \sum_0^{\infty} \frac{c_k \tau^k}{k!} \sum_0^{\infty} \frac{d_k \tau^k}{k!} - \phi_0 \right)^{1/2}$$

Then, since

$$\sum_0^{\infty} \frac{c_k \tau^k}{k!} \sum_0^{\infty} \frac{d_k \tau^k}{k!} = \sum_0^{\infty} \frac{1}{k!} \left[ \sum_v^k \binom{k}{v} c_v d_{k-v} \right] \tau^k$$

where  $\binom{k}{v}$  is the binomial coefficient, the equation can be written

$$\sum_1^{\infty} \frac{c_k}{(k-1)!} \tau^{k-1} = \kappa_1 (A_3)_n \left\{ \sum_0^{\infty} \frac{1}{k!} \left[ b_k - \phi_1 c_k - \theta_0 d_k - \theta_1 \sum_v^k \binom{k}{v} c_v d_{k-v} \right] \tau^k - \phi_0 \right\}^{1/2} \sum_0^{\infty} \frac{\alpha_k \tau^k}{k!}$$

Now define

$$\beta_k = b_k - \phi_1 c_k - \theta_0 d_k - \theta_1 \sum_{\nu=0}^k \binom{k}{\nu} c_\nu d_{k-\nu}$$

so that

$$\begin{aligned} \sum_1^{\infty} \frac{c_k}{(k-1)!} \tau^{k-1} &= \kappa_1 (A_3)_n \left( \sum_0^{\infty} \frac{\beta_k}{k!} \tau^k - \phi_0 \right)^{1/2} \sum_0^{\infty} \frac{\alpha_k}{k!} \tau^k \\ &= \kappa_1 (A_3)_n \left( \beta_0 - \phi_0 + \sum_1^{\infty} \frac{\beta_k}{k!} \tau^k \right)^{1/2} \sum_0^{\infty} \frac{\alpha_k}{k!} \tau^k \\ &= \kappa_1 (A_3)_n \sqrt{\beta_0 - \phi_0} \left( 1 + \frac{1}{\beta_0 - \phi_0} \sum_1^{\infty} \frac{\beta_k}{k!} \tau^k \right)^{1/2} \sum_0^{\infty} \frac{\alpha_k}{k!} \tau^k \end{aligned} \tag{31}$$

But returning to equation (28b) and inserting the initial conditions

$$b_0 = (x_2)_n$$

$$c_0 = (x)_n$$

$$c_1 = (\dot{x})_n$$

$$d_0 = (y)_n$$

one finds

$$c_1 = \kappa_1 (A_3)_n \sqrt{b_0 - \phi_1 c_0 - \theta_0 d_0 - \theta_1 c_0 d_0 - \phi_0}$$

$$c_1 = \kappa_1 (A_3)_n \sqrt{\beta_0 - \phi_0}$$

This may be used in equation (31) which then gives

$$\sum_1^{\infty} \frac{c_k}{(k-1)!} \tau^{k-1} = c_1 \left( 1 + 2\eta_1 \sum_1^{\infty} \frac{\beta_k}{k!} \tau^k \right)^{1/2} \sum_0^{\infty} \frac{\alpha_k}{k!} \tau^k$$

where also

$$\eta_1 = \frac{1}{2(\beta_0 - \phi_0)}$$

The expression within the parentheses raised to the one-half power in the above equation may be expanded now by the binomial theorem

$$(1 + s)^{1/2} = 1 + \frac{1}{2} s - \frac{1}{8} s^2 + \frac{1}{16} s^3 + \dots$$

When this is applied to the problem at hand, it follows that

$$\sum_1^{\infty} \frac{c_k}{(k-1)!} \tau^{k-1} = c_1 \left[ 1 + \eta_1 \sum_1^{\infty} \frac{\beta_k}{k!} \tau^k - \frac{1}{2} \eta_1^2 \left( \sum_1^{\infty} \frac{\beta_k}{k!} \tau^k \right)^2 + \right. \\ \left. \frac{1}{2} \eta_1^3 \left( \sum_1^{\infty} \frac{\beta_k}{k!} \tau^k \right)^3 \right] \sum_0^{\infty} \frac{\alpha_k}{k!} \tau^k$$

The expression within brackets here must be reduced to a single power series and then multiplied by the  $\alpha$  series. Finally, equating coefficients of like powers of  $\tau$  will yield:

$$\left. \begin{aligned}
 c_0 &= (x)_n \\
 c_1 &= \kappa_1 (A_3)_n \sqrt{\beta_0 - \phi_0} \\
 c_2 &= c_1 (\alpha_1 + \eta_1 \beta_1) \\
 c_3 &= c_1 (\alpha_2 + 2\alpha_1 \eta_1 \beta_1 + \eta_1 \beta_2 - \eta_1^2 \beta_1^2) \\
 c_4 &= c_1 \left[ \alpha_3 + \eta_1 \beta_3 + 3\alpha_2 \eta_1 \beta_1 + 3(\alpha_1 - \eta_1 \beta_1) (\eta_1 \beta_2 - \eta_1^2 \beta_1^2) \right]
 \end{aligned} \right\} (32)$$

where

$$\beta_k = b_k - \phi_1 c_k - \theta_0 d_k - \theta_1 \sum_{v=0}^k \binom{k}{v} c_v d_{k-v}$$

The solution of equation (28c) is similar to that of equation (28a) and yields

$$\left. \begin{aligned}
 d_0 &= (y)_n \\
 d_1 &= (\dot{y})_n \\
 d_k &= \kappa_2 b_{k-2} - \lambda_3^2 d_{k-2} \quad k > 1
 \end{aligned} \right\} (33)$$

Likewise, substituting and equating of coefficients in equation (28d) produce

$$\left. \begin{aligned}
 \alpha_0 &= 1 \\
 \alpha_1 &= c_1 \sigma_1 \\
 \alpha_2 &= c_2 \sigma_1 + c_1^2 \sigma_2 \\
 \alpha_3 &= c_3 \sigma_1 + 3c_1 c_2 \sigma_2
 \end{aligned} \right\} (34)$$

The last two equations (eqs. (28e) and (28f)) are easily handled. From equation (28e) it is evident that

$$b_k = a_k - c_k \quad (35)$$

Finally, equation (28f) is solved by substitution of the series for  $x_2$  and direct integration:

$$\left. \begin{aligned} \dot{\omega} &= \kappa_3 \sum_0^{\infty} \frac{b_k}{k!} \tau^k \\ \omega &= \kappa_3 \sum_0^{\infty} \frac{b_k}{(k+1)!} \tau^{k+1} + (\omega)_n \end{aligned} \right\} \quad (36)$$

Sufficient information has been amassed to find all of the coefficients  $a_k$ ,  $b_k$ ,  $c_k$ ,  $d_k$ , and  $\alpha_k$ . By inspection of the relations between the coefficients, it can be seen that starting from the coefficients determined by the initial conditions ( $a_0$ ,  $a_1$ ,  $c_1$ ,  $d_0$ ,  $d_1$ , and  $(A_3)_n$ ) the other coefficients can be found successively. This must be done in some such order as  $b_0$ ,  $c_1$ ,  $b_1$ ,  $\alpha_1$ ,  $a_2$ ,  $c_2$ ,  $b_2$ ,  $d_2$ ,  $\alpha_2$ , and so forth. The  $\omega$  series can be computed afterward, since the other equations do not depend on  $\omega$ .

Series solutions have now been found for the variables  $x_1$ ,  $x_2$ ,  $x$ ,  $y$ , and  $\omega$  in the interval of expansion. It would seem as if the solution were complete. However, there are still difficulties to be overcome. Since the natural frequency of the horizontal vibrations of the wheel is high, the series expansion for  $y$  converges too slowly to be of use in representing  $y$  in equation (28b).

It is possible (see appendix B) to obtain a more rapidly convergent solution for  $y(t)$  of the form

$$y = (d_0 - d_0') \cos \lambda_3 \tau + \frac{1}{\lambda_3} (d_1 - d_1') \sin \lambda_3 \tau + d_0' + d_1' \tau + \frac{1}{24} d_4' \tau^4 + \frac{1}{120} d_5' \tau^5 \quad (37)$$

where

$$d_0' = \frac{\kappa_2}{\lambda_3^2} b_0$$

$$d_1' = \frac{\kappa_2}{\lambda_3^2} b_1$$

$$d_4' = \kappa_2 b_2$$

$$d_5' = \kappa_2 b_3$$

This is a very rapidly converging solution but is still not suitable for use in equation (28b) since it contains trigonometric terms. It is necessary thus to fit a parabolic approximation to this curve using the initial value and slope plus a chosen quadratic (or cubic) term:

$$y = d_0 + d_1 \tau + \frac{1}{2} d_2^* \tau^2 \quad (38)$$

or

$$y = d_0 + d_1 \tau + \frac{1}{6} d_3^* \tau^3$$

The coefficients of this formula are used to represent  $y$  in equation (28b). The solution for  $y$ , equation (37), carried to the fourth power requires  $b_0$ ,  $b_1$ , and  $b_2$ , but these coefficients may be found before  $d_2^*$  is needed.

The series solution for  $x_1$  is adequate for use in equation (28b), but it still may sometimes be desirable to have a more rapidly convergent solution for this variable also. The same procedure as outlined in appendix B yields when applied here:

$$x_1 = b_0 \cos \lambda_1 \tau + \frac{1}{\lambda_1} b_1 \sin \lambda_1 \tau + c_0 + c_1 \tau + \frac{1}{2} W_1^* \tau^2 + \frac{1}{24} \lambda_1^2 (c_2 - W_1^*) \tau^4 + \frac{1}{120} \lambda_1^2 c_3 \tau^5 + \dots \quad (39)$$

When the approximate form, equation (37), for  $y$  is used, the solution is now complete and usable. One thing remains to be discussed, the question of the length of each interval. This depends on several factors. The interval is restricted by the need for accuracy of the approximations for  $A_3(x)$ ,  $f_1(x)$ , and  $f_2(x)$ . The  $A_3$  approximation especially must be made accurately, as the solution for  $x$  is very sensitive to this variable. As has been mentioned, the interval must end wherever there is a sharp break in the  $A_3$  curve. The length of the interval is also limited by the need of obtaining sufficient accuracy in the  $y(t)$  approximation. Finally, convergence of the series representation of  $x$  must be considered. One of these factors will determine the interval length.

The value of  $\dot{y} + rw$  must be watched as in the numerical integration method, since transition to phase three occurs when

$$\dot{y} + rw = V_h$$

After this time  $t = t_t$ , the deflection  $y$  is calculated in the same way as described for the numerical integration in phase three.

The interval need not necessarily end at  $t = t_t$ . Since  $y$  is continuous, the approximation equation (38) may still fit for some time beyond the transition to phase three.

Singular interval.— At the start of phase two ( $t = t_1$ ) the rate of stroke vanishes ( $\dot{x} = 0$ ) and the same happens again when the maximum stroke is reached and recoil begins. The vanishing of  $\dot{x}$  gives rise to a particular difficulty, the source of which is found in equation (23).

This equation may be written

$$\dot{x} = \kappa_1 A_3(x) \sqrt{\psi(t)} \quad (23')$$

with the abbreviation

$$\psi(t) = x_2 - \frac{A_1 P_0}{k_2 [1 - (A_1 x / A_0 z_0)]^\gamma} - \frac{\mu_s k_3}{k_2} \frac{2l - a - x}{a_x} |y|$$

Upon differentiating, one has

$$\ddot{x} = \kappa_1 \left( \dot{A}_3 \sqrt{\psi} + \frac{A_3 \dot{\psi}}{2\sqrt{\psi}} \right)$$

which, with the help of equation (23'), may be written as

$$\ddot{x} = \frac{\dot{A}_3}{A_3} \dot{x} - \frac{\kappa_1^2}{2} A_3^2 \frac{\dot{\psi}}{x} \tag{40}$$

Since  $\dot{\psi}$  does not happen to be zero at the start of phase two, this equation shows that  $\ddot{x}$  is infinite. Thus there is, at  $t = t_1$ , a singularity in the function  $x = x(t)$  which prevents the use of the ordinary power series (29).

Although power series (29) are not applicable in this interval, it is possible to handle it with series in half-powers of  $\tau = t - t_1$ :

$$\left. \begin{aligned} x_1 &= \sum_0^{\infty} \frac{\bar{a}_k}{k!} \tau^{k/2} \\ x_2 &= \sum_0^{\infty} \frac{\bar{b}_k}{k!} \tau^{k/2} \\ x &= \sum_0^{\infty} \frac{\bar{c}_k}{k!} \tau^{k/2} \\ y &= \sum_0^{\infty} \frac{\bar{d}_k}{k!} \tau^{k/2} \\ A_3 &= (A_3)_n \sum_0^{\infty} \frac{\bar{a}_k}{k!} \tau^{k/2} \end{aligned} \right\} \tag{41}$$

Equations (28a) and (28c) are solved as before by substituting and equating coefficients. The result for equation (28a) is

$$\left. \begin{aligned}
 \bar{a}_0 &= (x_1)_n \\
 \bar{a}_1 &= \bar{a}_3 = 0 \\
 \bar{a}_2 &= (\dot{x}_1)_n \\
 \bar{a}_4 &= -12\lambda_1^2 \bar{b}_0 + 12W_1^* \\
 \bar{a}_k &= -4(k-1)(k-3)\lambda_1^2 \bar{b}_{k-4} \quad (k > 4)
 \end{aligned} \right\} (42)$$

Similarly, for equation (28c):

$$\left. \begin{aligned}
 \bar{d}_0 &= (y)_n \\
 \bar{d}_1 &= \bar{d}_3 = 0 \\
 \bar{d}_2 &= 2(\dot{y})_n \\
 \bar{d}_k &= 4(k-1)(k-3)(\kappa_2 \bar{b}_{k-4} - \lambda_3^2 \bar{d}_{k-4}) \quad (k > 3)
 \end{aligned} \right\} (43)$$

Next consider equation (28d) which expresses  $A_3$  in terms of  $x$  and introduce series (41). Since it will be shown a little later that  $\bar{c}_1 = \bar{c}_2 = 0$ , the expressions for the first few coefficients  $\bar{a}_k$  become extremely simple:

$$\left. \begin{aligned}
 \bar{a}_0 &= 1 \\
 \bar{a}_1 &= \bar{a}_2 = 0 \\
 \bar{a}_3 &= \sigma_1 \bar{c}_3
 \end{aligned} \right\} (44)$$

Equation (28b) must be considered in more detail. After substitution of the series, equations (41), this equation becomes

$$\sum_0^{\infty} \frac{\bar{c}_k}{k!} \frac{k}{2} \tau^{\frac{k-2}{2}} = \kappa_1(A_3)_n \sum_0^{\infty} \frac{\bar{a}_k}{k!} \tau^{k/2} \left( \sum_0^{\infty} \frac{\bar{b}_k}{k!} \tau^{k/2} - \phi_1 \sum_0^{\infty} \frac{\bar{c}_k}{k!} \tau^{k/2} - \theta_0 \sum_0^{\infty} \frac{\bar{d}_k}{k!} \tau^{k/2} - \theta_1 \sum_0^{\infty} \frac{\bar{c}_k}{k!} \tau^{k/2} \sum_0^{\infty} \frac{\bar{d}_k}{k!} \tau^{k/2} - \phi_0 \right)^{1/2}$$

Using, as previously,

$$\sum_0^{\infty} \frac{\bar{c}_k}{k!} \tau^{k/2} \sum_0^{\infty} \frac{\bar{d}_k}{k!} \tau^{k/2} = \sum_0^{\infty} \frac{1}{k!} \left[ \sum_{\nu=0}^k \binom{k}{\nu} \bar{c}_\nu \bar{d}_{k-\nu} \right] \tau^{k/2}$$

one finds

$$\sum_1^{\infty} \frac{\bar{c}_k}{(k-1)!} \tau^{\frac{k-2}{2}} = 2\kappa_1(A_3)_n \sum_0^{\infty} \frac{\bar{a}_k}{k!} \tau^{k/2} \left\{ \sum_0^{\infty} \frac{1}{k!} \left[ \bar{b}_k - \phi_1 \bar{c}_k - \theta_0 \bar{d}_k - \theta_1 \sum_{\nu=0}^k \binom{k}{\nu} \bar{c}_\nu \bar{d}_{k-\nu} \right] \tau^{k/2} - \phi_0 \right\}^{1/2}$$

The expression within the braces to the one-half power may be simplified by introducing

$$\bar{\beta}_k = \bar{b}_k - \phi_1 \bar{c}_k - \theta_0 \bar{d}_k - \theta_1 \sum_{\nu=0}^k \binom{k}{\nu} \bar{c}_\nu \bar{d}_{k-\nu}$$

which yields

$$\sum_1^{\infty} \frac{\bar{c}_k}{(k-1)!} \tau^{\frac{k-2}{2}} = 2\kappa_1(A_3)_n \left( \bar{\beta}_0 - \phi_0 + \sum_1^{\infty} \frac{\bar{\beta}_k}{k!} \tau^{k/2} \right)^{1/2} \sum_0^{\infty} \frac{\bar{a}_k}{k!} \tau^{k/2}$$

(45)

It is profitable at this point to look at the result of applying the initial conditions to equation (28b). For  $\tau = 0$  each of the series of equations (41) consists only of its first term, and one has

$$\begin{aligned} (\dot{x})_n &= \kappa_1(A_3)_1 \left( \bar{b}_0 - \phi_1 \bar{c}_0 - \theta_0 \bar{a}_0 - \theta_0 \bar{c}_0 \bar{a}_0 - \phi_0 \right)^{1/2} \\ &= \kappa_1(A_3)_1 \left( \bar{\beta}_0 - \phi_0 \right)^{1/2} \end{aligned}$$

and, since  $(\dot{x})_n$  is zero, it follows that

$$\bar{\beta}_0 - \phi_0 = 0$$

Therefore, equation (45) reads simply

$$\sum_1^{\infty} \frac{\bar{c}_k}{(k-1)!} \tau^{\frac{k-2}{2}} = 2\kappa_1(A_3)_n \left( \sum_1^{\infty} \frac{\bar{\beta}_k}{k!} \tau^{k/2} \right)^{1/2} \sum_0^{\infty} \frac{\bar{a}_k}{k!} \tau^{k/2} \quad (46)$$

Some preliminary conclusions may now be drawn before the complete solution of the equation is attempted. The above equation in expanded form reads

$$\begin{aligned} \bar{c}_1 \tau^{-1/2} + \bar{c}_2 + \bar{c}_3 \tau^{1/2} + \dots &= 2\kappa_1(A_3)_n \left( \bar{\beta}_1 \tau^{1/2} + \right. \\ &\left. \frac{1}{2} \bar{\beta}_2 \tau + \dots \right)^{1/2} \sum_0^{\infty} \frac{\bar{a}_k}{k!} \tau^{k/2} \end{aligned}$$

Inspection of this equation shows that the terms of the right-hand side start with  $\tau^{1/4}$ . Therefore, the coefficients of  $\tau^{-1/2}$  and  $\tau^0$  on the left-hand side must vanish:

$$\bar{c}_1 = 0$$

$$\bar{c}_2 = 0$$

Further, since

$$\bar{a}_1 = 0$$

$$\bar{d}_1 = 0$$

(eqs. (42) and (43)), and since

$$\bar{b}_1 = \bar{a}_1 - \bar{c}_1 = 0$$

it follows that

$$\bar{\beta}_1 = \bar{b}_1 - \phi_1 \bar{c}_1 - \theta_0 \bar{d}_1 - \theta_1 (\bar{c}_0 \bar{d}_1 + \bar{c}_1 \bar{d}_0) = 0$$

Returning to equation (46) and using those results, one has

$$\sum_3^{\infty} \frac{\bar{c}_k}{(k-1)!} \tau^{\frac{k-2}{2}} = 2\kappa_1 (A_3)_n \left( \frac{1}{2} \bar{\beta}_2 \tau + \sum_3^{\infty} \frac{\bar{\beta}_k}{k!} \tau^{k/2} \right)^{1/2} \sum_0^{\infty} \frac{\bar{a}_k}{k!} \tau^{k/2}$$

and, hence,

$$\sum_3^{\infty} \frac{\bar{c}_k}{(k-1)!} \tau^{\frac{k-2}{2}} = 2\kappa_1 (A_3)_n \sqrt{\frac{\bar{\beta}_2}{2}} \tau^{1/2} \left( 1 + \frac{2}{\bar{\beta}_2} \sum_3^{\infty} \frac{\bar{\beta}_k}{k!} \tau^{\frac{k-2}{2}} \right)^{1/2} \sum_0^{\infty} \frac{\bar{a}_k}{k!} \tau^{k/2}$$

The expression within parentheses to the one-half power may be expanded by means of the binomial theorem. Also the  $\bar{a}$  series can be written in simple form making use of equation (44):

$$\begin{aligned} \sum_3^{\infty} \frac{\bar{c}_k}{(k-1)!} \tau^{\frac{k-2}{2}} &= 2\kappa_1 (A_3)_n \sqrt{\frac{\bar{\beta}_2}{2}} \tau^{1/2} \left[ 1 + \frac{1}{\bar{\beta}_2} \left( \sum_3^{\infty} \frac{\bar{\beta}_k}{k!} \tau^{\frac{k-2}{2}} \right) - \right. \\ &\quad \left. \frac{1}{2} \frac{1}{\bar{\beta}_2} \left( \sum_3^{\infty} \frac{\bar{\beta}_k}{k!} \tau^{\frac{k-2}{2}} \right)^2 + \frac{1}{2\bar{\beta}_2^3} \left( \sum_3^{\infty} \frac{\bar{\beta}_k}{k!} \tau^{\frac{k-2}{2}} \right)^3 + \dots \right] \times \\ &\quad \left( 1 + \frac{\bar{a}_3}{6} \tau^{3/2} + \dots \right) \end{aligned}$$

When the right-hand side is reduced to a single power series and the coefficients of like powers are equated, the results are these:

$$\left. \begin{aligned}
 \bar{c}_0 &= (x)_n \\
 \bar{c}_3 &= 4\kappa_1 (A_3)_n \sqrt{\frac{\bar{\beta}_2}{2}} \\
 \bar{c}_4 &= \frac{1}{2} \bar{c}_3 \frac{\bar{\beta}_3}{\bar{\beta}_2} \\
 \bar{c}_5 &= \frac{1}{6} \bar{c}_3 \left( 3 \frac{\bar{\beta}_4}{\bar{\beta}_2} - \frac{\bar{\beta}_3^2}{\bar{\beta}_2^2} \right) \\
 \bar{c}_6 &= \frac{1}{36} \bar{c}_3 \left[ \left( 18 \frac{\bar{\beta}_5}{\bar{\beta}_2} - 15 \frac{\bar{\beta}_3 \bar{\beta}_4}{\bar{\beta}_2^2} + 5 \frac{\bar{\beta}_3^3}{\bar{\beta}_2^3} \right) + 360 \bar{\alpha}_3 \right]
 \end{aligned} \right\} \quad (47)$$

A solution for the singular interval has now been found. However, it is necessary here as in the regular interval to use an altered form for  $y$  obtained in a manner similar to that of appendix B. This solution is found to be

$$\begin{aligned}
 y &= \left( \bar{a}_0 - \frac{\kappa_2}{\lambda_3^2} \bar{b}_0 \right) \cos \lambda_3 \tau + \frac{1}{2\lambda_3} \left( \bar{a}_2 - \frac{\kappa_2}{\lambda_3^2} \bar{b}_2 \right) \sin \lambda_3 \tau + \\
 &\frac{\kappa_2}{\lambda_3^2} \bar{b}_0 + \frac{1}{2} \frac{\kappa_2}{\lambda_3^2} \bar{b}_2 \tau + \frac{2}{105} \kappa_2 \bar{b}_3 \tau^{7/2} + \frac{1}{288} \kappa_2 \bar{b}_4 \tau^4 + \\
 &\frac{1}{1890} \kappa_2 \bar{b}_5 \tau^{9/2} + \dots \quad (48)
 \end{aligned}$$

Since this is not a pure power series, the coefficients of the powers of  $\tau$  cannot be used as  $\bar{a}_k$  in the computation of  $\bar{\beta}_k$  and hence of  $\bar{c}_k$  (eqs. (47)). A plot of the equation is therefore made (fig. 19) and a curve of the form

$$y = \bar{a}_0 + \frac{1}{2} \bar{a}_2 \tau + \frac{1}{24} \bar{a}_4 \tau^2 \quad (49)$$

is fitted to it by varying  $\bar{d}_4^*$ . The coefficients of this parabola are used to represent  $y$  in equations (47).

A similar formula for  $x_1$  may be useful for its calculation. It is found to be

$$x_1 = \bar{a}_0 \cos \lambda_1 \tau + \frac{1}{2} \frac{\bar{e}_2}{\lambda_1} \sin \lambda_1 \tau + \frac{1}{24} W_1^* \tau^2 + \frac{2}{105} \lambda_1^2 \bar{e}_3 \tau^{7/2} + \frac{1}{288} \lambda_1^2 (\bar{c}_4 - W_1^*) \tau^4 + \frac{1}{1890} \lambda_1^2 \bar{e}_5 \tau^{9/2} + \dots \quad (50)$$

Finally, equation (28c) may be solved by substitution of the series for  $x_2$  and direct integration:

$$\left. \begin{aligned} \dot{\omega} &= \kappa_3 \sum_0^{\infty} \frac{\bar{b}_k}{k!} \tau^{k/2} \\ \omega &= 2\kappa_3 \sum_0^{\infty} \frac{\bar{b}_k}{k!(k+2)} \tau^{\frac{k+2}{2}} + (\omega)_n \end{aligned} \right\} \quad (51)$$

A complete, usable solution has now been found for the singular interval  $n$ . The same considerations which cause termination of a regular interval will govern this interval.

Procedure.- A procedure is given here outlining the analytical method which has been derived. The steps are given for both the singular and regular intervals with differences noted.

- (1) Determine values of  $m_1, m_2, m_3, W_1, k_2, k_3, A_0, A_1, A_2, \mu_s, \mu_r, p_0, \rho, \gamma, z_0, l, a, V, V_h, r,$  and  $I$ .

(2) Calculate the parameters

$$\lambda_1^2 = k_2/m_1$$

$$\lambda_3^2 = k_3/m_3$$

$$\kappa_1 = \sqrt{2k_2/\rho A_2^3}$$

$$\kappa_2 = \mu_T k_2/m_3$$

$$\kappa_3 = \mu_T r k_2/I$$

(3) Construct graphs of

$$f_1(x) = \frac{A_1 p_0}{k_2} \left( 1 - \frac{A_1}{A_0 z_0} x \right)^{-\gamma}$$

$$f_2(x) = \frac{\mu_B k_3}{k_2} \frac{2l - a - x}{a + x}$$

$$A_3(x)$$

Phase one: The steps for phase one are as follows:

(4) Determine the time  $t_1$  at the end of interval 0 by iteration of equations (14).

(5) Calculate values of  $(\dot{x}_1)_1$ ,  $(\ddot{x}_1)_1$ ,  $(y)_1$ , and  $(\dot{y})_1$  from equations (13).

(6) Calculate  $(\omega)_1$  and  $(\dot{y} + r\omega)_1$  from equation (15).

Phase two: For phase two the procedure is as follows:

(7) Estimate the length of the interval to insure accuracy of:

(a) Parabolic curve for  $A_3(x)$

(b) Linear approximations for  $f_1(x)$  and  $f_2(x)$

(c) Parabolic curve for  $y(t)$

(d) Convergence of series for  $x$  and  $\dot{x}_1$

(8) Determine  $\sigma_1$ ,  $\sigma_2$ ,  $\phi_0$ ,  $\phi_1$ ,  $\theta_0$ , and  $\theta_1$  in the interval to give the best approximations:

$$A_3(x) = (A_3)_n (1 + \sigma_1 \xi + \sigma_2 \xi^2)$$

with

$$\xi = x - (x)_n$$

$$f_1(x) = \phi_0 + \phi_1 x$$

$$f_2(x) = \theta_0 + \theta_1 x$$

Singular interval

(S9) From step (5) calculate

$$\bar{a}_0 = (x_1)_n$$

$$\bar{a}_2 = 2(\dot{x}_1)_n$$

$$\bar{d}_0 = (y)_n$$

$$\bar{d}_2 = 2(\dot{y})_n$$

(S10) Using table 4, compute successively  $\bar{b}_0$ ,  $\bar{a}_4$ ,  $\bar{b}_2$ ,  $\bar{a}_6$ ,  $\bar{\beta}_2$ ,  $\bar{c}_3$ ,  $\bar{b}_3$ ,  $\bar{\beta}_3/\bar{\beta}_2$ , and  $\bar{c}_4$ .

(S11) Calculate and plot  $y(\tau)$  in the interval from equation (48). Determine  $\bar{d}_4^*$  to give the best approximation from equation (49). Record  $\bar{d}_4^*$  in table 1. All higher values of  $\bar{d}_k$  are made zero.

Regular interval

(R9) From step (5) calculate

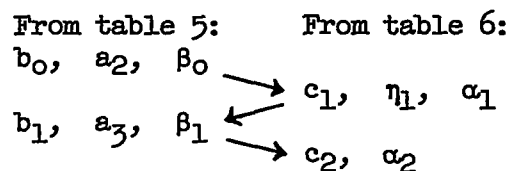
$$a_0 = (x_1)_n$$

$$a_1 = (\dot{x}_1)_n$$

$$d_0 = (y)_n$$

$$d_1 = (\dot{y})_n$$

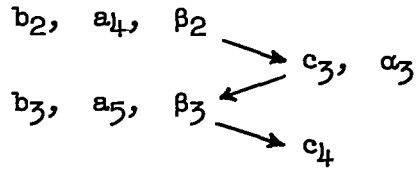
(R10) Using tables 5 and 6, calculate successively



(R11) Calculate and plot  $y(\tau)$  in the interval from equation (37). Determine  $d_2^*$  to give the best approximation from equation (38). Record  $d_2^*$  in table 3. All higher values of  $d_k$  are made zero.

(S12) In table 4 calculate successively  $\bar{\beta}_4/\bar{\beta}_2$ ,  $\bar{c}_5$ ,  $\bar{b}_5$ ,  $\bar{\beta}_5/\bar{\beta}_2$ ,  $\bar{c}_6$ , and  $\bar{b}_6$ .

(R12) Calculate successively From table 5: From table 6:



(S13) Form series

$$x_1 = \sum_0^{\infty} \frac{\bar{a}_k}{k!} \tau^{k/2}$$

$$x = \sum_0^{\infty} \frac{\bar{c}_k}{k!} \tau^{k/2}$$

(R13) Form series

$$x_1 = \sum_0^{\infty} \frac{a_k}{k!} \tau^k$$

$$x = \sum_0^{\infty} \frac{c_k}{k!} \tau^k$$

(14) If the end of the interval is determined by value of  $x$ , find by trial the value of  $\tau$  for which  $x = (x)_{n+1}$ . Then calculate  $(x_1)_{n+1}$ ,  $(\dot{x}_1)_{n+1}$ ,  $(y)_{n+1}$ , and  $(\dot{y})_{n+1}$ . If the value of  $\tau$  ends the interval, all the values may be computed immediately.

(S15) Compute  $(\omega)_{n+1}$  from equation (51).

(R15) Compute  $(\omega)_{n+1}$  from equation (36).

(16) Determine  $(\dot{y} + r\omega)_{n+1}$ . In some interval the condition

$$\dot{y} + r\omega = V_h \quad \text{at} \quad t = t_t$$

will be satisfied. This terminates phase two.

Phase three: The procedure for phase three is the same as that for phase two except for the following changes:

(a) Replace step (R11) as follows:

(R11') Calculate and plot  $y(\tau)$  using equation (37). Determine  $d_2^*$  to give the best approximation from equation (38).

(b) In step (14)  $(y)_{n+1}$  and  $(\dot{y})_{n+1}$  need not be calculated.

(c) Omit steps (R15) and (R16).

Application of method to numerical example.- The analytical method is applied in this section to the example used for the numerical integration. The procedure of the preceding section is followed, so that here only results and special remarks need be given. The data for this example have been listed in the section "Numerical example." From these the computation parameters are found to be.

$$\lambda_1^2 = 120.7 \text{ sec}^{-2}$$

$$\lambda_3^2 = 2,008 \text{ sec}^{-2}$$

$$\kappa_1 = 68.63 \text{ in.}^{-3/2} \text{ sec}^{-1}$$

$$\kappa_2 = 1,607 \text{ sec}^{-2}$$

$$\kappa_3 = 182.2 \text{ in.}^{-1} \text{ sec}^{-2}$$

Figures 17, 18, and 9 show graphs of the functions

$$f_1(x) = 0.9870 \left(1 - \frac{x}{23.5}\right)^{-1.1}$$

$$f_2(x) = 0.06248 \frac{67 - x}{13 + x}$$

and  $A_3(x)$ , respectively. The parameters for the approximate representations of these functions in each interval are collected in table 7. These are all secant approximations, except for one parabola in the case of  $A_3(x)$ .

The computations for interval  $n = 0$  (phase one) are the same as those given in the section "Numerical example." Interval 1 at the start of phase two is a singular interval since  $(\dot{x})_1$  is zero. The interval length is limited by the break in the  $A_3(x)$  curve at  $x = 2.036$  inches. However, to obtain a good approximation for  $y(t)$  and sufficient convergence for  $x(t)$ , it is better to restrict the interval to  $\tau = 0.3$  second ( $x \approx 0.7$  inch). When the interval length has been chosen, the computation proceeds without incident as shown in table 4. In figure 19 the graph of  $y(t)$  in this interval found by use of equation (48) is shown. In this graph the fitted parabola, equation (49), is also plotted. The fitted curve has the same initial value and slope and is chosen to give the least percentage error. This procedure is handled similarly in each interval.

Interval 2 is the first regular interval and extends until  $x = 2.036$  inches. The computations for this and the following intervals are displayed in tables 5 and 6.

The next interval ( $n = 3$ ) may be carried to  $x = 3.350$  inches where a second break occurs in the  $A_3(x)$  curve. This needs no special discussion.

Although  $A_3(x)$  becomes a smooth curve for some distance after  $x = 3.350$  inches, interval 4 is terminated at  $x = 8.156$  inches which maintains convergence of the  $x$  series and permits a good approximation for  $y(t)$ . In this interval transition occurs. For  $t = t_1 = 0.1086$  second,  $(\dot{y} + w)_t = 1,672$  inches per second  $= V_h$ . At this time the differential equation for  $y(t)$  changes form and is no longer coupled to the other dependent variables. However, since  $y$  and  $\dot{y}$  remain continuous through transition, it proves possible in this example to carry the approximation for  $y(t)$  past the transition point.

The series solutions for all variables in each interval are given in table 8. These results when plotted give almost identical results to those found by numerical integration (figs. 12 to 14).

#### Analytic Start of Numerical Integration

When using the numerical integration method, it is necessary to make the first step with an integration formula of poor accuracy. This does not matter if it is 1 step out of 40 or 50, but it does, if the integration is to be made with large steps. And it matters still more in the present case because of the singularity of  $\ddot{x}$  at  $t = t_1$ . This infinite value of the derivative makes all finite-difference work non-convergent at the time  $t = t_1$ , and therefore the outcome of the first step is not reliable.

It is therefore advisable to use the analytical method just described at least for getting started in phase two, even if numerical integration is to be employed for the rest of the work.

In this case only one singular interval needs to be handled, and one may follow the instructions as given in the left-hand column of the procedure. The interval is chosen as long as possible, and near its end the variables  $x_1$ ,  $x_2$ ,  $x$ , and  $y$  and their derivatives are evaluated for three or four equidistant times. These values are entered in the first lines of an integration table, and from there on the numerical integration is run as shown before.

This is the procedure if one wants to deal with the most exact set of equations used in this report, that is, with those which neglect  $m_2$  but keep  $m_3$ . If the mass  $m_3$  of the spring-back motion is to be neglected, equations (43) must be replaced by a simpler set, representing the static values of the horizontal deflection:

$$\begin{aligned} y &= \frac{\mu_T F_1}{k_3} \\ &= \frac{\mu_T k_2}{k_3} x_2 \\ &= \frac{\mu_T k_2}{k_3} \sum_0^{\infty} \frac{\bar{b}_k}{k!} \tau^{k/2} \end{aligned}$$

This yields the simple relation

$$\bar{d}_k = \frac{\mu_T k_2}{k_3} \bar{b}_k$$

which takes the place of equations (43). With these coefficients convergence of the  $y$  series is just as good as that of the  $x_2$  series, and it is not necessary to apply the curve-fitting procedure described in connection with equations (48) and (49).

#### GENERALIZATIONS OF THEORY

In this section two of the most stringent restrictions are dropped, namely, that the axis of the shock strut lies in the plane of the wheel and that this axis is vertical. In both cases it is found that the computation, though more realistic, is also more laborious. It will depend on the particular case whether the results justify the greater effort. This should be checked in all practical cases. When the shock strut makes an angle with the vertical, the possibility of a divergent motion (self-excited vibration) appears, which deserves further investigation.

#### Eccentric Wheel

While landing gears for large loads often have two wheels arranged symmetrically on both sides of the oleo strut, small landing gears have

only one wheel. In nose gears (and tail gears) symmetry is maintained by the use of a fork, but in the main gears the wheel usually is arranged eccentrically as shown in figure 20 and a pair of shears is provided to prevent the wheel from castering. The eccentricity of the drag force  $D$  presents an additional problem which must be worked into the general equations.

Figure 21 shows a free-body diagram of the lower part of the landing gear in three projections. The wheel has been taken off, and the force  $H$  at the axle has been introduced. The following equations of equilibrium may be written:

$$H'e' = He$$

$$N_1 = H \frac{l - a - x}{a + x}$$

$$N_2 = H \frac{l}{a + x}$$

$$N_1' = H' \frac{l' - a - \frac{x}{2}}{a + x} - F_1 \frac{e}{a + x}$$

$$N_2' = H' \frac{l' + \frac{x}{2}}{a + x} - F_1 \frac{e}{a + x}$$

In the first equation, the arm  $e'$  depends on  $x$  according to a simple trigonometric relation. This variability may be taken into account when it is worth while, or  $e'$  may be assumed as an average value. In the other equations the contributions of the friction forces  $\mu_s N$  have been neglected, as before.

The forces  $N_1$  and  $N_1'$  and  $N_2$  and  $N_2'$  combine to two resultants

$$\sqrt{N_1^2 + (N_1')^2}$$

and

$$\sqrt{N_2^2 + (N_2')^2}$$

and these resultants give rise to friction forces:

$$\left. \begin{aligned} T_1 &= \frac{\mu_s |H|}{a+x} \left\{ (l-a-x)^2 + \left[ (l' - a - \frac{x}{2}) \frac{e}{e'} - \frac{F_1}{H} e \right]^2 \right\}^{1/2} \\ T_2 &= \frac{\mu_s |H|}{a+x} \left\{ l^2 + \left[ (l' + \frac{x}{2}) \frac{e}{e'} - \frac{F_1}{H} e \right]^2 \right\}^{1/2} \end{aligned} \right\} \quad (52)$$

The sum of these forces takes the place of the term

$$\mu_s |H| \frac{2l - a - x}{a+x}$$

in equation (7). Here again the forces  $T$  do not change direction if  $H$  does, and consequently  $|H|$  has been written outside of the braces, but not inside.

It may be observed here that the second term in the expressions for  $N_1'$  and  $N_2'$  changes sign if the shears are placed on the rear side of the landing gear. This may easily be seen from figure 20. When the airplane is supposed to move from left to right the shears are to the rear, and the directions of  $H$  and  $H'$  must be inverted. The friction forces are then

$$\left. \begin{aligned} T_1 &= \frac{\mu_s |H|}{a+x} \left\{ (l-a-x)^2 + \left[ (l' - a - \frac{x}{2}) \frac{e}{e'} + \frac{F_1}{H} e \right]^2 \right\}^{1/2} \\ T_2 &= \frac{\mu_s |H|}{a+x} \left\{ l^2 + \left[ (l' + \frac{x}{2}) \frac{e}{e'} + \frac{F_1}{H} e \right]^2 \right\}^{1/2} \end{aligned} \right\} \quad (53)$$

Evidently, it is better to place the shears on the front side since this will result in lower piston friction.

In the most general case, the force  $T_1 + T_2$  depends on  $x$ ,  $F_1$ , and  $H$ , and its value must be computed in every line of the numerical integration. This leads to a substantial increase in computation labor.

A considerable simplification is obtained if the masses  $m_2$  and  $m_3$  in equations (9d) and (10b) are neglected. Since, by definition,  $H = k_3 y$ , one has then

$$\frac{F_1}{H} = \frac{F_1}{k_3 y} = \frac{k_2 x_2}{\mu_r k_2 x_2} = \frac{1}{\mu_r}$$

and, except for the factor  $|H|$ , the friction forces depend only on  $x$ . One may then put

$$T_1 + T_2 = \beta |H|$$

with

$$\beta = \frac{\mu_s}{a + x} \left\{ \left[ (l - a - x)^2 + e^2 \left( \frac{l' - a - x/2}{e'} + \frac{1}{\mu_r} \right)^2 \right]^{1/2} + \left[ l^2 + e^2 \left( \frac{l' + x/2}{e'} + \frac{1}{\mu_r} \right)^2 \right]^{1/2} \right\}$$

and it is possible to prepare a diagram similar to figure 11 representing  $\beta$  as a function of  $x$ . Although the formula does not look very pleasant, the preparation of the diagram is an easy job, since only a few points are needed to trace the curve. Once this has been done, phase two may be dealt with in exactly the same way as when the wheel has no eccentricity.

In phase three the deflection  $y$  and hence  $H$  may be computed in advance and, therefore, the ratio  $F_1/H$  cannot have a fixed value.

Whether one uses the correct values of  $y$  or the average of  $|y|$ , as explained before, there is no way of avoiding the repeated use of equations (52) at every step of the numerical integration.

#### Inclined Shock Strut

So far it has been assumed in this report that the axis of the shock strut makes a right angle with the runway. This is usually not the case, the shock strut being inclined by a moderate angle  $\alpha$  from the vertical.

If this inclination is to be taken into account, all the equations must be reexamined and most of them rewritten. In order to keep the relations as simple as possible, this will be done here under the

assumptions that in phases one and two the masses  $m_2$  and  $m_3$  can be neglected and that in phase three  $m_2$  at least need not be considered. As shown before, it is not possible to neglect  $m_3$  in the spring-back motion, because then the influence of the wheel drag would be lost entirely.

The notations are shown in figure 22, where  $F_1$  is the force in the shock strut and  $x$ , the stroke measured in axial direction. The deflection  $y$  is at right angles to the shock-strut axis, but  $F_2$  and  $D$  are vertical and horizontal, respectively.

The equation of the shock strut, equation (7), may be retained as it stands, if  $H$  is interpreted as the force normal to the shock strut; that is,

$$H = D \cos \alpha - F_2 \sin \alpha$$

The equations of motion must be investigated separately for the three phases of motion.

Phase one.— In the prestress phase equations (9) were used. Equation (9a) is still applicable. To find the replacement for equation (9b), one must start from the more general equation

$$m_1 \ddot{x}_1 = W_1 - F_2$$

Here, equation (9a) may again be used to eliminate  $F_2$ , but  $x_1$  and  $x_2$  are no longer equal since the deflection  $y$  has a vertical component  $y \sin \alpha$ . Therefore,

$$x_1 = x_2 - y \sin \alpha$$

and when this is introduced in the preceding equation, one has instead of equation (9b):

$$m_1 \ddot{x}_2 + k_2 x_2 - m_1 \sin \alpha (\ddot{y}) = W_1 \quad (54a)$$

This is no longer an equation for  $x_2$  alone, and it must be considered simultaneously with the replacement for equation (9d). When the dynamic term  $m_3 \ddot{y}$  is dropped from that equation, it states simply that the lateral force  $H = k_3 y$  which deflects the shock strut is equal to the drag  $\mu_r F_2$ . Under the present conditions  $k_3 y$  must be equated to the external force normal to the shock strut:

$$k_3 y = D \cos \alpha - F_2 \sin \alpha = F_2 (\mu_r \cos \alpha - \sin \alpha)$$

and with equation (9a) it becomes

$$k_3 y = (\mu_r \cos \alpha - \sin \alpha) k_2 x_2 \quad (54b)$$

This equation may readily be used to eliminate  $y$  from equation (54a):

$$m_1 \left[ 1 - \frac{k_2}{k_3} (\mu_r \cos \alpha - \sin \alpha) \sin \alpha \right] \ddot{x}_2 + k_2 x_2 = W_1 \quad (54a')$$

It appears here that by a suitable (or rather an unsuitable) choice of the data one may obtain a negative mass coefficient, that is, an exponential increase of  $x_2$  with time.

Equation (9c) indicates that  $F_1 = F_2$  if  $m_2 = 0$ . In the present case this must be replaced by the relation

$$F_1 = F_2 \cos \alpha + D \sin \alpha$$

which may be read from figure 22. With  $D = \mu_r F_2$  and equation (9a) it becomes

$$F_1 = k_2 x_2 (\cos \alpha + \mu_r \sin \alpha) \quad (54c)$$

Equation (9e), the last of the group, remains as it stands.

Since all equations in phase one are linear, the solution may be easily obtained. The phase will not be of long duration, and hence a power-series method will be most convenient. The unknown  $x_2$  is assumed in the form

$$x_2 = \sum_{k=0}^{\infty} \frac{b_k}{k!} t^k$$

and is introduced into equation (54a'). With the initial conditions

$$t = 0: \quad x_2 = \dot{x}_2 = 0$$

this yields

$$x_2 = \frac{W_1}{m_1^*} t^2 \left[ \frac{1}{2!} - \frac{1}{4!} \left( \frac{k_2 t^2}{m_1^*} \right) + \frac{1}{6!} \left( \frac{k_2 t^2}{m_1^*} \right)^2 - \dots \right]$$

where

$$m_1^* = m_1 \left[ 1 - \frac{k_2}{k_3} (\mu_r \cos \alpha - \sin \alpha) \sin \alpha \right]$$

The other variables depend on  $x_2$ :

$$y = \frac{k_2}{k_3} (\mu_r \cos \alpha - \sin \alpha) x_2$$

$$x_1 = \frac{m_1^*}{m_1} x_2$$

Phase two.- In phase two equations (9a) and (10a) are still valid, which may be combined to

$$m \dot{x}_1 = W_1 - k_2 x_2 \quad (55a)$$

Equations (54b) and (54c) are applicable also, but  $x$  enters now into the relation between  $x_1$ ,  $x_2$ , and  $y$ :

$$x_1 - x_2 = x \cos \alpha + y \sin \alpha \quad (55b)$$

When  $y$  from equation (54b) is introduced here, one obtains

$$x_2 = \frac{k_3}{k_3 - k_2 \sin \alpha (\mu_r \cos \alpha - \sin \alpha)} (x_1 - x \cos \alpha) \quad (55c)$$

In addition, there is still the shock-strut equation (eq. (7)) which is best written in the form of equation (17). But, in the present case

$$\begin{aligned} F_1 - \beta y &= k_2 (\cos \alpha + \mu_r \sin \alpha) x_2 - \mu_s \frac{2l - a - x}{a + x} k_2 (\mu_r \cos \alpha - \sin \alpha) x_2 \\ &= k_2 x_2 \left[ \cos \alpha + \mu_r \sin \alpha - \mu_s \frac{2l - a - x}{a + x} (\mu_r \cos \alpha - \sin \alpha) \right] \end{aligned}$$

One may write this as

$$F_1 - \beta y = \beta' x_2$$

with the coefficient

$$\beta' = k_2 \left[ \cos \alpha + \mu_r \sin \alpha - \mu_s (\mu_r \cos \alpha - \sin \alpha) \frac{2l - a - x}{a + x} \right] \quad (56)$$

depending on  $x$ . Equation (17) assumes then the simple form

$$\dot{x} = \frac{A_3}{A_2} \sqrt{\frac{2}{\rho A_2}} \sqrt{\beta' x_2 - F_a} \quad (57)$$

Equations (55a), (55c), and (57) are three differential equations for  $x_1$ ,  $x_2$ , and  $x$ . They may be solved by the methods described in the section "Differential Equations of Landing Impact."

When  $x_2$  is eliminated from equations (55a) and (55c), an equation will result which contains terms with  $\ddot{x}_1$  and  $x_1$ . In general, both will have the same sign, but it may happen that their signs are opposite, depending on the denominator in equation (55c). This hints at the possibility of a divergent motion.

The end of phase two is reached when the wheel is completely spun up, that is, when

$$r\omega = V_h$$

Here the term  $\dot{y}$  used previously has been dropped, since it is insignificant when only the static deflection  $y$  is considered ( $m_3 = 0$ ). The angular velocity  $\omega$  of the wheel is found from equation (9e) which still applies.

Phase three.— The only difference between phases two and three is that the drag  $D$  is no longer proportional to the wheel force  $F_2$ .

One may, therefore, keep all those equations which do not contain the coefficient of runway friction  $\mu_r$ . They are equations (9a), (55a), and (55b).

In addition, there are now equations (1a) and (1b) and the kinematic condition of rolling without skidding, but they all need a careful revision. In equation (1a), the term  $\mu F$  describes the force on the wheel in the direction of the displacement  $y$ . This is now the force  $H$ , and the equation reads

$$m_3 \ddot{y} = H - k_3 y$$

In equation (1b) the term  $\mu F$  is the drag force  $D$  which has the moment  $D r$  and accelerates the rotatory motion of the wheel:

$$I\dot{\omega} = D r$$

The horizontal velocity of the airplane is  $V_h$ . Relative to the airplane the axle of the wheel has a backward velocity  $\dot{x} \sin \alpha + \dot{y} \cos \alpha$ , and the lowest point of the wheel rim has still the additional velocity  $r\omega$ , also directed backwards. The resultant velocity of this point must be zero:

$$V_h - \dot{x} \sin \alpha - \dot{y} \cos \alpha - r\omega = 0$$

Finally, there is the relation between the forces acting on the wheel:

$$H = D \cos \alpha - F_2 \sin \alpha$$

which has already been used in phase one.

From these equations one may easily eliminate  $H$ ,  $D$ , and  $\omega$ , and then equation (9a) may be used to eliminate also  $F_2$ . The result is the following differential equation:

$$\left(m_3 + \frac{I}{r^2} \cos^2 \alpha\right) \ddot{y} + k_3 y + \frac{I}{r^2} \cos \alpha \sin \alpha \ddot{x} + k_2 \sin \alpha x_2 = 0 \quad (58a)$$

This and equations (55a) and (55b) are three equations for the four unknowns  $x_1$ ,  $x_2$ ,  $x$ , and  $y$ . The fourth equation is the equation of the oleo strut, equation (7). It must now be used in the following way:  $F_1$  is the force in the shock strut; that is,

$$\begin{aligned} F_1 &= F_2 \cos \alpha + D \sin \alpha \\ &= k_2 x_2 \cos \alpha - \frac{I}{r^2} (\ddot{x} \sin \alpha + \ddot{y} \cos \alpha) \sin \alpha \end{aligned}$$

The first and second terms on the right-hand side of equation (7) remain as they stand. In the third term,  $H$  is the force  $k_3 y$  that deflects the shock strut laterally. If these expressions are introduced, equation (7) reads as follows:

$$\frac{I}{r^2} \cos \alpha \sin \alpha \ddot{y} + \beta y - k_2 \cos \alpha x_2 + \frac{I}{r^2} \sin^2 \alpha \ddot{x} + \frac{\rho A_2^3}{2A_3^2} \dot{x}^2 + F_a = 0 \quad (58b)$$

Equations (58) may be considered as a pair of linear equations for the second derivatives  $\ddot{y}$  and  $\ddot{x}$ . When they are solved for these unknowns, the following relations are obtained:

$$m_3 \ddot{y} + (k_3 - \beta \cot \alpha) y + \frac{k_2}{\sin \alpha} x_2 - \left( \frac{\rho A_2^3}{2A_3^2} \dot{x}^2 + F_a \right) \cot \alpha = 0 \quad (59a)$$

$$\frac{m_3 \sin^2 \alpha}{\frac{m_3 r^2}{I} + \cos^2 \alpha} \ddot{x} + \frac{\rho A_2^3}{2A_3^2} \dot{x}^2 + F_a - \left( \frac{k_3 \cos \alpha \sin \alpha}{\frac{m_3 r^2}{I} + \cos^2 \alpha} - \beta \right) y -$$

$$k_2 \cos \alpha \left( 1 + \frac{\sin^2 \alpha}{\frac{m_3 r^2}{I} + \cos^2 \alpha} \right) x_2 = 0 \quad (59b)$$

These and equation (55a) may be used to find by numerical integration  $y$ ,  $x$ , and  $x_1$ , and  $x_2$  will then be found from equation (55b).

#### BINDING OF SHOCK STRUT

So far it has been assumed that the friction between piston and barrel depends only on the forces  $N_1$  and  $N_2$  in figure 6, which in turn depend directly on the force  $H$  transmitted from the wheel to the lower end of the shock strut.

The shock-strut barrel is a rather thin-walled tube, and in the usual cantilever construction it is subjected to a large bending moment. It is known that in such cases a slight ovalization of the cross section is part of the elastic deformation. Since the piston will locally

prevent this ovalization, it must be feared that the resulting pressure between the wall of the barrel and the piston may lead to a considerable increase in friction.

It will be seen on the following pages that this problem leads into the nonlinear theory of elasticity and a good deal into the bending theory of cylindrical shells. It is not possible to make such calculations part of a routine stress analysis, and it is even beyond the scope of this report to present them in detail. But it is possible to indicate the lines of thought and the final conclusions, which seem to be fairly general.

Consider a long thin-walled tube of circular cross section subjected to pure bending by couples  $M$  applied at both ends. Figure 23 shows an element of this tube. According to elementary formulas there are bending stresses

$$\sigma = \frac{M \cos \theta}{\pi a^2 t}$$

and they produce a curvature of the tube

$$\frac{d\phi}{dx} = \frac{M}{E \pi a^3 t}$$

Because of this curvature, the stresses on opposite ends of the element do not have the same direction, and the stresses acting on corresponding elements of both cross sections have an upward or downward resultant. For an element  $a \, d\theta \, t$  of the cross sections this resultant is

$$a \, d\theta \, t \sigma \, d\phi$$

and it may be considered as being distributed over a strip of the middle surface of the cylinder, having the length  $dx$  and width  $a \, d\theta$ . The resultant force per unit area of this strip is

$$q = t \sigma \frac{d\phi}{dx} = \frac{M^2 \cos \theta}{E \pi^2 a^5 t}$$

In the lower half of the cylinder ( $\cos \theta > 0$ ) it is directed upward and in the upper half, downward, as indicated in the cross section in figure 23.

It is this load which causes the ovalization of the tube. One may find the magnitude of this deformation by cutting a ring of unit width

from the tube and applying to it the well-known theory of stresses in circular rings. If the deformation due to direct stress is neglected, it will be found that the maximum radial displacement is

$$w_0 = \frac{M^2(1 - \nu^2)}{\pi^2 E^2 a t^4}$$

where  $\nu$  is, as usual, Poisson's ratio. This displacement is directed inward at the ends of the vertical diameter and outward at the ends of the horizontal diameter. In between it varies as  $\cos 2\theta$ . Since the load  $q$  is proportional to  $M^2$ , the ovalization is a nonlinear effect.

The ovalization of the shock-strut barrel will be less than indicated by the formula, because of the additional rigidity which comes from the closing of the upper end and from local reinforcements of its wall, for example, those necessary for attaching the drag strut. This reserve in rigidity will be neglected here, since it is rather difficult and not worth while to evaluate it.

To get an idea of what this ovalization really amounts to, it is useful to express it in terms of the maximum bending stress  $\sigma_{\max} = M/\pi a^2 t$ . One finds

$$\frac{w_0}{a} = \left( \frac{\sigma_{\max}}{E} \right)^2 (1 - \nu^2) \frac{a^2}{t^2}$$

In shock struts one may expect  $\sigma_{\max}/E = 0.5 \times 10^{-3}$  or less and perhaps  $t/a = 0.1$ . This yields

$$w_0/a = 0.228 \times 10^{-6}$$

and for  $a = 4$  inches the displacement is  $0.9 \times 10^{-4}$  inch. This is rather small, but one may easily get more by assuming a higher ratio  $a/t$ .

Unless the ovalization is smaller than the clearance between piston and barrel, the piston will locally prevent it. It will exert such radial forces on the wall that at this particular cross section the tube remains almost or completely circular. Since the deviation of the ovalized tube from a circle is  $w_0 \cos 2\theta$ , radial forces proportional to  $\cos 2\theta$  are needed to remove this deformation. Such forces would be negative in two quarters of the circumference, but the piston cannot exert a negative (i.e., inward) pressure on the wall. However, it is

possible to superpose a constant pressure such that the total force per unit of circumference is

$$P = P_0(1 + \cos 2\theta)$$

(see diagram on left in fig. 24). If one neglects the deformation due to direct stress and considers only the bending deformation of the cylinder, this load would really lead to a displacement of the required type. But since the constant term  $P = P_0$  will produce a uniform outward displacement of all points of the cross section, the piston would lose contact on part of the circumference. The real load distribution will therefore look like that shown on the right in figure 24. The deviation from the distribution on the left in figure 24 will be less pronounced the thinner the cylinder is, that is, the more the deformation due to bending of the wall prevails. In any case, when the real load distribution is expanded in a Fourier series, it may be expected that the term with  $\cos 2\theta$  will be predominant.

An exact solution of the problem would require the determination of a radial load

$$P = P_0 + P_2 \cos 2\theta + P_4 \cos 4\theta + \dots$$

to be applied in a certain cross section of the cylinder and satisfying the following condition:

In every point of this cross section there must be either  $P > 0$  and the radial displacement just compensating the one due to ovalization or  $P = 0$  and the radial displacement more than compensating, so that there will be a clearance between cylinder and piston.

Problems of this kind are very hard to solve, in particular if the bending theory of a cylindrical shell is involved. In the present case one may take advantage of the predominance of the second harmonic, and on this basis the following procedure has been worked out:

A line load  $P = P_2 \cos 2\theta$  as shown in figure 25 was applied to a cylindrical shell of infinite length. The bending theory of cylindrical shells was used to find the stresses and in particular the radial displacement of the points of the loaded circle. This is a lengthy computation which is not presented here. It was made for several ratios

of the wall thickness  $t$  of the cylinder to its mean radius  $a$ . The following results were obtained:

$t/a$ , percent	$Ew_2/P_2$
6.00	480
9.33	163.0
10.96	113.0
13.42	67.8
15.50	45.4

Now a ring of width  $b$  is cut from the shell, and the same load  $P = P_2 \cos 2\theta$  is applied to it in its central plane. Using elementary ring theory, one may determine the deflections of this ring, which will also be distributed as  $w = w_2 \cos 2\theta$ . The amplitude  $w_2$  will be inversely proportional to the width  $b$ , and one may choose  $b$  so that the deflection  $w_2$  equals the one obtained for the cylindrical shell. The width  $b$  thus determined is the effective width of the shell with respect to the problem under consideration.

The computation yielded the following values:

$t/a$ , percent	$b/a$
6.00	12.83
9.33	10.10
10.96	8.97
13.42	8.14
15.50	7.91

They are surprisingly large. This indicates that through a direct stress system a rather considerable length of the cylinder cooperates in carrying the load. Real shock-strut cylinders may be expected to be less rigid, because of their finite length.

The values of  $b/a$  may be plotted with  $t/a$  as abscissa (fig. 26) and this curve may be used for all deflection problems in which the second harmonic is preponderant.

The following application may be made of this result. Assume a pressure distribution between piston and barrel as shown in figure 27 and described by the equation

$$P = P_2^* \cos 2\theta$$

applicable for  $-45^\circ < \theta < 45^\circ$  and for  $135^\circ < \theta < 225^\circ$ . From elementary ring theory the following bending moments in a circular ring will be found:

In the loaded parts of the circumference:

$$M = \frac{1}{3} P_2^* a^2 \left[ -\sqrt{2}(1 - \cos \theta) + 2 \sin^2 \theta \right] - M_1$$

In the free parts:

$$M = \frac{1}{3} P_2^* a^2 \left[ 1 - \sqrt{2}(1 - \sin \theta) \right] - M_1$$

with

$$M_1 = 0.1803 P_2^* a^2$$

Neglecting the influence of the direct stress, one may compute from this moment distribution the following outward deflection of the points  $\theta = 0^\circ$  and  $\theta = 180^\circ$ :

$$w = 0.230 \frac{P_2^* a^4}{EI}$$

where  $I = \frac{bt^3}{12}$  is the moment of inertia of the cross section of the ring.

This deflection must be equal to the inward deflection  $w_o$  due to ovalization, which was found to be

$$w_o = (1 - \nu^2) \left( \frac{\sigma_{\max}}{E} \right)^2 \frac{a^3}{t^2}$$

This will yield the maximum  $P_2^*$  of the piston-ring pressure. If the deformation due to direct stress were taken into account, a smaller value for  $P_2^*$  would result.

Now take some typical figures from a shock-strut barrel:

$$a = 4 \text{ in.}$$

$$t = 0.4 \text{ in.}$$

$$E = 3 \times 10^7 \text{ lb/sq in. (steel)}$$

$$\nu = 0.3$$

and assume  $\sigma_{\max}/E = 5 \times 10^4$  and  $b = 5a = 20$  inches. Then

$$I = 0.1067 \text{ in.}^4$$

and

$$P_2^* = 4.94 \text{ lb/in.}$$

The total friction force due to this load is

$$T = 4\mu_s \int_0^{45^\circ} P_2^* \cos 2\theta a \, d\theta = 2\mu_s P_2^* a$$

Assuming, as before, that  $\mu_s = 0.1$ , one has

$$T = 3.94 \text{ lb}$$

which is entirely insignificant.

Going to extremes in  $\sigma_{\max}/E$  and in  $t/a$ , one may get 10 or 20 times this value, but this still would be without significance. One may, therefore, expect that binding of the piston in the cylinder will not be a serious problem except in very unusual designs, and it does not seem necessary to include it in the analysis.

Stanford University,  
Stanford, Calif., April 8, 1953.

## APPENDIX A

PROOF THAT SPRING-BACK MOTION CANNOT BE  
INTERRUPTED BY SLIPPING OF TIRE

When the vertical force is increased linearly with time, the spin-up deflection is given by equations (6). At a certain time  $t = t_t$ , the spin-up is completed and the ensuing spring-back deflection is given by equation (5a). Introducing here  $y(t_t)$  from equations (6) one finds

$$y = \frac{\mu \dot{F}}{k} \left[ \left( t_t - \frac{1}{\lambda} \sin \lambda t_t \right) \cos \lambda' (t - t_t) + \frac{1}{\lambda'} (1 - \cos \lambda t_t) \sin \lambda' (t - t_t) \right]$$

The corresponding drag is, according to equation (5c),

$$D = \frac{I}{I + mr^2} ky$$

and the admissible drag force is  $\mu \dot{F} t$ . It is asked whether the quotient  $D/\mu \dot{F} t$  will always be smaller than 1.

Now,

$$\frac{D}{\mu \dot{F} t} = \frac{I}{I + mr^2} \left[ \left( \frac{t_t}{t} - \frac{1}{\lambda t} \sin \lambda t_t \right) \cos \lambda' (t - t_t) + \frac{1}{\lambda' t} (1 - \cos \lambda t_t) \sin \lambda' (t - t_t) \right]$$

If the bracketed expression is differentiated with respect to time and the result equated to zero, the following relation is obtained:

$$\left( t_t - \frac{1}{\lambda} \sin \lambda t_t \right) \cos \lambda' (t - t_t) + \frac{1}{\lambda'} (1 - \cos \lambda t_t) \sin \lambda' (t - t_t) =$$

$$t(1 - \cos \lambda t_t) \cos \lambda' (t - t_t) - \lambda' t \left( t_t - \frac{1}{\lambda} \sin \lambda t_t \right) \sin \lambda' (t - t_t)$$

This equation is valid at those times  $t$  at which extreme values of  $D/\mu\dot{F}t$  will occur. For these values of  $t$  it may be used to give the right-hand side of the preceding equation another form:

$$\left(\frac{D}{\mu\dot{F}t}\right)_{\text{extr}} = \frac{I}{I + mr^2} \left[ (1 - \cos \lambda t_t) \cos \lambda'(t - t_t) - \frac{\lambda'}{\lambda} (\lambda t_t - \sin \lambda t_t) \sin \lambda'(t - t_t) \right]$$

Since  $y_t$  and  $\dot{y}_t$  are both positive, the first maximum of  $y$  and hence of  $D$  occurs while  $\lambda'(t - t_t) < \pi/2$ ; and, since the denominator is increasing with  $t$ , the maximum of the above quotient must still occur earlier. Then  $\sin \lambda'(t - t_t) \geq 0$  and, since certainly  $\lambda t_t - \sin \lambda t_t > 0$ , the bracketed expression cannot be greater than its first term.

Now,

$$0 \leq 1 - \cos \lambda t_t \leq 2$$

$$0 < \cos \lambda'(t - t_t) < 1$$

Hence the bracketed expression is smaller than 2, and, since  $mr^2 > I$ , the first maximum of the right-hand side is smaller than 1. All following maximums and minimums of  $D$  have the same absolute value, but the admissible drag  $\mu\dot{F}t$  increases continually and the quotient can never again reach the first maximum.

It follows that once the spring-back motion has begun, slipping between tire and ground will never occur again and equation (5a) describes the motion for  $t_t \leq t < \infty$ .

## APPENDIX B

MODIFIED POWER-SERIES SOLUTION FOR LATERAL  
DEFLECTION  $y$  OF SHOCK STRUT

A series solution has been found in the text for the harmonic equation

$$\ddot{y} + \lambda_3^2 y = \kappa_2 x_2$$

where the forcing function or right-hand member is expressed as a power series

$$\kappa_2 x_2 = \kappa_2 \left( b_0 + b_1 \tau + \frac{1}{2} b_2 \tau^2 + \dots \right)$$

The displacement  $y$  represents an oscillation of the mass  $m_3$  on the spring  $k_3$  and will therefore contain the terms  $\cos \lambda_3 \tau$  and  $\sin \lambda_3 \tau$  representing the free vibrations of this spring-mass system. It is therefore not surprising that it cannot be well represented by the first few terms of the power series in  $\tau$  when  $\tau$  approaches the half-period  $\pi/\lambda_3$  of this vibration, and it is desirable to find a better representation of the function  $y(\tau)$ . This is found by splitting off the free vibration, writing

$$y = D_1 \cos \lambda_3 \tau + D_2 \sin \lambda_3 \tau + \sum_0^{\infty} \frac{d_k'}{k!} \tau^{k/2} \quad (B1)$$

When this is introduced into equation (28c), the same expression

$$d_k' = -\lambda_3^2 d_{k-2}' + \kappa_2 b_{k-2} \quad \text{for } k > 1 \quad (B2)$$

results, and  $d_0'$  and  $d_1'$  are again left undetermined. But now there are four coefficients,  $D_1$ ,  $D_2$ ,  $d_0'$ , and  $d_1'$ , which must be chosen so as to satisfy the two initial conditions, and the question arises how to make best use of the arbitrariness thus provided.

Since the differential equation is linear, its solution may be considered as composed of several parts. Each term of the forcing

function produces a forced nonoscillatory motion plus an induced oscillation such that the two together satisfy the initial conditions  $y = \dot{y} = 0$  at  $t = t_0$ . Additional to the sum of all these terms there is the oscillation which satisfies the actual initial conditions. Some of the particular solutions for zero initial conditions are listed below.

Forcing term	Solution $y(t)$
$\kappa_2 b_0$	$\kappa_2 \frac{b_0}{\lambda_3^2} (1 - \cos \lambda_3 \tau)$
$\kappa_2 b_1 \tau$	$\kappa_2 \frac{b_1}{\lambda_3^3} (\lambda_3 \tau - \sin \lambda_3 \tau)$
$\frac{1}{2} \kappa_2 b_2 \tau^2$	$-\kappa_2 \frac{b_2}{\lambda_3^4} (1 - \cos \lambda_3 \tau) + \frac{1}{2} \kappa_2 \frac{b_2}{\lambda_3^2} \tau^2$
$\frac{1}{6} \kappa_2 b_3 \tau^3$	$-\kappa_2 \frac{b_3}{\lambda_3^5} (\lambda_3 \tau - \sin \lambda_3 \tau) + \frac{1}{6} \kappa_2 \frac{b_3}{\lambda_3^2} \tau^3$

In the power-series solution using the coefficients, equations (33), the oscillations due both to nonzero initial conditions and to the forcing terms are expressed in series form, and it is this series which converges slowly.

The solution equation (B1) contains a sine and cosine, and the coefficients  $D_1$  and  $D_2$  may be chosen to put in closed form the oscillation due to nonzero initial conditions plus any desired number of the oscillations due to the forcing terms. Inspection of the solutions listed above shows that the amplitude of the sine or cosine due to a forcing term

$$\kappa_2 \frac{b_k}{k!} \tau^k$$

is

$$\kappa_2 \frac{b_k}{\lambda_3^{k+2}}$$

The  $k + 2$  power of  $\lambda_3$  in the denominator makes the induced oscillations due to the higher terms diminish in importance. Thus it is most advantageous to absorb in the sine and cosine of solution (B1) the two oscillations due to first two forcing terms  $\kappa_2 b_0$  and  $\kappa_2 b_1$ . This is accomplished by choosing

$$D_1 = (y)_n - \kappa_2 \frac{b_0}{\lambda_3^2}$$

$$D_2 = \frac{1}{\lambda_3} (y)_n - \kappa_2 \frac{b_1}{\lambda_3^3}$$

When now the initial conditions are applied to equation (B1), it follows that

$$(y)_n = D_1 + d_0'$$

$$(\dot{y})_n = \lambda_3 D_2 + d_1'$$

Hence:

$$d_0' = \kappa_2 \frac{b_0}{\lambda_3^2}$$

$$d_1' = \kappa_2 \frac{b_1}{\lambda_3^2}$$

Then from equation (B2):

$$d_2' = 0$$

$$d_3' = 0$$

$$d_4' = \kappa_2 b_2$$

$$d_5' = \kappa_2 b_3$$

## REFERENCES

1. Schmitz, G.: Beanspruchungsmessungen am Fahrwerk des Bugradflugzeuges Me 262 bei der Landung (Stress Tests on the Landing Gear of the Nose-Wheel Airplane Me 262 in Landing). Untersuchungen und Mitteilungen Nr. 1391/1, Oct. 13, 1944. (Available in English translation as Translation No. F-TS-966-RE, Air Materiel Command, Army Air Forces, Apr. 1947.)
2. Flügge, W.: Landing-Gear Impact. NACA TN 2743, 1952.
3. Tischbein, Hans W.: Reibung an Kolbenringen (The Friction of Piston Rings). Kraftstoff, vol. 15, Dec. 1939, pp. 83-87; vol. 16, Jan. 1940, pp. 6-8; Feb. 1940, pp. 39-42; Mar. 1940, pp. 71-75. (Available in English translation as NACA TM 1069.)
4. Milne, W. E.: Numerical Calculus. Princeton Univ. Press (Princeton), 1949.

TABLE 1  
COMPUTATIONAL FORM FOR STEP-BY-STEP INTEGRATION

①	②	③	④	⑤	⑥	⑦	⑧	⑨	⑩	⑪	⑫	⑬	⑭	⑮
t	$x_1$	$\dot{x}_1$	$x_2$	x	y	$\dot{y}$	$F_1$	$\dot{x}$	$\dot{x}_2$	$W_1 - F_1$	$\dot{x}_1$	$\ddot{y}$	$\int F_1 dt$	$rw + \dot{y}$
$t_1$	*	*	*	② and ④	*	*	Eq. (16b)	Eq. (16d)	③ and ⑨		Eq. (16a)	Eq. (16c)	⑧	⑦ and ⑭

TABLE 2  
COMPUTATIONAL FORM FOR NUMERICAL INTEGRATION  
USING MILNE AND SIMPSON FORMULAS

①	②	③	④	⑤	⑥	⑦	⑧	⑨	⑩	⑪	⑫	⑬	⑭	⑮
t	$\dot{x}_2$	$x_2$	$\dot{x}_1$	$\dot{x}_1$	$x_1$	$\ddot{y}$	$\dot{y}$	y	x	$F_1$	$\dot{x}$	$W_1 - F_1$	$\int F_1 dt$	$rw + \dot{y}$
$t_0$	(5) and (12)	*	Eq. (16a)	*	*	Eq. (16c)	*	*	⑥ and ③	Eq. (16b)	Eq. (16d)			

TABLE 3  
APPROXIMATE INTEGRATION USING STATIC  $\gamma$  AND LARGE STEPS

t, sec	t - t <sub>0</sub> , sec	$\dot{x}_2$ , in./sec	x <sub>2</sub> , in.	$\ddot{x}_1$ , in./sec <sup>2</sup>	$\dot{x}_1$ , in./sec	x <sub>1</sub> , in.	F <sub>1</sub> , lb	x, in.	F <sub>a</sub> , lb	$\beta$ , lb/in.	0.8ax <sub>2</sub> , lb	$\sqrt{-2}$ , lb	A <sub>3</sub> , sq in.	$\dot{x}$ , in./sec	$\int x_2 dt$ , in. sec
0.0111	0	119.2	1.332	-160.7	119.2	1.332									0.0074
.0311	.02	87.85	3.402	-411	113.48	3.659	42,600	0.257	12,500	3,930	10,710	19,390	0.300	23.63	
.0511	.04	69.23	4.951	-595	105.20	5.841	61,600	.910	12,900	3,710	14,630	34,070	.300	33.97	.1399
.0711	.06	50.21	6.168	-745	89.91	7.767	77,100	1.599	13,350	3,500	17,260	46,490	.300	39.70	.2523
.0911	.08	-19.95	6.598	-796	74.05	9.420	82,500	2.822	14,220	3,175	16,730	51,530	.673	94.0	.3812
	.10	-43.35	5.682	-686	59.15	10.735	71,100	3.053	16,130	2,685	12,190	42,780	.807	102.5	.5072
.1033	.0922	-34.22	6.059	-729	64.96	10.222	75,550	4.185	15,380	2,875	13,970	46,190		99.2	

t, sec	t - t <sub>1</sub> , sec	$\dot{x}_2$ , in./sec	x <sub>2</sub> , in.	$\ddot{x}_1$ , in./sec <sup>2</sup>	$\dot{x}_1$ , in./sec	x <sub>1</sub> , in.	F <sub>1</sub> , lb	x, in.	F <sub>a</sub> , lb	$\beta$ , lb/in.	$\beta \gamma $ , lb	$\sqrt{-2}$ , lb	A <sub>3</sub> , sq in.	$\dot{x}$ , in./sec	$ \gamma $ , in.	$ \cos \lambda_3'(t - t_1) $	$\lambda_3'(t - t_1)$ , deg
0.1033	0	-34.22	6.059	-729	64.96	10.222	75,550	4.185	15,380	2,860	13,810		0.822	99.2	4.85	1	0
.1233	.02	-44.77	5.250	-634	51.33	11.385	65,600	6.135	17,240	2,487	8,820	39,540	.787	96.1	3.545	.734	42.8
.1433	.04	-44.28	4.322	-521	39.72	12.289	54,000	7.967	19,500	2,200	814	33,690	.746	84.0	.370	.0767	85.6
.1633	.06	-26.88	3.592	-433	30.32	12.989	44,900	9.397	21,670	2,005	6,015	17,215	.710	57.2	3.000	.621	128.4
.1833	.08	-14.97	3.210	-387.0	22.10	13.510	40,100	10.300	23,300	1,900	9,060	7,740	.686	37.07	4.77	.988	171.2
.2033	.10	-13.29	2.925	-353.3	14.76	13.879	36,600	10.954	24,610	1,827	7,510	4,680	.668	28.05	4.00	.829	214.0

TABLE 4  
COMPUTATIONAL FORM FOR  $\bar{a}_k$ ,  $\bar{b}_k$ ,  $\bar{c}_k$ , AND  $\bar{f}_k$  IN SINGULAR INTERVAL

(1)	(2)	(3)	(4)	(5)	(6)	(7)	(8)	(9)	(10)	(11)	(12)	(13)
k	$\bar{a}_k$	$\bar{c}_k$	$\bar{d}_k$	$\bar{b}_k$ (2)-(3)	$4(k+1)(k+5)$	$\bar{b}_{k+4}$ -120.7(3)×(6)	$\phi_1 \bar{b}_k$ 0.0506 × (3)	$\theta_0 \bar{a}_k$ 0.3220 $\bar{d}_k$	$\bar{v}_k^a$	$\theta_1 \bar{v}_k$ -0.0256 $\bar{v}_k$	$\bar{f}_k$ (5)-(8) (9)-(11)	$\bar{f}_k/\bar{f}_2$
0	0.9954	0	0.0182	0.9954	12	-1,439						
1	0	0	0	0	32	0						
2	239.0	0	13.09	239.0	60	-1.731 × 10 <sup>6</sup>						
3	0	892.4		-892.4			45.15	4.215	0	0	234.8	
4	-1,439	-1,781	(30,000)	342			-90.12	0	16,24	-0.416	-937.1	-3.991
5	0	-19,900		19,900			-1,007	9,660	-32.41	0.830	-9,229	-39.31
6	-1.731 × 10 <sup>6</sup>	-20,820		0				0	116,400	-2,980	23,890	101.7

$$\bar{v}^a = \sum_{k=0}^k (\bar{b}_k) \bar{a}_{k-v}$$

$$\bar{v}_0 = \bar{c}_0 \bar{d}_0$$

$$\bar{v}_1 = \bar{c}_0 \bar{d}_1 + \bar{c}_1 \bar{d}_0$$

$$\bar{v}_2 = \bar{c}_0 \bar{d}_2 + 2\bar{c}_1 \bar{d}_1 + \bar{c}_2 \bar{d}_0$$

$$\bar{v}_3 = \bar{c}_0 \bar{d}_3 + 3\bar{c}_1 \bar{d}_2 + 3\bar{c}_2 \bar{d}_1 + \bar{c}_3 \bar{d}_0$$

.....

(1)	(2)	(3)	(4)	(5)	(6)	(7)	(8)	(9)	(10)	(11)	(12)	(13)
n	$\phi_1$	$(A_3)_n$	$\sigma_1$	$\bar{f}_2$	$8\bar{f}_2$	$\sqrt{8\bar{f}_2}$	$\kappa_1(A_3)_n$ 68.65 × (3)	$\bar{c}_3$ (7) × (8)	$\frac{\bar{f}_3}{\bar{f}_2}$	$\bar{c}_4$ $\frac{1}{2} \times (9) \times (10)$	$\frac{\bar{f}_4}{\bar{f}_2}$	$\frac{\bar{f}_4}{\bar{f}_2}$
1	0.0506	0.3	0	234.8	1,878	43.34	20.59	892.4	-3.991	-1,781	-39.31	-117.9

(1)	(14)	(15)	(16)	(17)	(18)	(19)	(20)	(21)	(22)	(23)	(24)	(25)
n	$\left(\frac{\bar{f}_2}{\bar{f}_2}\right)^2$	Difference, (15) - (14)	$\bar{c}_5$ $\frac{1}{6} \times (9) \times (15)$	$\frac{\bar{f}_5}{\bar{f}_2}$	$18 \frac{\bar{f}_5}{\bar{f}_2}$	$15 \frac{\bar{f}_5 \bar{f}_4}{\bar{f}_2^2}$ $15 \times (10) \times (12)$	$\left(\frac{\bar{f}_3}{\bar{f}_2}\right)^3$ (10) <sup>3</sup>	$5 \frac{\bar{f}_5^3}{\bar{f}_2^3}$	$\bar{c}_6$ $\frac{(4) \times (9)}{(3)}$	360 $\bar{c}_5$	Sum, (18) - (19) + (21) + (23)	$\bar{c}_6$ $\frac{1}{36} (9) \times (24)$
1	15.93	-133.8	-19,900	101.7	1,831	2,333	-63.58	-317.9	0	0	-839.9	-20,820

TABLE 5  
COMPUTATIONAL FORM FOR  $a_k$ ,  $b_k$ , AND  $\beta_k$  IN REGULAR INTERVAL

(1)	(2)	(3)	(4)	(5)	(6)	(7)	(8)	(9)	(10)	(11)	(12)	(13)	(14)	(15)	(16)
$n - k$	$a_k$	$c_k$	$d_k$	$b_k$ (2)-(3)	$a_{k+2}$ $-120.7 \times$ (5)	$\phi_1$	$\phi_1 c_k$	$\theta_0$	$\theta_0 d_k$	$\theta_1$	$\psi_k^a$	$\theta_1 \psi_k$	$\beta_k$ (7)-(8) (11)-(13)	$\eta_1$	$\eta_1 \beta_k$
2 - 0	4.469	0.679	1.427	3.790	-457.4	0.0506	0.0344	0.3220	0.4595	-0.0256	0.9689	-0.0248	3.321	0.2142	
1	110.6	31.46	94.85	79.14	-9,552	↓	1.592	↓	30.54	↓	109.3	-2.798	49.81	↓	10.67
2	-457.4	335.7	(2,000)	-795.1	95,730	↓	16.99	↓	644	↓	7,805	-199.8	-1,254	↓	-268.6
3	-9,552	-12,050	0	2,478	-299,100	↓	-608.7	↓	0	↓	267,100	-6,838	9,925	↓	2,126
4	95,730	$4.521 \times 10^5$	0	0	0	↓	0	↓	0	↓	0	0	0	↓	0
5	-299,100	0	0	0	0	↓	0	↓	0	↓	0	0	0	↓	0
3 - 0	8.245	2.056	6.213	6.209	-749.4	0.0600	0.1222	0.3112	1.933	-0.0203	12.65	-0.257	4.411	0.1452	
1	87.32	38.22	119.7	49.10	-5,926	↓	2.295	↓	37.25	↓	481.2	-9.768	19.33	↓	2.807
2	-749.4	2,935	(-3,540)	-3,684	$4.447 \times 10^5$	↓	176.1	↓	-1,102	↓	20,180	-409.6	-2548	↓	-340.9
3	-5,926	169,900	0	-175,800	$2.122 \times 10^7$	↓	10,190	↓	0	↓	$1.704 \times 10^6$	-34,590	-151,400	↓	-21,980
4	$4.447 \times 10^5$	$-1.179 \times 10^6$	0	0	0	↓	0	↓	0	↓	0	0	0	↓	0
5	$2.122 \times 10^7$	0	0	0	0	↓	0	↓	0	↓	0	0	0	↓	0
4 - 0	9.684	3.350	7.802	6.334	-764.5	0.0684	0.2811	0.2921	2.279	-0.0146	26.13	-0.381	4.155	0.1530	
1	75.47	103.2	48.17	-29.7	3,585	↓	8.669	↓	14.07	↓	966.6	-14.11	-58.33	↓	-5.864
2	-764.5	-851.0	(-7,600)	66.5	-8,026	↓	-69.80	↓	-2,220	↓	-22,000	321.2	2,035	↓	311.4
3	3,585	33,050	0	-29,470	$3.557 \times 10^6$	↓	2,776	↓	0	↓	$-2.215 \times 10^6$	32,340	-64,590	↓	-9,882
4	-8,026	-808,900	0	0	0	↓	0	↓	0	↓	0	0	0	↓	0
5	$3.557 \times 10^6$	0	0	0	0	↓	0	↓	0	↓	0	0	0	↓	0
5 - 0	12.57	8.156	0	4.41	-532.3	0.152	1.240	0.2517	0	-0.0095	0	0	3.170	0.1772	
1	39.26	86.47	297.3	-47.21	5,698	↓	13.14	↓	74.85	↓	2,425	-25.04	-112.1	↓	-19.86
2	-532.3	-1,994	0	1,462	-176,500	↓	-305.1	↓	0	↓	51,400	-488.5	2,255	↓	399.2
3	5,698	17,790	(-369,000)	-12,090	$1.459 \times 10^6$	↓	2,704	↓	-92,880	↓	$-4.788 \times 10^6$	45,490	32,600	↓	5,777
4	-176,500	83,360	0	0	0	↓	0	↓	0	↓	0	0	0	↓	0
5	$1.459 \times 10^6$	0	0	0	0	↓	0	↓	0	↓	0	0	0	↓	0

$$\psi_k = \sum_{v=0}^k (5) a_v d_{k-v}$$

$$\psi_0 = c_0 d_0$$

$$\psi_1 = c_0 d_1 + c_1 d_0$$

$$\psi_2 = c_0 d_2 + 2c_1 d_1 + c_2 d_0$$

$$\psi_3 = c_0 d_3 + 3c_1 d_2 + 3c_2 d_1 + c_3 d_0$$

.....

TABLE 6  
COMPUTATIONAL FORM FOR  $\alpha_k$ ,  $\alpha_k$ , AND  $\eta_1$  IN REGULAR INTERVAL

(1)	(2)	(3)	(4)	(5)	(6)	(7)	(8)	(9)
n	$\phi_0$	$(A_3)_n$	$\sigma_1$	$\sigma_2$	$\beta_0$	$\beta_0 - \phi_0$	$\sqrt{(7)}$	$*1(A_3)_n,$ $68.63 \times (3)$
2	0.9870	0.3	0	0	3.321	2.334	1.528	20.59
3	0.968	0.3	1.976	-0.892	4.411	3.443	1.856	20.59
4	0.887	0.832	-0.0212	0	4.155	3.268	1.808	57.10
5	0.348	0.730	-0.0370	0	3.170	2.822	1.680	51.47

(1)	(10)	(11)	(12)	(13)	(14)	(15)	(16)	(17)
n	$\alpha_1,$ (8) x (9)	$\eta_1,$ $1/2 \times (7)$	$\eta_1 \beta_1$	$\alpha_1,$ (4) x (10)	$\alpha_1 + \eta_1 \beta_1$	$\alpha_2,$ (10) x (14)	$\alpha_1 \alpha_2,$ (4) x (15)	$\alpha_2 \alpha_1^2,$ (3) x (10) x (10)
2	31.46	0.2142	10.67	0	10.67	335.7	0	0
3	38.22	0.1432	2.807	73.99	76.80	2,955	5,682	-1,305
4	103.2	0.1530	-5.864	-2.188	-8.052	-851.0	17.62	0
5	86.47	0.1772	-19.86	-3.199	-23.06	-1,994	73.78	0

(1)	(18)	(19)	(20)	(21)	(22)	(23)	(24)	(25)
n	$\alpha_2,$ (16) + (17)	$2\alpha_1 \eta_1 \beta_1,$ $2 \times (12) \times (13)$	$\eta_1 \beta_2$	$\eta_1^2 \beta_1^2,$ (12) x (12)	$\alpha_1,$ (20) - (21)	Sum, (18) + (19) + (22)	$\alpha_3,$ (10) x (23)	$3\alpha_2 \alpha_1 \alpha_2,$ $3 \times (5) \times (10) \times (15)$
2	0	0	-268.6	113.8	-382.4	-382.4	-12,050	0
3	4,379	415.4	-340.9	7.879	-348.8	4,445	169,900	-300,200
4	17.62	25.66	311.4	34.39	277.0	320.3	55,050	0
5	73.78	127.1	559.2	394.4	4.6	205.7	17,790	0

(1)	(26)	(27)	(28)	(29)	(30)	(31)	(32)	(33)
n	$\alpha_1 \alpha_3,$ (4) x (24)	$\alpha_3,$ (25) + (26)	$3\alpha_2 \eta_1 \beta_1,$ $3 \times (12) \times (12)$	$\alpha_2,$ (13) - (12)	$3\alpha_1 \alpha_2,$ $3 \times (22) \times (23)$	$\eta_1 \beta_3$	Sum, (27) + (28) + (30) + (31)	$\alpha_4,$ (10) x (32)
2	0	0	0	-10.67	12,240	2,126	14,370	$4.521 \times 10^5$
3	328,900	28,700	36,880	71.18	-74,450	-21,980	-30,850	$-1.179 \times 10^6$
4	-700.7	-700.7	-509.9	3.676	3,055	-9,882	-7,858	-808,900
5	-658.2	-658.2	-4,395	16.66	239.9	5,777	964	85,360

TABLE 7  
PARAMETERS FOR APPROXIMATE REPRESENTATION OF  
FUNCTIONS  $f_1(x)$ ,  $f_2(x)$ , AND  $A_3(x)$

$$\left[ f_1(x) = \phi_0 + \phi_1 x; f_2(x) = \theta_0 + \theta_1 x; \right.$$

$$A_3(x) = (A_3)_n \left( 1 + \sigma_1 \xi + \frac{1}{2} \sigma_2 \xi^2 \right)$$

$$\left. \xi = x - (x)_n \right]$$

Interval	$\phi_0$	$\phi_1$	$(A_3)_n$	$\sigma_1$	$\sigma_2$	$\theta_0$	$\theta_1$
1,2	0.987	0.0506	0.3	0	0	0.3220	-0.0256
3	.968	.060	.3	1.936	-.892	.3112	-.0203
4	.887	.084	.832	-.0212	0	.2921	-.0146
5	.348	.152	.750	-.0370	0	.2517	-.0095
6	-1.254	.285	.639	-.0469	0		

TABLE 8  
SOLUTION FOR EXAMPLE ILLUSTRATING ANALYTIC METHOD

## Phase one

Interval 0:  $0 < t < 0.00829$  sec

$$x_1 = 120t(1 - 20.12t^2 + \dots)$$

$$x = 0$$

$$y = 32,140t^3(1 - 106.4t^2 + \dots)$$

$$\omega = 10,930t^2\left(1 - \frac{1}{12}t^2 + \dots\right)$$

## Phase two

Interval 1:  $0.00829 < t < 0.03829$  sec;  $0 < x < 0.679$  in.

$$x_1 = 0.9934 \cos 10.99\tau + 10.87 \sin 10.99\tau + 2,052\tau^{7/2} - 746.4\tau^4 + \dots$$

$$x = 148.7\tau^{3/2} - 74.21\tau^2 - 165.8\tau^{5/2} - 28.92\tau^3 + \dots$$

$$y = -0.7768 \cos 44.81\tau - 1.988 \sin 44.81\tau + 0.7950 + 95.65\tau - 27,320\tau^{7/2} + 1,908\tau^4 + \dots$$

$$\omega = 182.2\left(0.9934\tau + 59.75\tau^2 - 59.48\tau^{5/2} + \dots\right) + 0.751$$

Interval 2:  $0.03829 < t < 0.0761$ ;  $0.679 < x < 2.036$ 

$$x_1 = 4.469 + 110.6\tau - 228.7\tau^2 - 1,592\tau^3 + 3,989\tau^4 - 2,492\tau^5 + \dots$$

$$x = 0.679 + 31.46\tau + 167.8\tau^2 - 2,005\tau^3 + 18,840\tau^4 + \dots$$

$$y = 0.7040 \sin 44.81\tau - 1.605 \cos 44.81\tau + 3.032 + 63.31\tau - 53,100\tau^4 + 33,180\tau^5 + \dots$$

$$\omega = 182.2\left(3.790\tau + 39.57\tau^2 - 132.2\tau^3 + 103.2\tau^4 + \dots\right) + 14.29$$

TABLE 8.- Continued

## SOLUTION FOR EXAMPLE ILLUSTRATING ANALYTIC METHOD

Interval 3:  $0.0761 < t < 0.0940$ ;  $2.036 < x < 3.350$ 

$$x_1 = 8.245 + 87.32\tau - 374.7\tau^2 - 987.7\tau^3 + 18,530\tau^4 + 176,800\tau^5 + \dots$$

$$x = 2.036 + 38.22\tau + 1,468\tau^2 + 28,320\tau^3 - 49,120\tau^4 + \dots$$

$$y = 1.795 \sin 44.81\tau + 1.246 \cos 44.81\tau + 4.967 + 39.28\tau - 246,700\tau^4 - 2.345 \times 10^6\tau^5 + \dots$$

$$\omega = 182.2(6.209\tau + 24.55\tau^2 - 614\tau^3 + \dots) + 49.4$$

Interval 4:  $0.0940 < t < 0.1464$ ;  $3.350 < x < 8.126$ 

$$x_1 = 9.684 + 73.47\tau - 382.2\tau^2 + 597.5\tau^3 - 334.4\tau^4 + 29640\tau^5 + \dots$$

$$x = 3.350 + 103.2\tau - 415.5\tau^2 + 5,508\tau^3 - 33,700\tau^4 + \dots$$

$$y = 2.735 \cos 44.81\tau + 1.605 \sin 44.81\tau + 5.067 + 23.76\tau + 4,453\tau^4 + \dots$$

$$\omega = 182.2(6.334\tau - 14.85\tau^2 + 11.08\tau^3 + \dots) + 70.4$$

Phase three

Interval 4 (continued):  $t_t = 0.1073$ 

Same as before except:

$$y = 7.915 \cos 37.32\tau' - 0.884 \sin 37.32\tau' \quad (\tau' = t - t_t)$$

$$\omega = \frac{1,672 - \dot{y}}{20}$$

## TABLE 8.- Concluded

## SOLUTION FOR EXAMPLE ILLUSTRATING ANALYTIC METHOD

Interval 5:  $0.1464 < t < \dots$ ;  $8.156 < x < \dots$

$$x_1 = 12.57 + 39.26\tau - 266.2\tau^2 + 9,497\tau^3 - 7,354\tau^4 + 12,160\tau^5 + \dots$$

$$x = 8.156 + 86.47\tau - 997\tau^2 + 2,965\tau^3 + 34,730\tau^4 + \dots$$

$$y = 7.966 \sin 37.32\tau$$

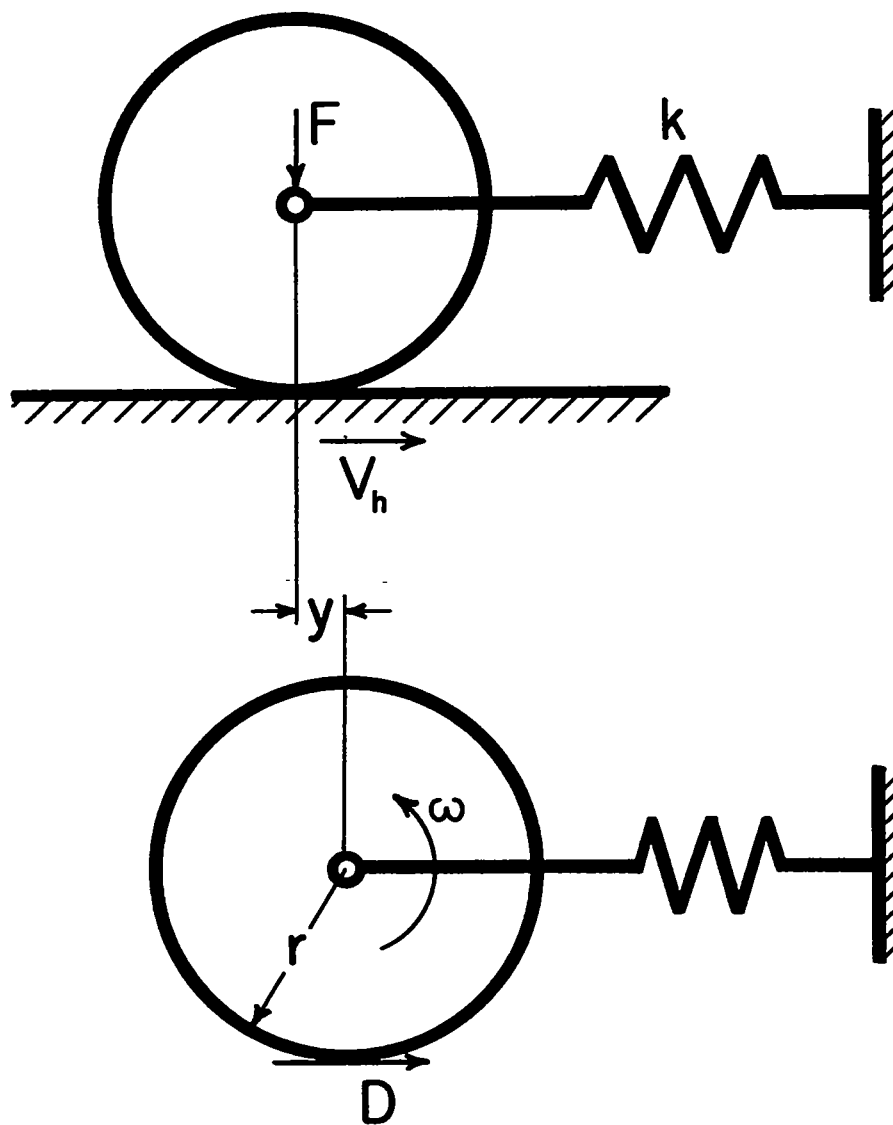


Figure 1.- Wheel with horizontal constraint.

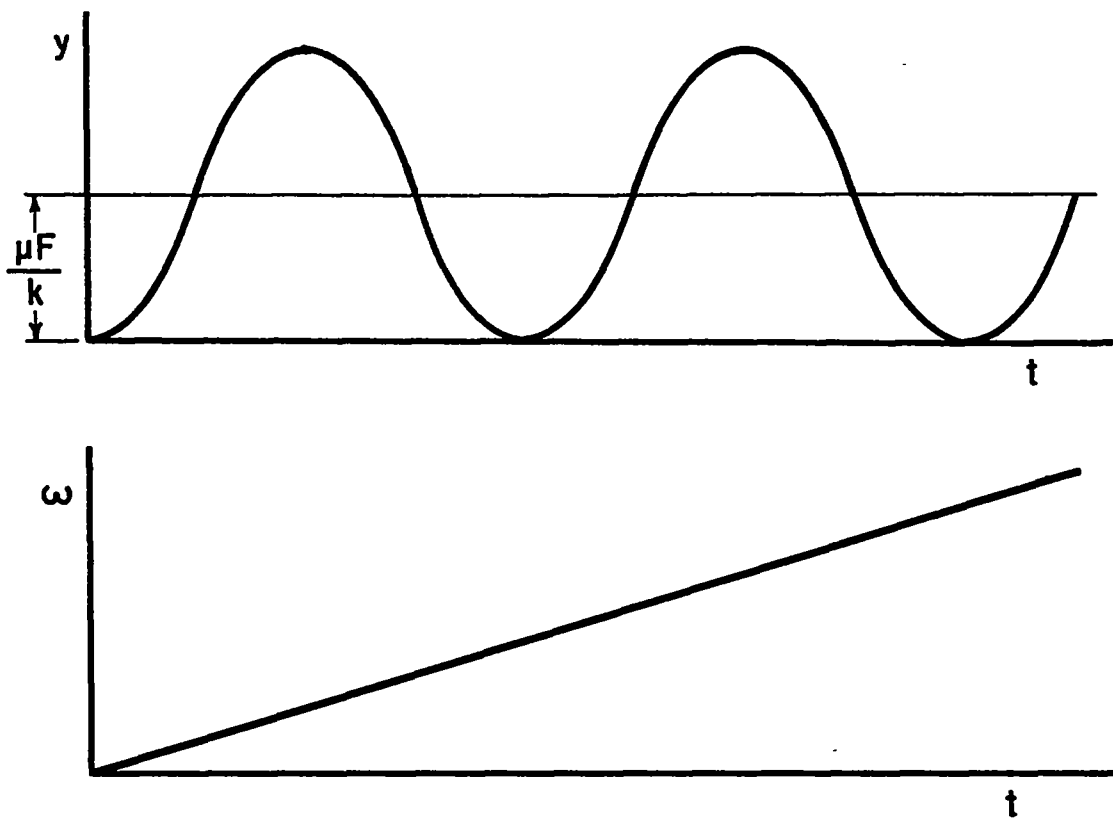


Figure 2.- Horizontal movement of wheel during spin-up.

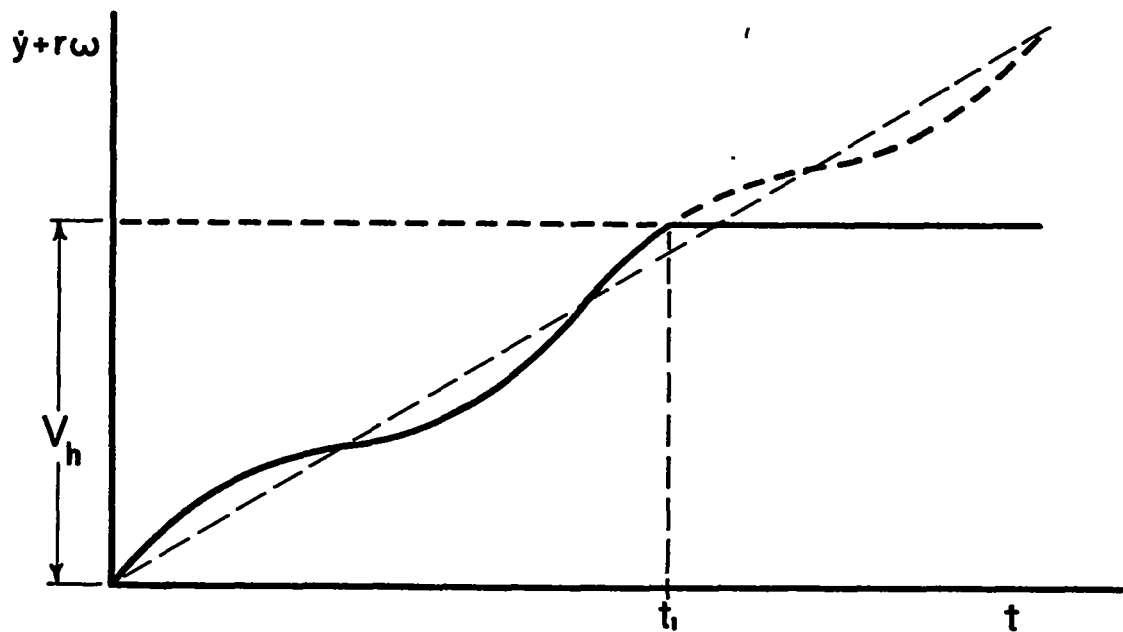


Figure 3.- Spinning-up of wheel.

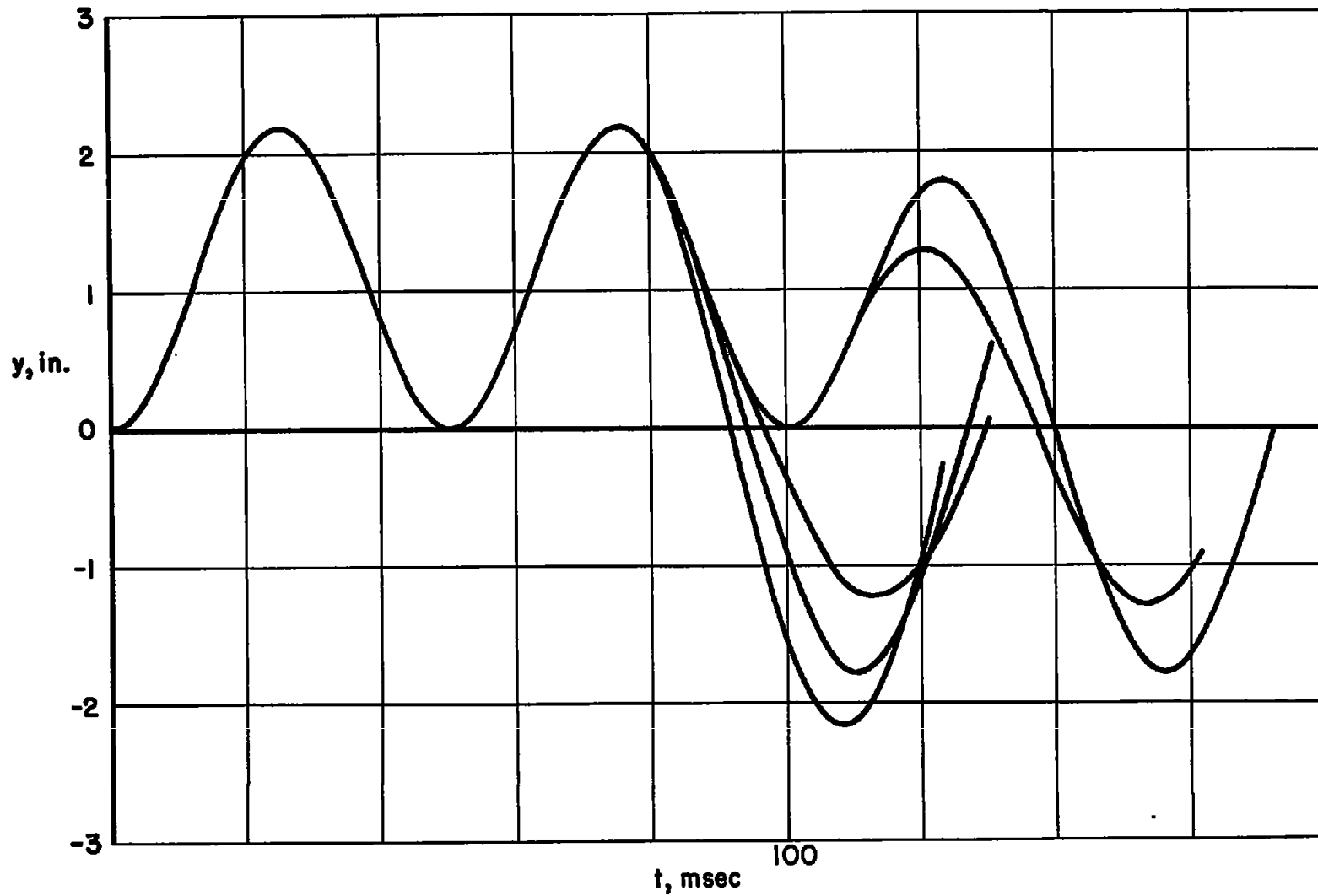


Figure 4.- Horizontal deflection  $y$  for different spin-up times  $t_t$ .  
Constant load.

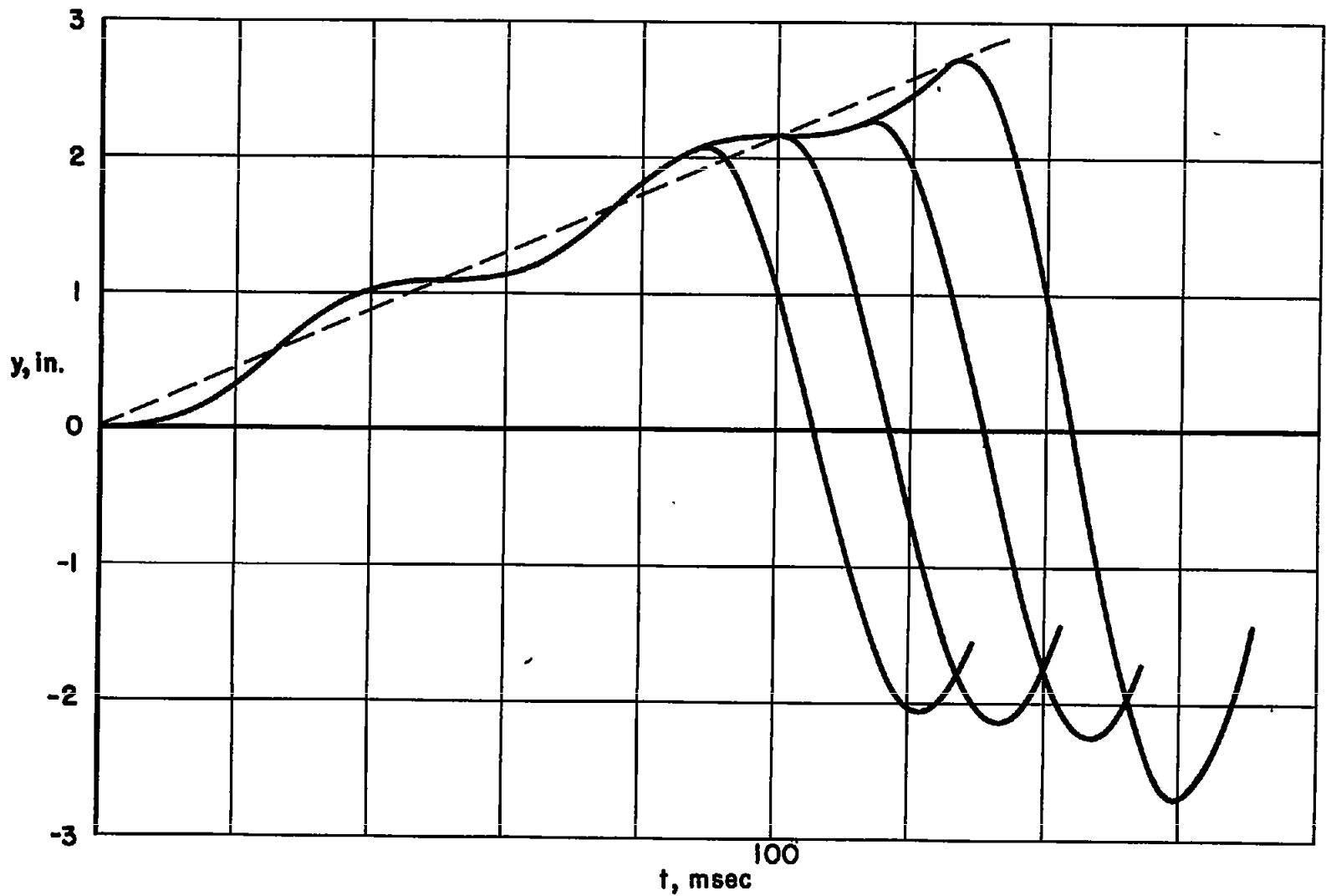


Figure 5.- Horizontal deflection  $y$  for different spin-up times  $t_t$ .  
Linearly increasing load.

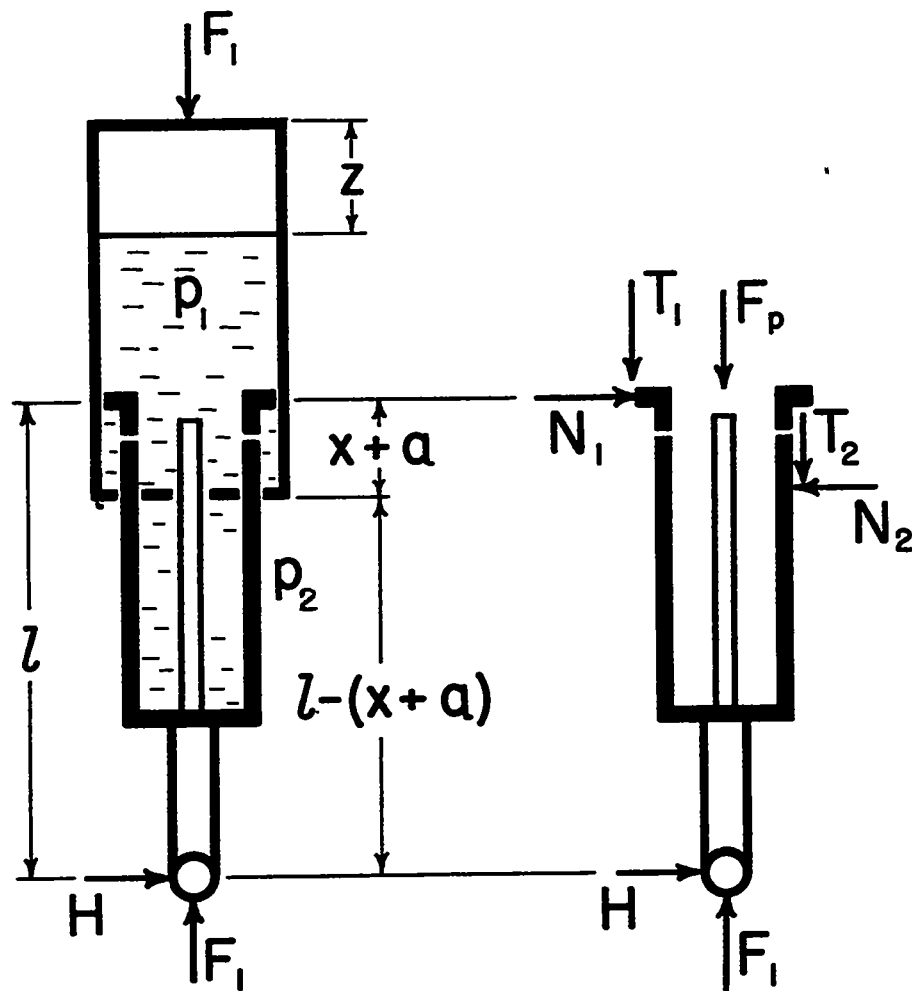


Figure 6.- Forces in oleo shock strut.

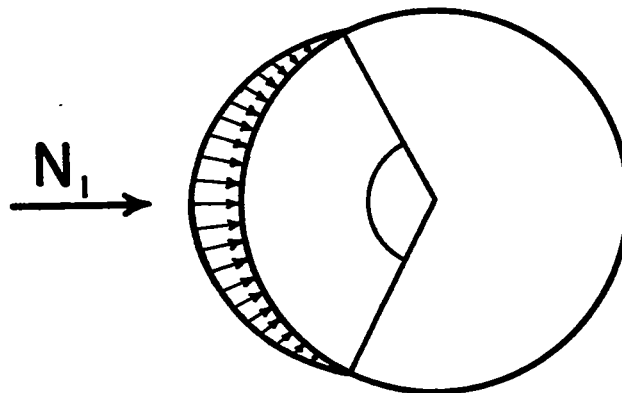


Figure 7.- Forces between piston and barrel.

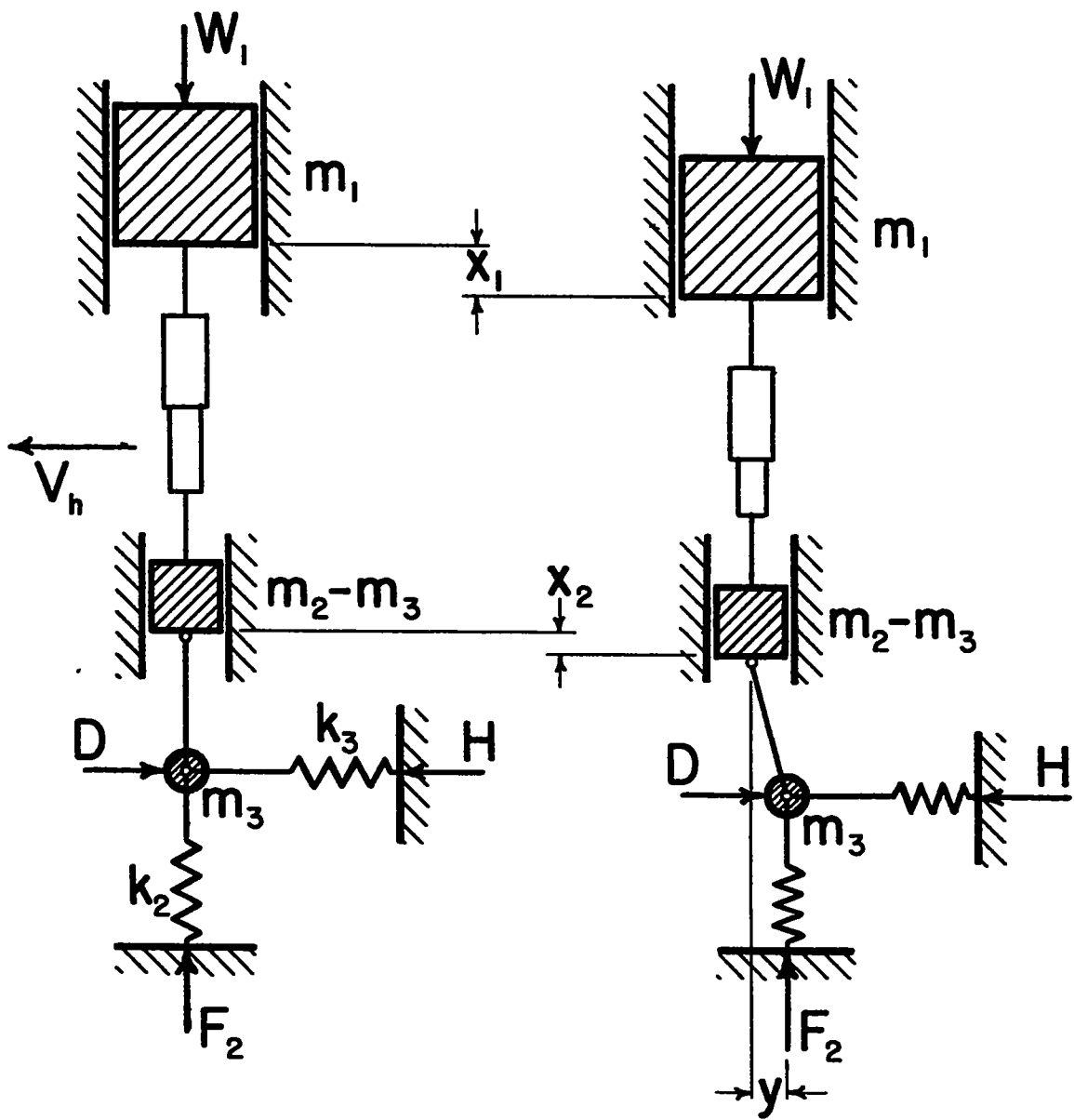


Figure 8.- Mass-spring model of landing gear.

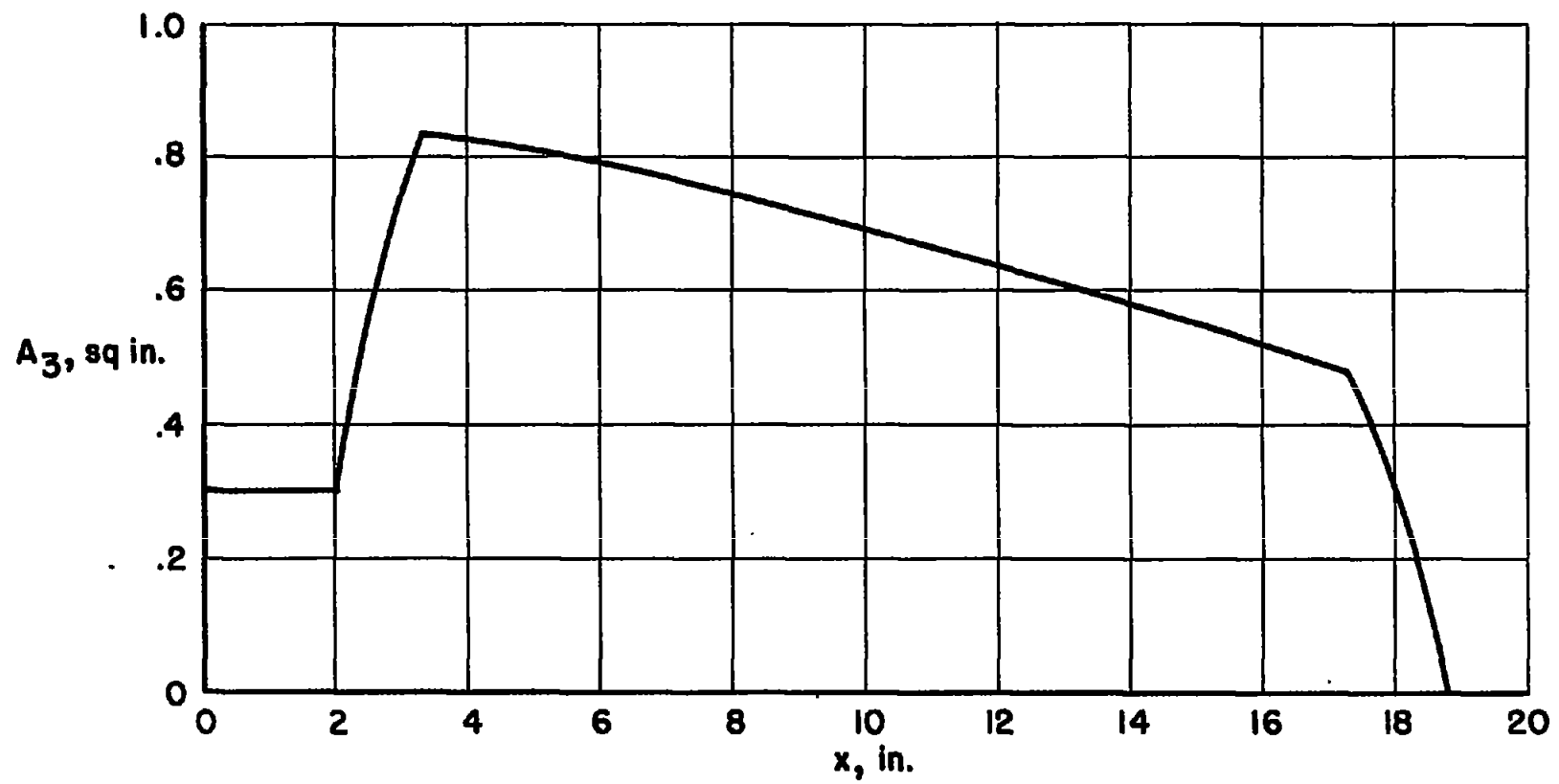


Figure 9.- Graph of orifice area  $A_3$  versus stroke  $x$ .

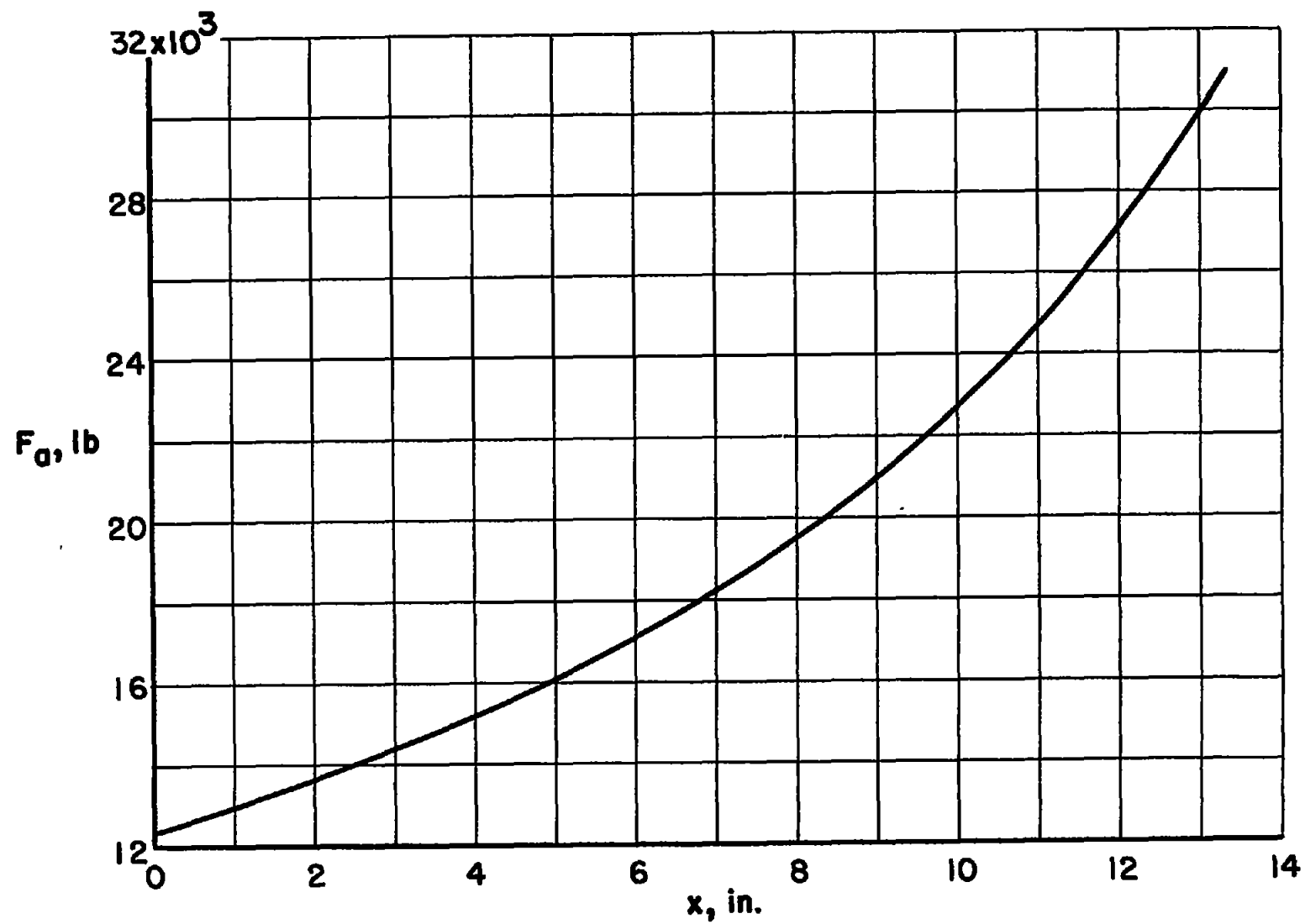


Figure 10.- Graph of air force  $F_a$  versus stroke  $x$ .

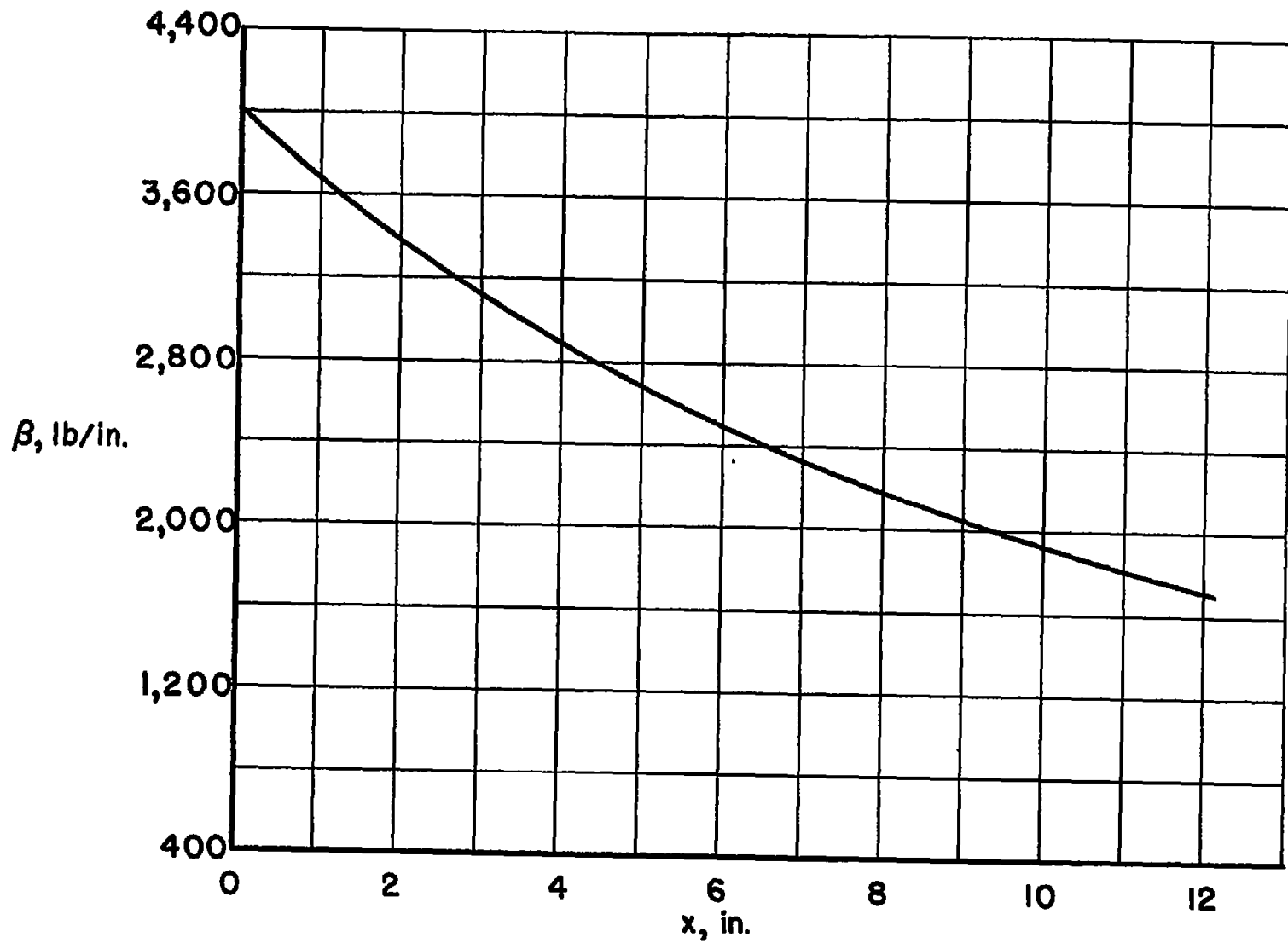


Figure 11.- Graph of factor  $\beta$  used in equation (1.7) versus stroke  $x$ .

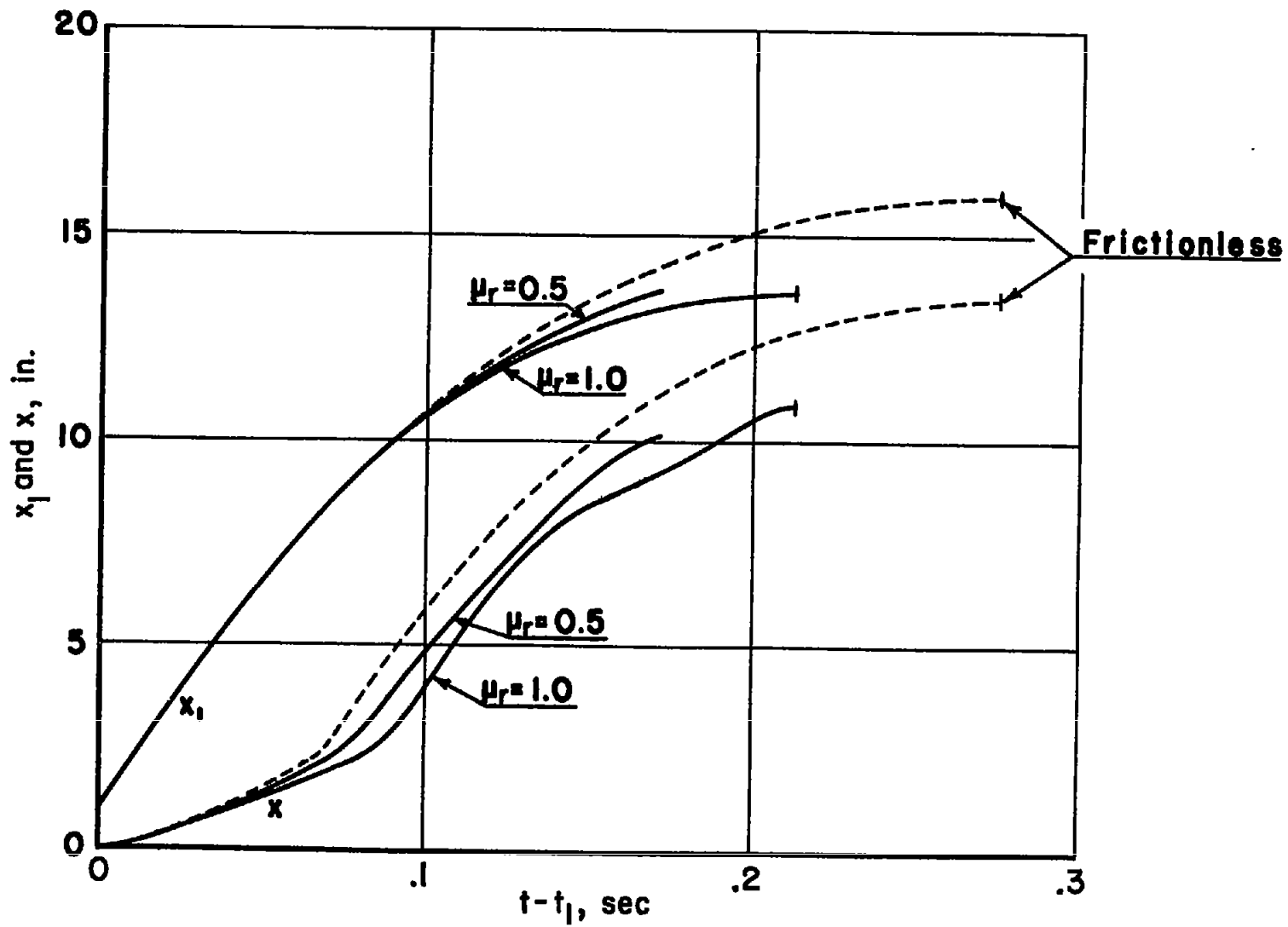


Figure 12.- Displacement  $x_1$  and stroke  $x$  for different values of  $\mu_r$ .

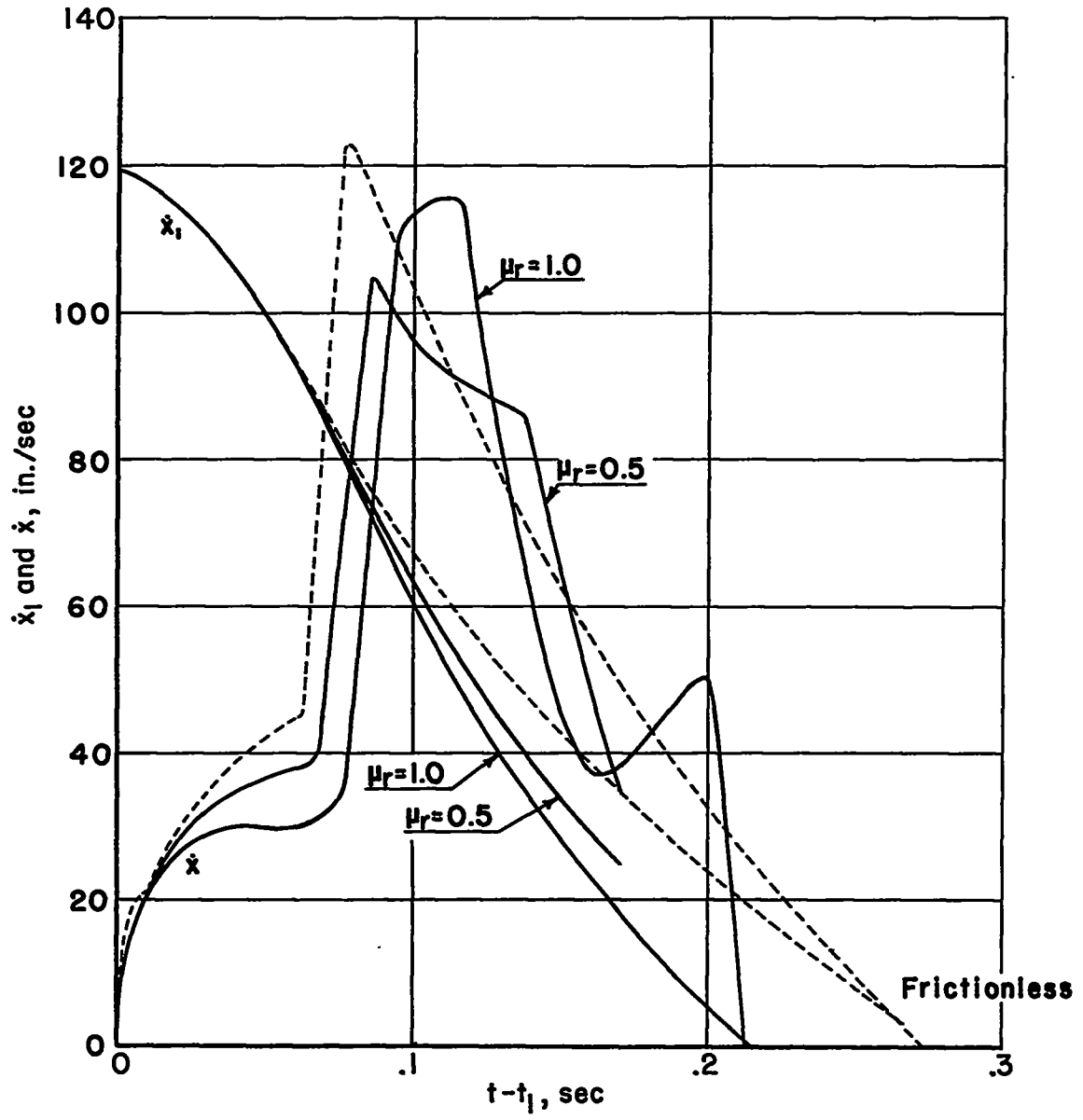


Figure 13.- Vertical velocity  $\dot{x}_1$  and rate of stroke  $\dot{x}$  for different values of  $\mu_r$ .

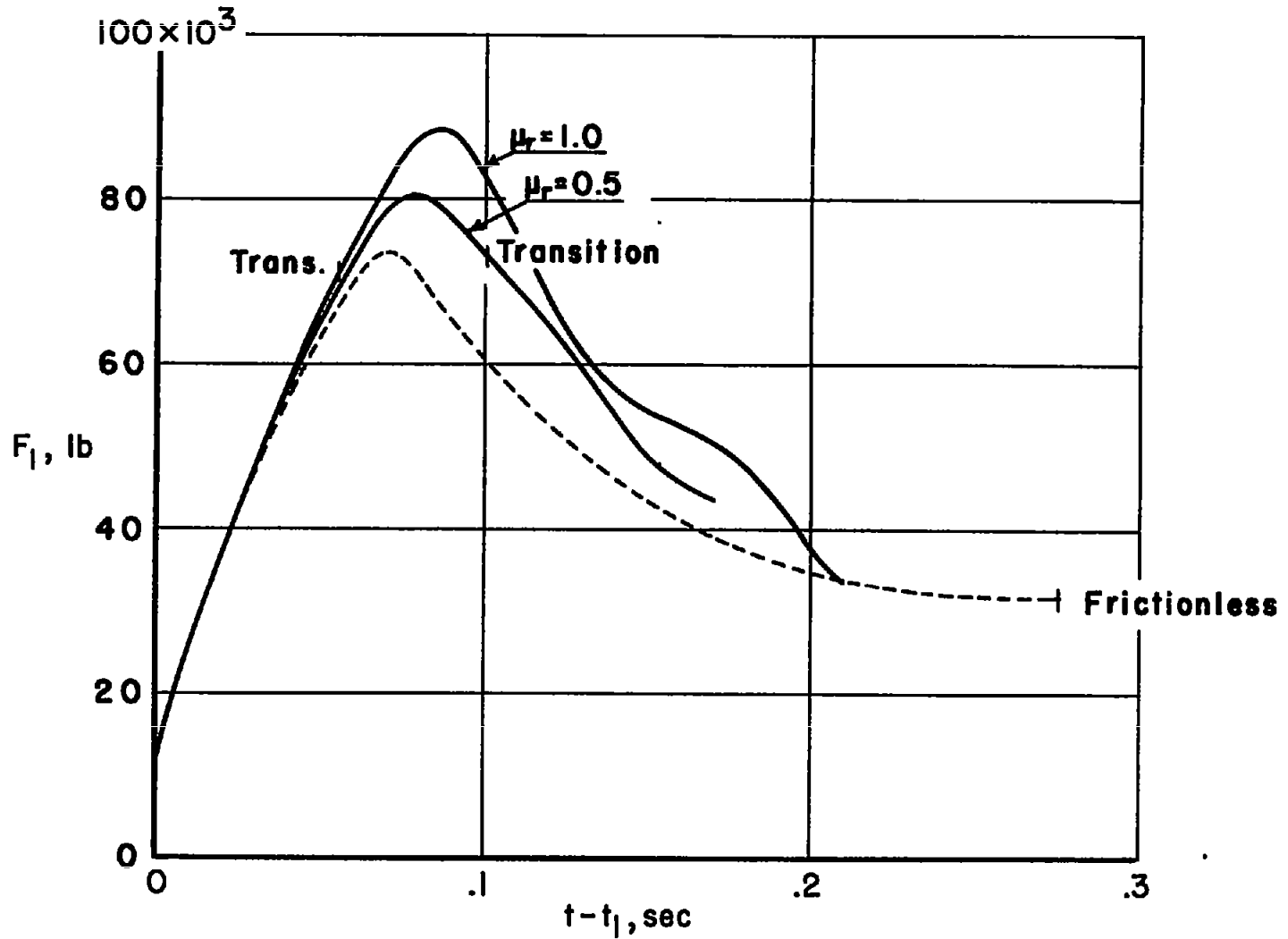


Figure 14.- Time history of impact force  $F_1$ . Transition point indicates time when wheel is spun up.

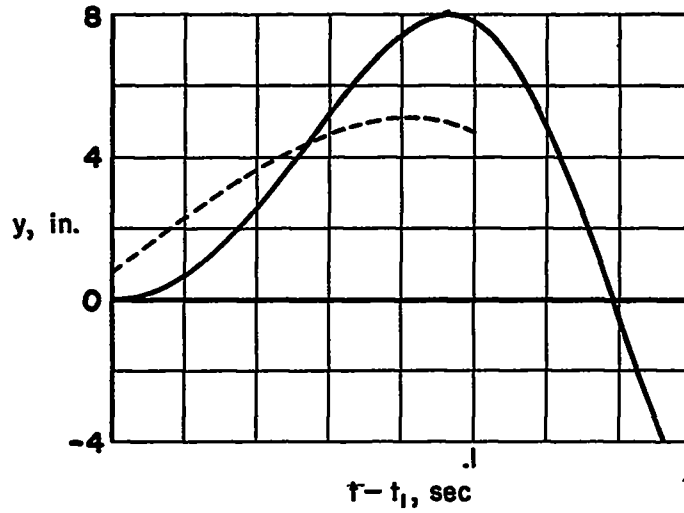


Figure 15.- Lateral deflection  $y$  of the shock strut. Solid line, exact values; broken line, static values.

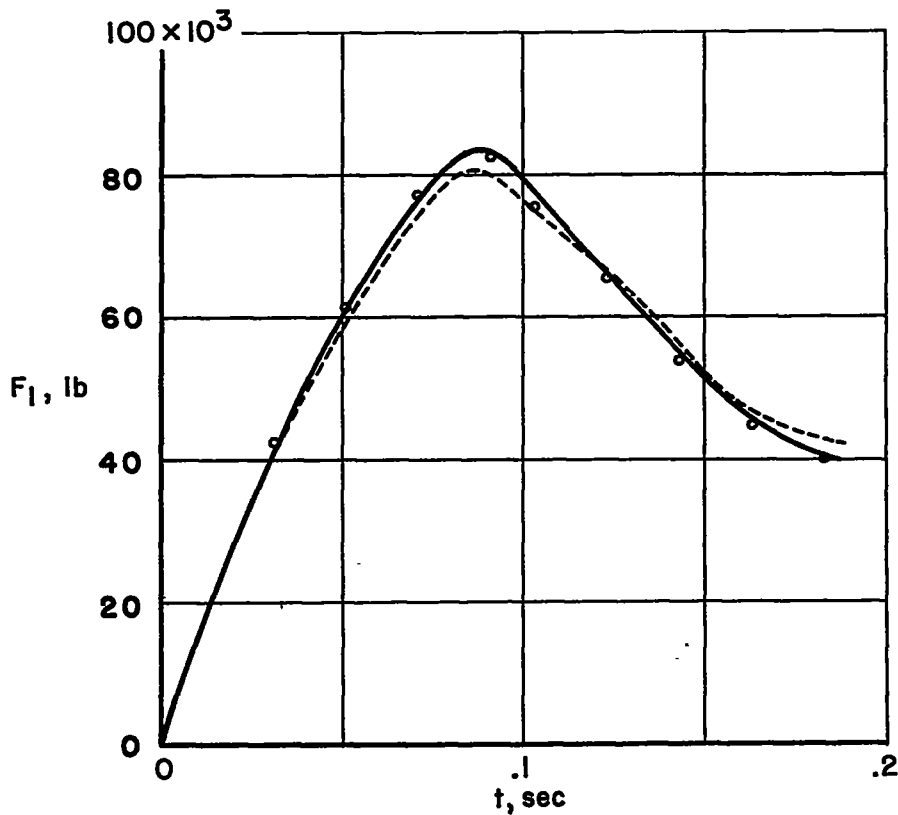


Figure 16.- Time history of impact force  $F_1$ . Broken line, exact values from figure 14; solid line, approximation based on static  $y$ ; circles, same approximation but from a large-step integration.

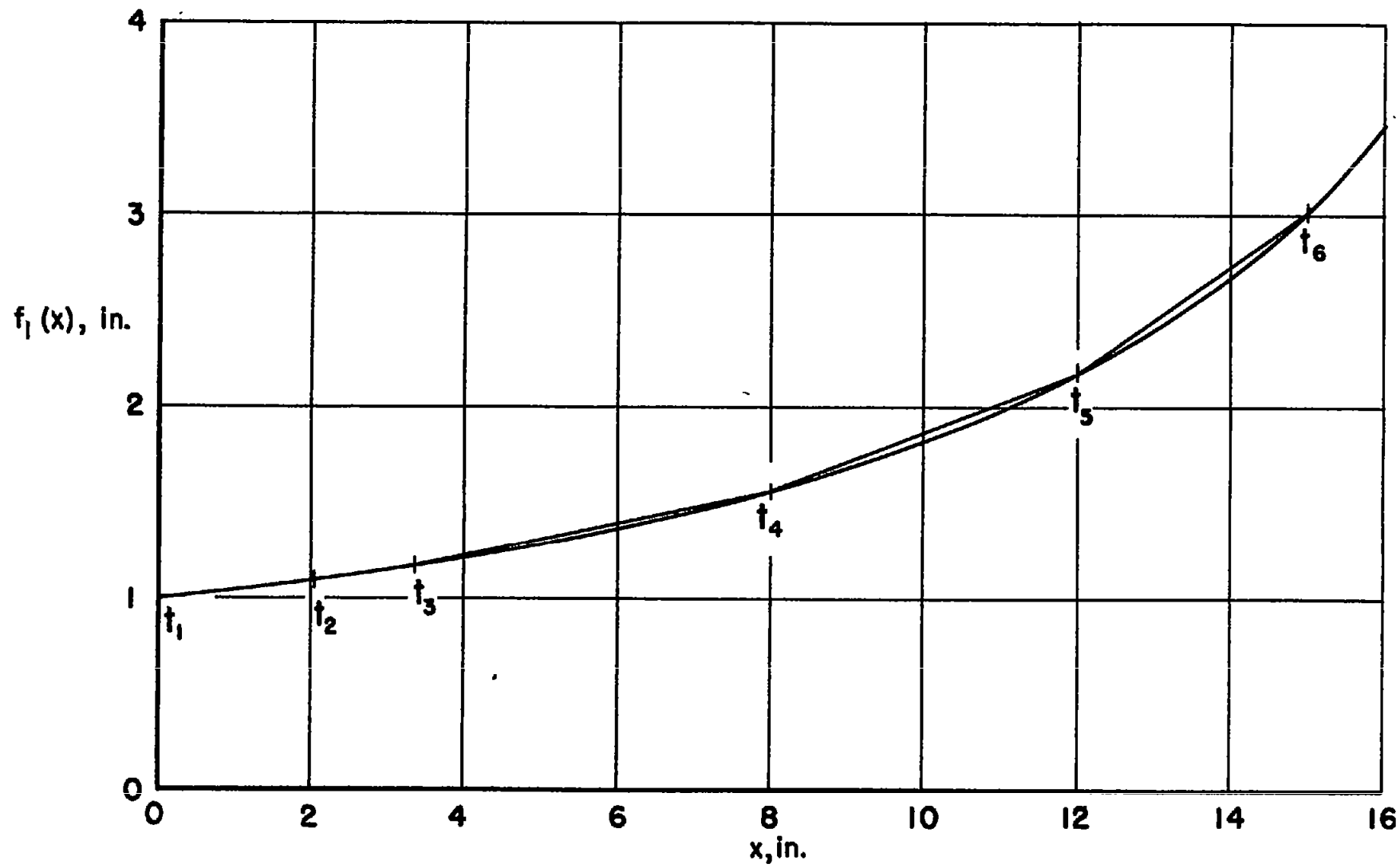


Figure 17.- Straight-line approximation of  $f_1(x)$ , equation (24).

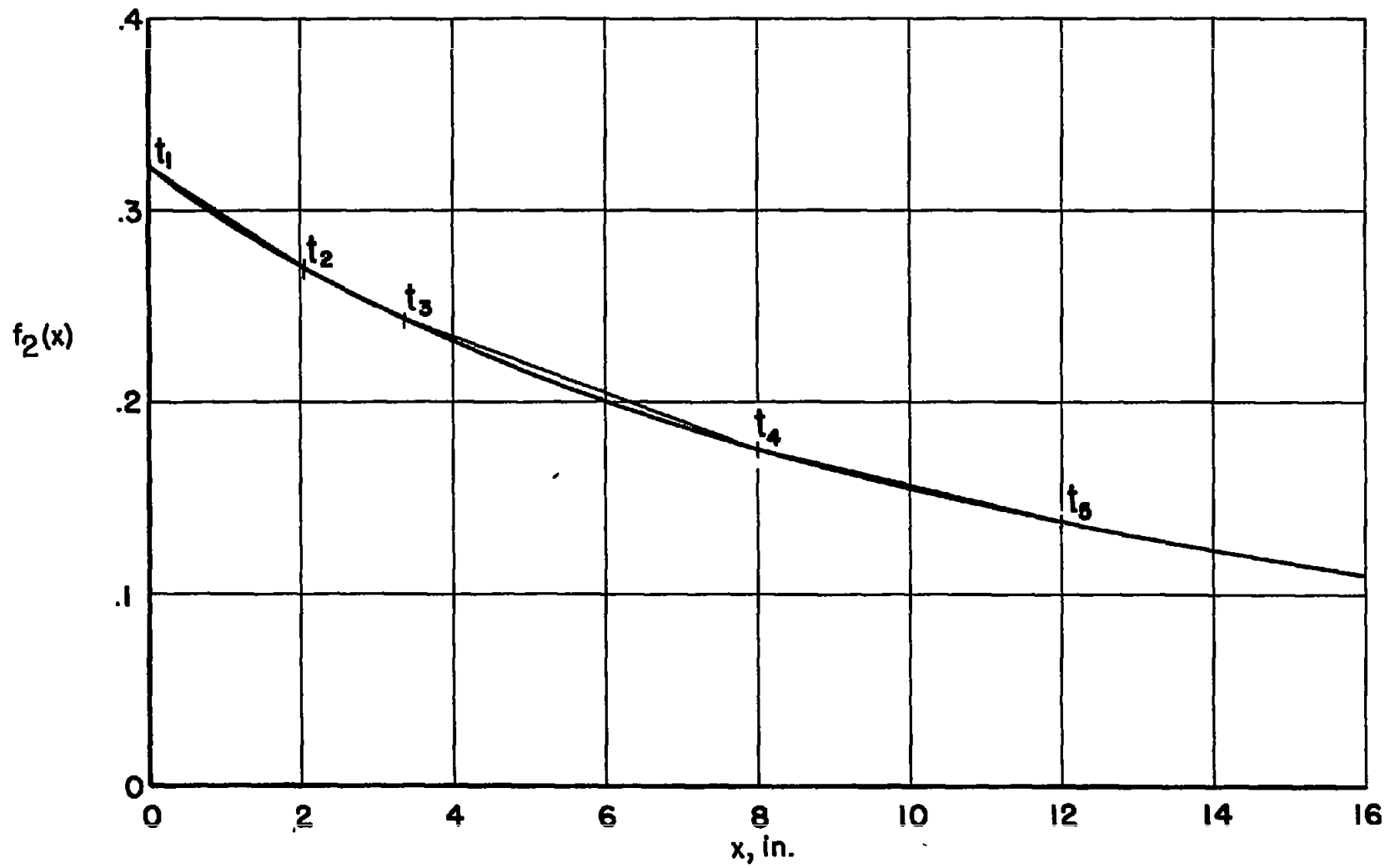


Figure 18.- Straight-line approximation of  $f_2(x)$ , equation (25).

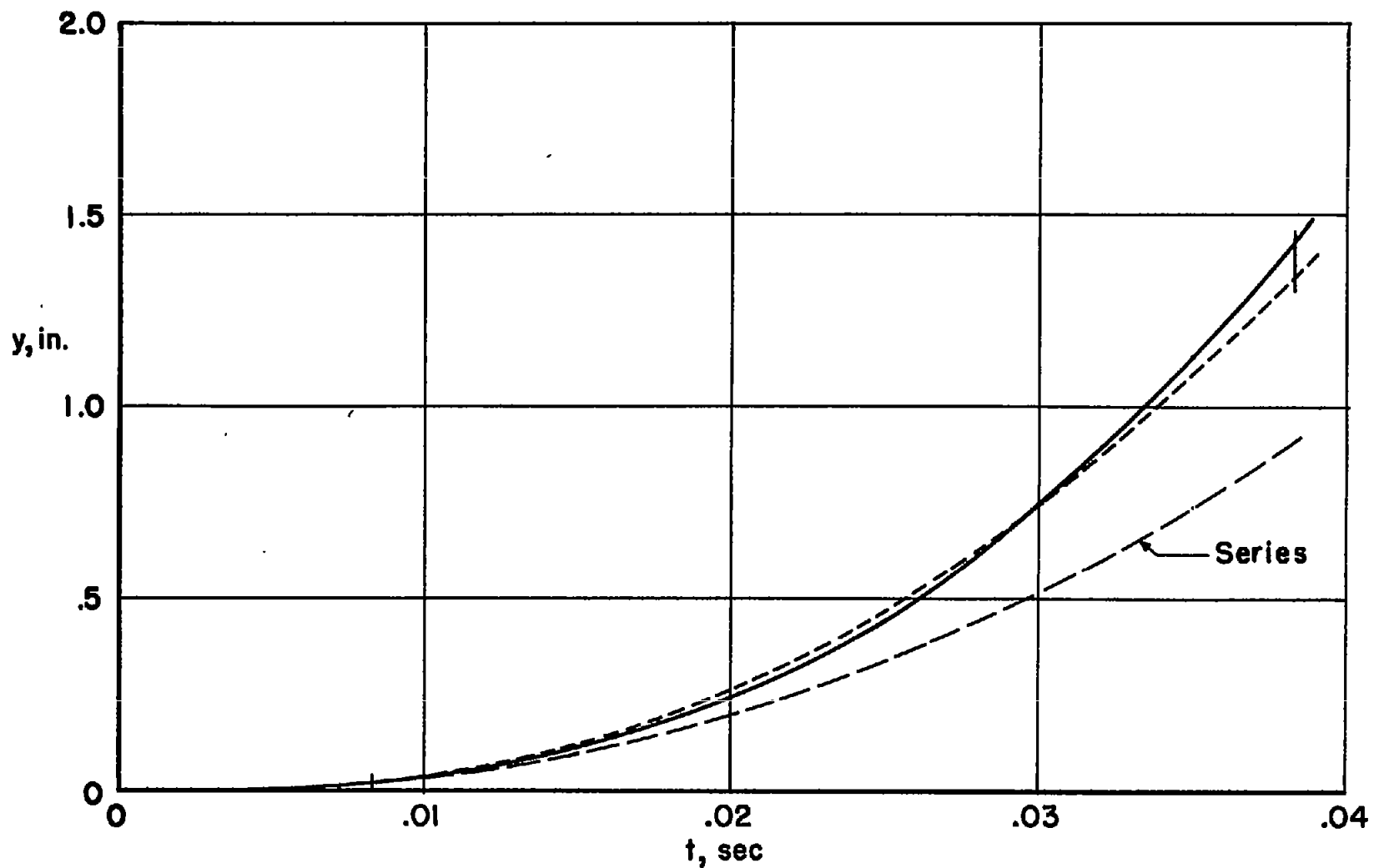


Figure 19.- Approximations for  $y$ . Solid line, equation (48); short dashes, equation (49); long dashes, equation (41).

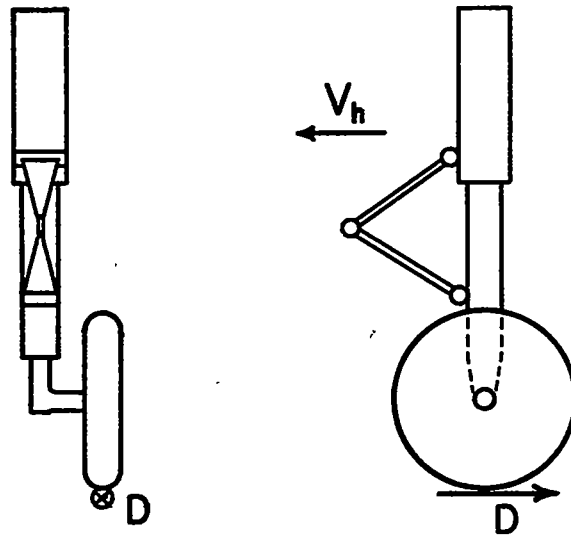


Figure 20.- Shock strut with eccentric wheel.

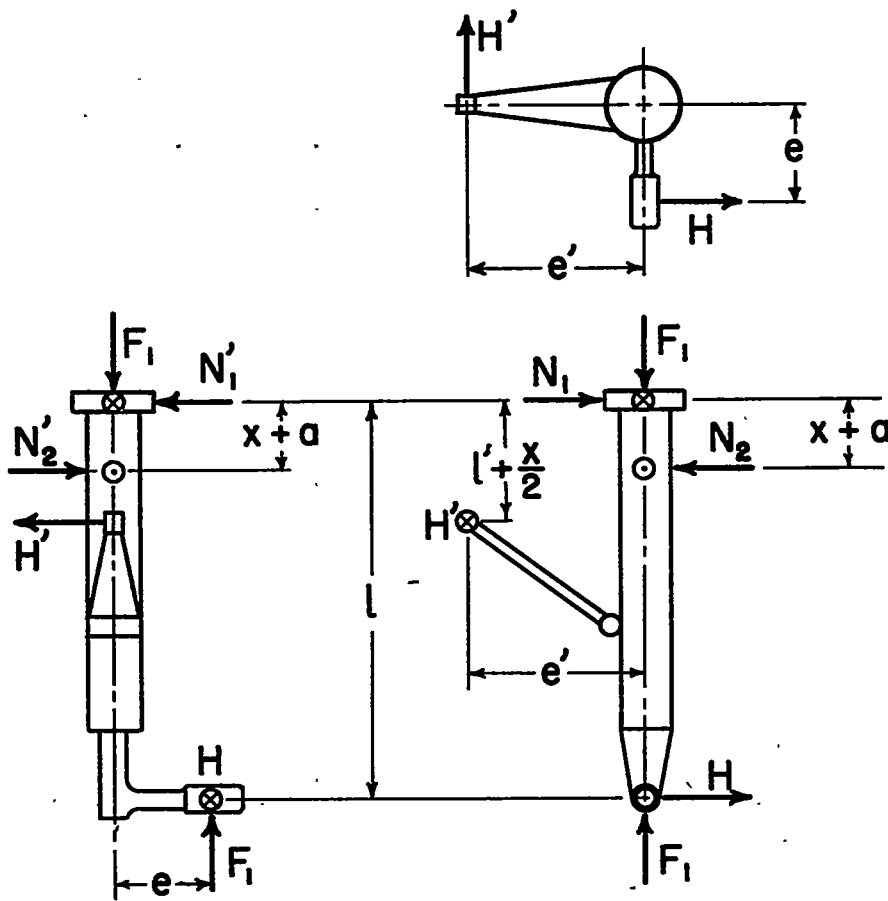


Figure 21.- Free-body diagram of piston.

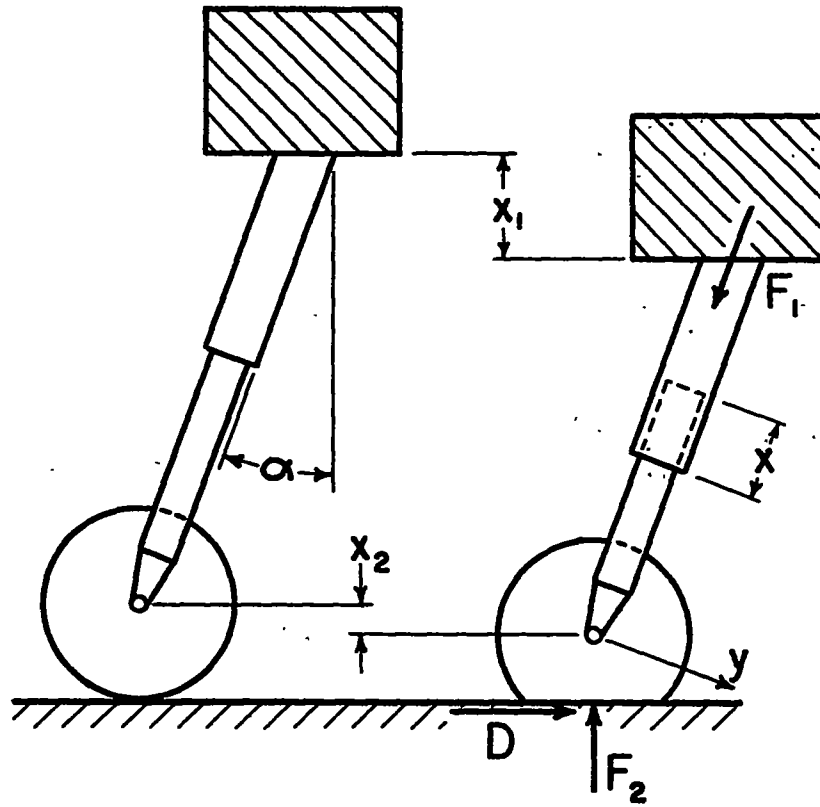


Figure 22.- Inclined shock strut.

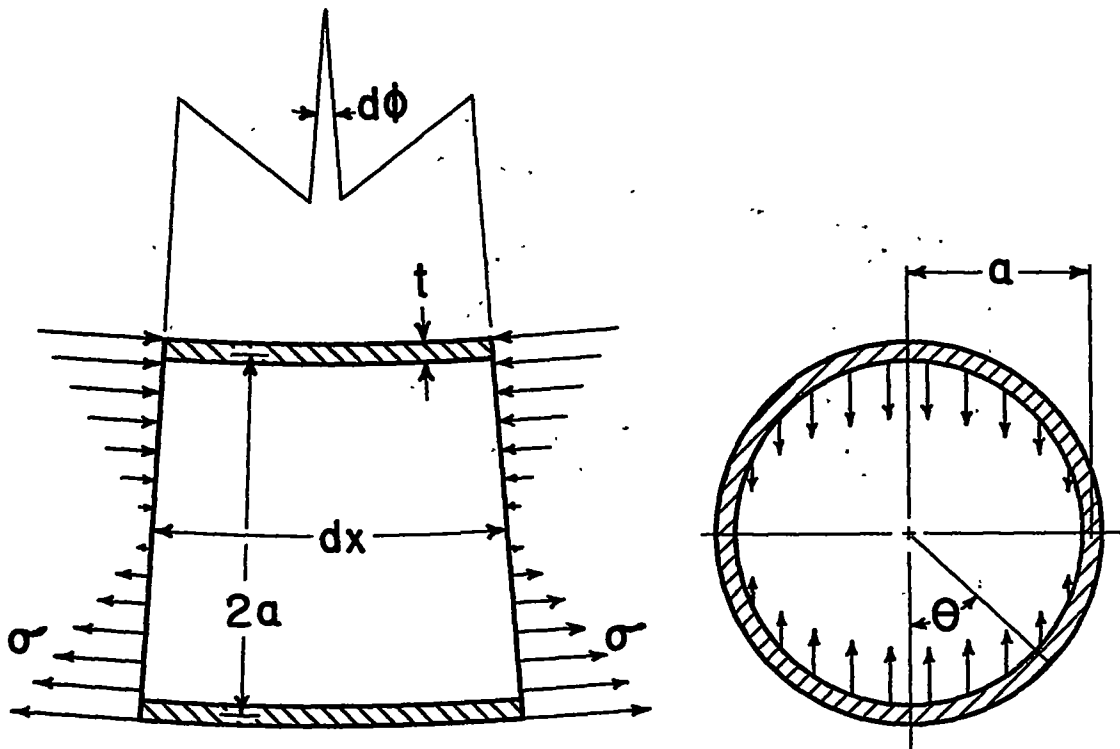


Figure 23.- Element of tube, showing forces which produce ovalization.